BRNO UNIVERSITY OF TECHNOLOGY

VYSOKÉ UČENÍ TECHNICKÉ V BRNĚ

FACULTY OF MECHANICAL ENGINEERING

FAKULTA STROJNÍHO INŽENÝRSTVÍ

ENERGY INSTITUTE

ENERGETICKÝ ÚSTAV

QUANTIFICATION AND OPTIMIZATION OF BLOOD FLOW PATTERNS

KVANTIFIKACE A OPTIMALIZACE VZORCŮ PRŮTOKU KRVE

BACHELOR'S THESIS

BAKALÁŘSKÁ PRÁCE

AUTHOR AUTOR PRÁCE	Michael Macek
CONSULTANT KONZULTANT	Andreas Linninger, Ph.D.
SUPERVISOR VEDOUCÍ PRÁCE	doc. Ing. Marek Baláš, Ph.D.

BRNO 2025

BRNO UNIVERSITY OF TECHNOLOGY
FACULTY OF MECHANICAL ENGINEERING

Assignment Bachelor's Thesis

Institut:	Energy Institute
Student:	**Michael Macek**
Degree programm:	Energy
Branch:	no specialisation
Consultant:	**Andreas Linninger, Ph.D.**
Supervisor:	**doc. Ing. Marek Baláš, Ph.D.**
Academic year:	2024/25

As provided for by the Act No. 111/98 Coll. on higher education institutions and the BUT Study and Examination Regulations, the director of the Institute hereby assigns the following topic of Bachelor's Thesis:

Quantification and optimization of blood flow patterns

Brief Description:

This thesis is a proposal of a new method of processing in vivo measurements to enhance the quality of measured data sets and apply this method in multiple case studies. The proposal is based on the hypothesis that by simulating more anatomically accurate models it is possible to achieve precise results, which has never been done before.
To be able to avoid risking someone's health when planning a neurovascular surgical procedure, it is necessary to have a validation for essential decisions. The cerebrovascular blood flow (CBF) can theoretically be simulated like any other fluid system.

For any simulation, it is essential to measure accurate flow rates. Cerebral blood flow cannot be measured the same way as sewers or rivers. Flow values have to be obtained without direct contact with the fluid. A common way of measuring CBF is by using MRI technology.

Static flow simulations can be simulated using the Hagen–Poiseuille and mass conservation equations. MRI technology has shown one major issue when used for CBF measurements – this technology can only detect the largest vessels. The vessels, even though small can withdraw large amounts of blood, the incapability of detecting them when measuring causes an inflow/outflow discrepancy. This discrepancy prevents flow simulations due to the mass balance not being satisfied. This effect cannot be eliminated or reconciled even with optimization–based parameter estimation techniques.
This thesis will be contains the hypothesis that the discrepancy is caused by the mentioned small vessels. This thesis will test this hypothesis by developing a new estimation technique which accounts the CBF in non–detectable vessels.

Bachelor's Thesis goals:

List the basic approaches to modelling blood flow in human organs.
Propose a procedure to test the hypothesis of the influence of small vessels on the accuracy of simulations.
Verify the hypothesis and report the results of your study.

Recommended bibliography:

CENGEL, Yunus A. a John M. CIMBALA. Fluid Mechanics - Fundamentals and Applications. 2. Boston: McGraw Hill, 2010.

Park C.S., Hartung G., Alaraj A., Du X., Charbel F.T., Linninger A.A. Quantification of blood flow patterns in the cerebral arterial circulation of individual (human) subjects. Int J Numer Meth Biomed Engng. 2020; 36:e3288. https://doi.org/10.1002/cnm.3288

Deadline for submission Bachelor's Thesis is given by the Schedule of the Academic year 2024/25

In Brno,

L. S.

prof. Ing. Jiří Pospíšil, Ph.D.
Director of the Institute

doc. Ing. Jiří Hlinka, Ph.D.
FME dean

Summary

To minimize risks to a patient's health in neurovascular surgical planning, establishing precise and validated methods to determine the status of blood supply of the brain is crucial for critical decision-making. This thesis proposes a new method of processing in-vivo measurements to reconstruct the blood flow distribution across the cerebral circulation and enhance the quality of measured data sets. The proposal is based on the hypothesis that the increase of anatomical detail of the cerebrovascular tree leads to a significant improvement in accuracy of flow estimations, resulting in unprecedented levels of accuracy in determining patterns of blood flow distributions in vivo.

Cerebral blood flow simulations are highly dependent on the quality of in vivo measurements. Volumetric blood flow in the cerebral circulation can be measured with non-invasively with cine phase contrast MRI (NOVA), which limits the ability to measure vessels smaller than the spatial resolution of the technology employed. The consequence of this limitation results in discrepancies in data sets. The flow, which is distributed into vessels below the resolution threshold cannot be accounted for, thus portions of the blood flow will be diverted to these invisible vessels thus seemingly disappear from the circuitry of measured flows. Fluid mechanical simulations cannot use flow measurements that include discrepancies.

We present a novel flow estimation method with the goal of reconciling such discrepancies in flow measurements. We wish to preserve all explicit measurements to acquire an anatomically accurate flow distribution in all vessels contained in the system. The method also accounts for flows in small blood vessels, whose existence is an undisputed anatomical fact, but whose caliber is too small to be detected by MR. The method is based on a multi-objective constrained optimization method accepting both explicit flow measurements and flows expressed as a fraction of an arbitrary vessel. Once flows have been estimated in the entire cerebral network based on in vivo flow measurements, pressure distributions of network can be inferred using Hagen Poiseuille's law.

All mentioned methods have been introduced, tested, and validated on multiple small networks to examine the performance of the novel approach. Further, the techniques were applied to various data sets for real patients for the arterial and venous tree. We also reconciled all flows in the arterial and venous system simultaneously in a single program. To the best of our knowledge, this arterial venous flow estimation has never been attempted before. The results of all presented case studies have shown that the estimation of anatomically incomplete networks leads to not preserving the input measurements, which devaluates the results to such an extent that they are unreliable for practical use. All estimations of anatomically accurate networks have strictly preserved all measured values making the results suitable for precise practical use. These results support the notion that to achieve anatomically accurate results, it is crucial to consider all anatomical details.

This approach could be a significant milestone in neurology and a very useful tool for neurosurgeons to test their theories in unprecedented cases with accurate values. This tool could also be an important pre-requisite for potential heat models of the cerebral circulation, which could be crucial for predicting strokes, etc

Keywords

Flow estimation; Pressure estimation; Blood flow patterns; Discrepancy reconciliation; Neurovascular systems; Hemodynamic

Abstrakt

Pro minimalizaci vystavení pacienta riziku při plánování chirurgických zákroků, stanovení precizní a validované metody na kvantifikaci krevního zásobování je zásadní pro kritické rozhodování. Tato bakalářská práce představuje novou metodu zpracování měřených in-vivo hodnot pro rekonkstrukci distribuce krevních průtoku v krevním oběhu mozku a navýšit kvalitu naměřených dat. Představený návrh je založen na hypotéze, že navýšení anatomických detailů cerebrovaskulárního rozvětvení povede k výraznému navýšení přesnosti výsledných hodnot, což bude mít za následek bezprecedentní preciznost určování in-vivo krevní distribuce.

Simulace krevního průtoku jsou vysoce závislé kvalitě in-vivo měření. Objemový krevní průtok v cerebrovaskulárním oběhu lze měřit neinvazivně pomocí cine fázově kontrastní MR (NOVA), což limituje možnost měření cév menších něž minimálního rozlešení. Důsledky těchto limitů jsou nepřesnosti v naměřených datech. Průtoky, které jsou rozloženy do nerozeznatelných cév nemohou být zaznamenány, tudíž části krevního průtoku nezaznamenáme jako výtoky ze systému a zdánlivě zmizí z měřeného systému. Tekutinové simulace nejsou schopny příjmout naměřené hodnoty obsahující tyto nesrovnalosti.

Představujeme novou metodologii stanovení průtoků s cílem korekce nesrovnalostí. Cílem je ponechat všechny explicitně zadané naměřené hodnoty a získání anatomicky korekní krevní distribuce ve všech cévách systému. Tato metoda rovněž zohledňuje krevní průtoky ve vlásečnicích nerozeznatelních MR, jejíž existence je nepopřitelným anatomickým faktem. Tato metoda je založena na multi-objektivní vázanou optimalizační metodou příjimací jak explicitně zadané hodnoty, tak implicitně zadané průtoky jakožto zlomek průtoku jiné cévy. Po stanovení průtoku v celém cerebrovaskulárním systému založeným na in-vivo měření, tak budou následně stanoveny tlaky pomocí Hagen-Poiseuillového zákona.

Všechny zmíněné metody byly představeny, otestovány a validovány na několika malých systémech pro stanovení charakteru nové metodologie. Následně byly techniky aplikovány s různorodými daty na tepenných a žilných rozvětveních reálných pacientů. Všechny nesrovnalosti prošly korekcí samotnou metodologií pro jak tepenní, tak i žilný rozvětvení. Podle našich nejlepších znalostí nebyl takto přesný odhad arteriálního a žilnýho průtoku dosud nikdy dosažen. Výsledky všech představených případů prokázaly, že stanovení průtoků nedostatečně detailních systémů má za následek nedodržení explicitně zadaných hodnot, což znehodnocuje výsledky natolik, že jsou nespolehlivé pro praktické využití. Všechny odhady anatomicky korektních systému striktně dodržely explicitně zadané hodnoty, což činí výsledky hodnými pro užití v praxi. Tyto výsledky podporují myšlenku, že pro docílení anatomicky korektních výsledků, tak je kruciální zvažovat všechny anatomické detaily.

Tento přístup by mohl být významným milníkem v neurologii a velmi užitečným nástrojem pro neurochirurgy pro testování jejích hypotéz při bezprecedentních případech s přesnými výsledky. Tento nástroj by mohl být nezbytným pre-rekvizitem pro potenciální simulace tepelných pochodů cerebrální cirkulace, což by bylo zásadním, též bezprecedentním, způsobem předpovídání cévní mozkové příhody, apod.

Klíčová slova

Stanovení průtoku; Stanovení tlaku; Průtokové vzorce krve; Vyrovnání nesrovnalostí; Neurovaskulární systémy; Hemodynamika

Bibliographic citation

MACEK, Michael. *Quantification and optimization of blood flow patterns*. Online, bachelor's Thesis. Marek BALÁŠ (supervisor). Brno: Brno University of Technology, Faculty of Mechanical Engineering, 2025. Available at: https://www.vut.cz/en/students/final-thesis/detail/165968. [accessed 2025-05-22].

Declaration

I, Michael Macek, hereby declare that I have written this bachelor's thesis on the topic **Quantification and Optimization of Blood Flow Patterns** independently, using only the sources and literature listed in the bibliography, which forms an appendix to this thesis.

Date *Name and Surname*

First and foremost, I would like to express my sincere gratitude to prof. Linninger and the LPPD laboratory for their valuable lessons, guidance, and for allowing me to gain practical experience in a research environment. Their support and encouragement have been instrumental in introducing me to this field of study, and without their help, I would never have been able to undertake this bachelor's thesis on this topic. Your feedback has given me invaluable advice that has profoundly influenced my professional and personal approach to everything I do.

I would also like to thank my family for their encouragement, patience, and support. Their belief in me has been a fundamental resource of motivation in times of need. Furthermore, I would like to acknowledge my academic supervisor, doc. Baláš, for formally overseeing the completion of this thesis. I also wish to thank my colleagues at the Institute of Energy for their scholarly work and the inspiring environment they have created.

This thesis would not have been completed without the contributions, support, and presence of all the individuals mentioned above.

Michael Macek

Table of Contents

Chapter 1 – Neurovascular anatomy of the human brain.

Summary

This chapter introduces the neurovascular anatomy of the Circle of Willis, familiarizing the reader with the anatomy, which will be referenced and analyzed in subsequent sections of the thesis. By including the side draws in the simulated models, a more accurate neurovascular model is achieved. By increasing the accuracy of the model a more accurate flow estimation can be achieved resolving flow discrepancies contained in IN VIVO measurements, as well as acquiring anatomically correct flows in those vessels, which cannot be measured.

1.1. Anatomy of the Circle of Willis: The Circle of Willis (CoW) is a significant part of the neurovascular structure of the brain. It is responsible for distributing blood into the whole brain and its surroundings, it serves as a main blood vessel conjunction. The main CoW inlet vessels are the *Internal Carotid Arteries*– ICA (approximately 80% of the CoW feed), and the *Basilar Artery (combination of prior Vertebral Arteries)* – BA. The outlet arteries are the *Posterior Cerebral Arteries* – PCA, *Middle Cerebral Arteries* – MCA, and the *Anterior Cerebral Arteries* – ACA. The ICA and PCA are connected by the P*osterior Communicating Arteries* – PcoA, ACA are connected by the AcoA.

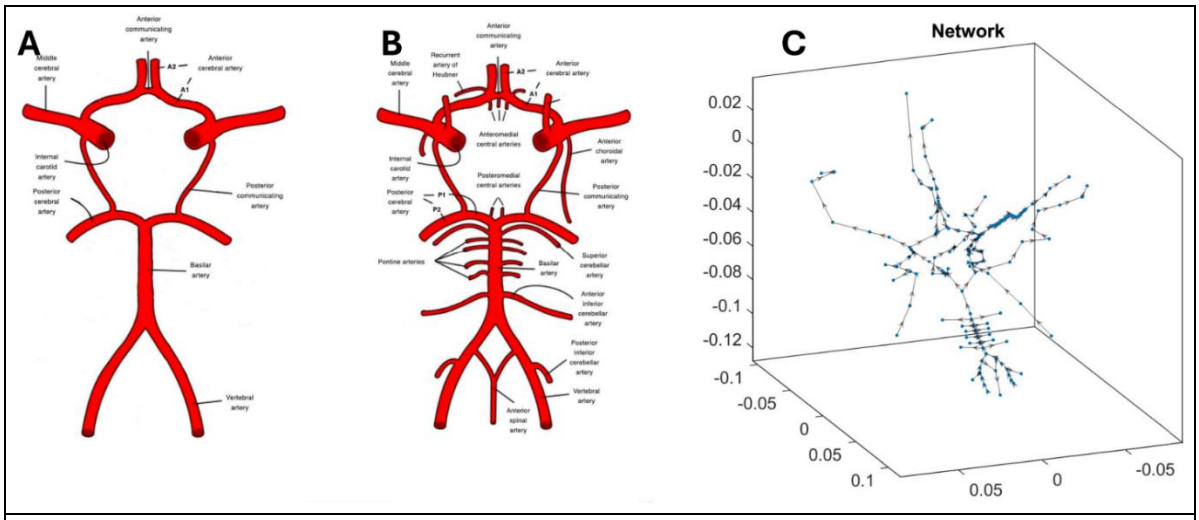

Figure 1 – A) NOVA view of the Circle of Willis, small vessels are missing.[1] B) Expanded view of the CoW including side draws invisible for MR technology.[1] C) 3D model of Expanded view of the of the CoW.

1.2. Vertebral Artery: The VA and the ICA supply blood to the brain, the VA supplies approximately 20% of all blood provided. The main VA blood withdrawal is caused by the *Posterior Inferior Cerebellar Artery* which supplies the cerebellum and the choroid plexus. A minor blood withdrawal is caused by the *Anterior Spinal Artery*.[2]

1.2.1. Posterior Inferior Cerebellar Artery: The PICA is one of the 3 main blood suppliers of the Cerebellum, in comparison to the Spinal Artery, it causes substantially more blood withdrawal from the VA.[2]

1.3. Basilar Artery: The Basilar Artery has 3 main side branches, *The Anterior Inferior Cerebellar Artery, the Pontine Branches*, and *the Superior Cerebellar Artery*. All mentioned withdrawals are visualized in Figure 2E. The PB, SCeA, and AICA supply blood to the Pons and the Cerebellum area.[2]

1.3.1. Anterior Inferior Cerebellar Artery: The AICA supplies blood to the middle cerebellar peduncle, lower lateral pons, the anteroinferior surface of the cerebellum, flocculus, and the choroid plexus of the lateral ventricle.[2]

1.3.2. Pontine Branches: The Pontine Branches branch from the BA at sides with a 90° angle, the amount of PB can vary from 3-5 on each side of the BA. They supply blood to the Pons and structures adjacent to them.[2]

1.3.3. Superior Cerebellar Artery: The SCeA branches from the BA right before the BA-PCA bifurcation and is the main blood supplier for the Cerebellum. Unlike the AICA, the SCeA is rarely absent, it rather duplicates and can branches from the PCA. [2]

1.4. Internal Carotid Artery: The ICAs are the main vessels supplying blood into the brain. They branch from the Common Carotid Arteries and then split into the MCA and the ACA. Before the bifurcation, there are *Meningeal Branches* and the *Ophthalmic Arteries* causing blood withdrawal, further branches are the *Inferior* and *Superior hypophyseal arteries.* To emphasize the importance of the ICA (more precisely CCA) – if hit into the neck, a blood clot can occur causing stroke, thrombosis, etc. by clogging the vessel. The blood withdrawals cannot be estimated, we would need to additionally measure either PcoA or the ICA near the ACA/MCA bifurcation.[2]

1.4.1. Ophthalmic Artery: The OA branches before the PcoA/MCA/ACA bifurcation and is responsible for the blood supply of the orbit, eye, nose, face, and the meninges (membranes wrapping around the brain and the spinal cord). The occlusion of OA can lead to sight-threatening conditions.[2]

1.4.2. Anterior Choroidal Artery: The AnCA branches from the ICA and has an extensive blood supply area. It is one of the main suppliers of the Choroid plexus.[2]

1.5. Limitations with in vivo flow measurements: The neurovascular anatomy is a very complex network, when taking measurements, the vessels must be recognizable by the measuring device – e.g. when getting measurements with an MR scan, the actual vessels we want to measure have to be visible on the scan. The absence of small vessel measurements results in seemingly disappearing flow from the system without any traces, **this discrepancy prevents the measurements from being simulated**.

1.6. The arterial network in the CoW:

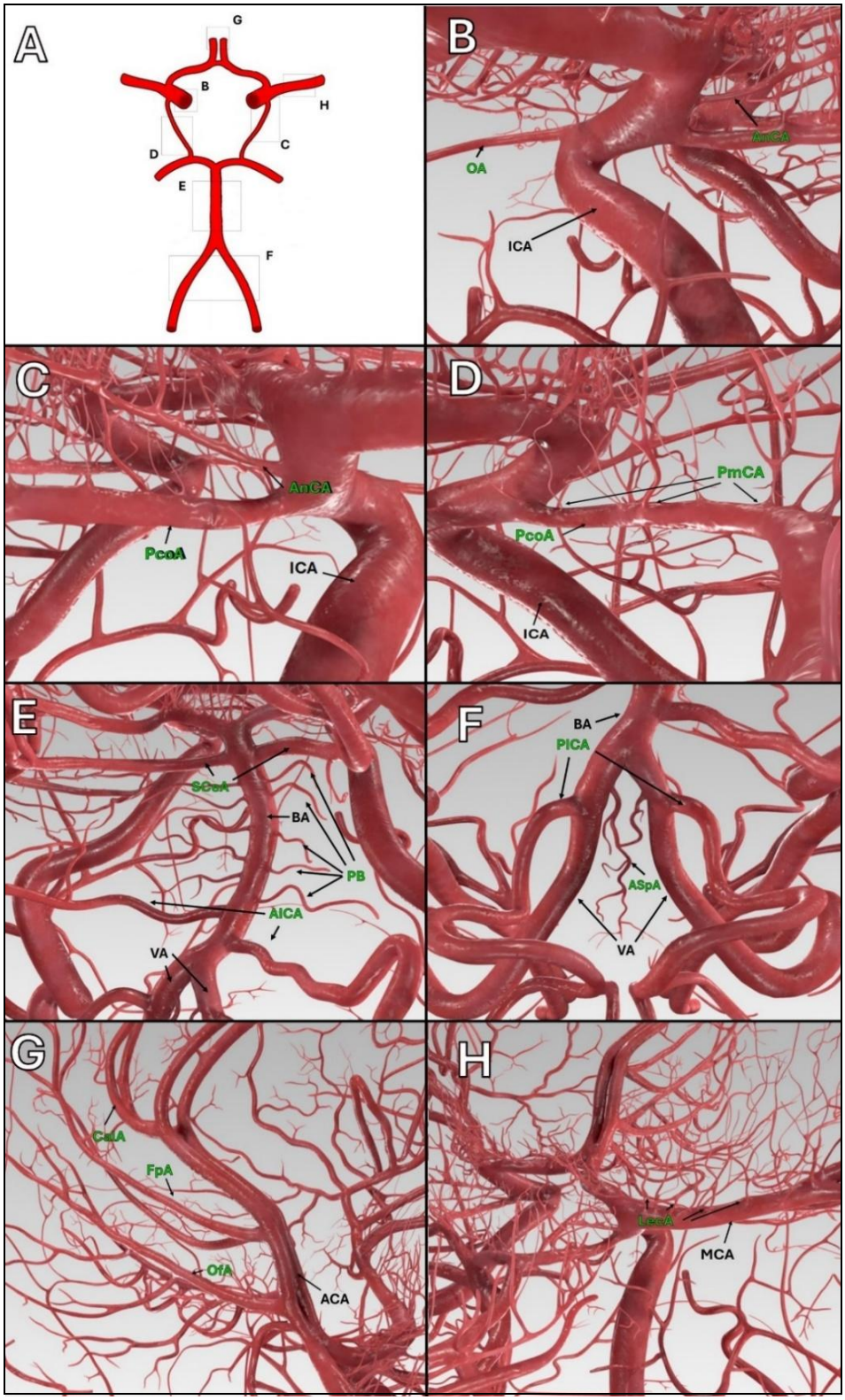

Side draw abbreviations:

OA *– Ophthalmic artery*
AnCA *– Anterior Choroidal Artery*
PcoA *– Posterior Communicating artery*
PmCA *– Posteromedial Central Arteries*
SCeA *– Superior Cerebellar Artery*
PB *– Pontine Branches*
AICA *– Anterior Inferior Cerebellar Artery*
ASpA *– Anterior Spinal Artery*
CalA *– Callosomarginal Artery*
FpA *– Frontopolar Artery*
OfA *– Orbitofrontal Artery*
LecA *– Lenticulostriatal Artery*

Artery abbreviations:

CCA *– Common Carotid Artery*
ECA – *External Carotid Artery*
ICA *– Internal Carotid Artery*
BA *– Basilar artery*
PCA – *Posterior Cerebral Artery*
MCA – *Middle Cerebral Artery*
ACA *– Anterior Cerebral Artery*
VA *– Vertebral Artery*

Vein abbreviations:

JV – *Jugular Vein*
STRAIGHT – *Straight Sinus*
SIGMOID – *Sigmoid Sinus*
SSS – *Superior Sagittal Sinus*
TRANS – *Transverse Sinus*

Figure 2 – Visualization of the main side withdrawals of the CoW[2], Black labels represent the main vessels of the CoW, the green labels represent the side vessels. A) A schematic of the Circle of Willis for marking where Fig. 2B-F are located. B-H) CoW model views with various side withdrawals to showcase the quantity of vessels that cause withdrawals, all vessels of interest are labelled. All vessel abbreviations are discussed.

In vivo blood flow measurements (NOVA)

1.7. Explanation of the measurement procedure: All patients underwent a MRI scan on a Phase Contrast Quantitative Magnetic Resonance Angiography (QMRA) 3.0 Tesla MRI on either a four or eight channel neurovascular coil. The volumetric flow rate was acquired using the Noninvasive Optimal Vessel Analysis (NOVA) software. Major extracranial arteries (such as the ICA, BA, etc.) were visualized with the 2D MRA Time-of-Flight (TOF) technique, afterwards a 3D MRA TOF scan of the head was obtained.

The MRA images were then sent to a different workstation running the NOVA software to acquire a 3D software-rendering of the vasculature. The 3D render is then used for an automated determination of scan planes perpendicular to the flows of the vessels of interest, which are used to determine where the measurements will be taken.

Volumetric flow rates based on said planes were then acquired using a cardiac-gated Phase Contrast MRA. To acquire accurate measurements, boundaries within the measured values may vary have been set with careful consideration – this process is called velocity encoding. The velocity encoding has been automatically verified by the NOVA software to ensure that aliasing doesn't occur for high velocities within the velocity range chosen for phase encoding of vessels.

To maximal accuracy of flow measurements, velocity encoding was individually adjusted for each vessel. The volumetric flow rate flow rate for each vessel was processed by the NOVA software.[3] This procedure results in a NOVA flow report, which presents a table of the systolic-diastolic cycle dependent on time.

1.8. NOVA flow report of Subject S58: The NOVA report of subject 58 (S58) presents for all main Veins and Arteries of interest, in **Error! Reference source not found.** there is a depiction of all planes, where S58's measurements of the Arterial tree were taken, the measurement planes of the main Veins are in Figure 4. The NOVA table of flows can be found in Appendix B.

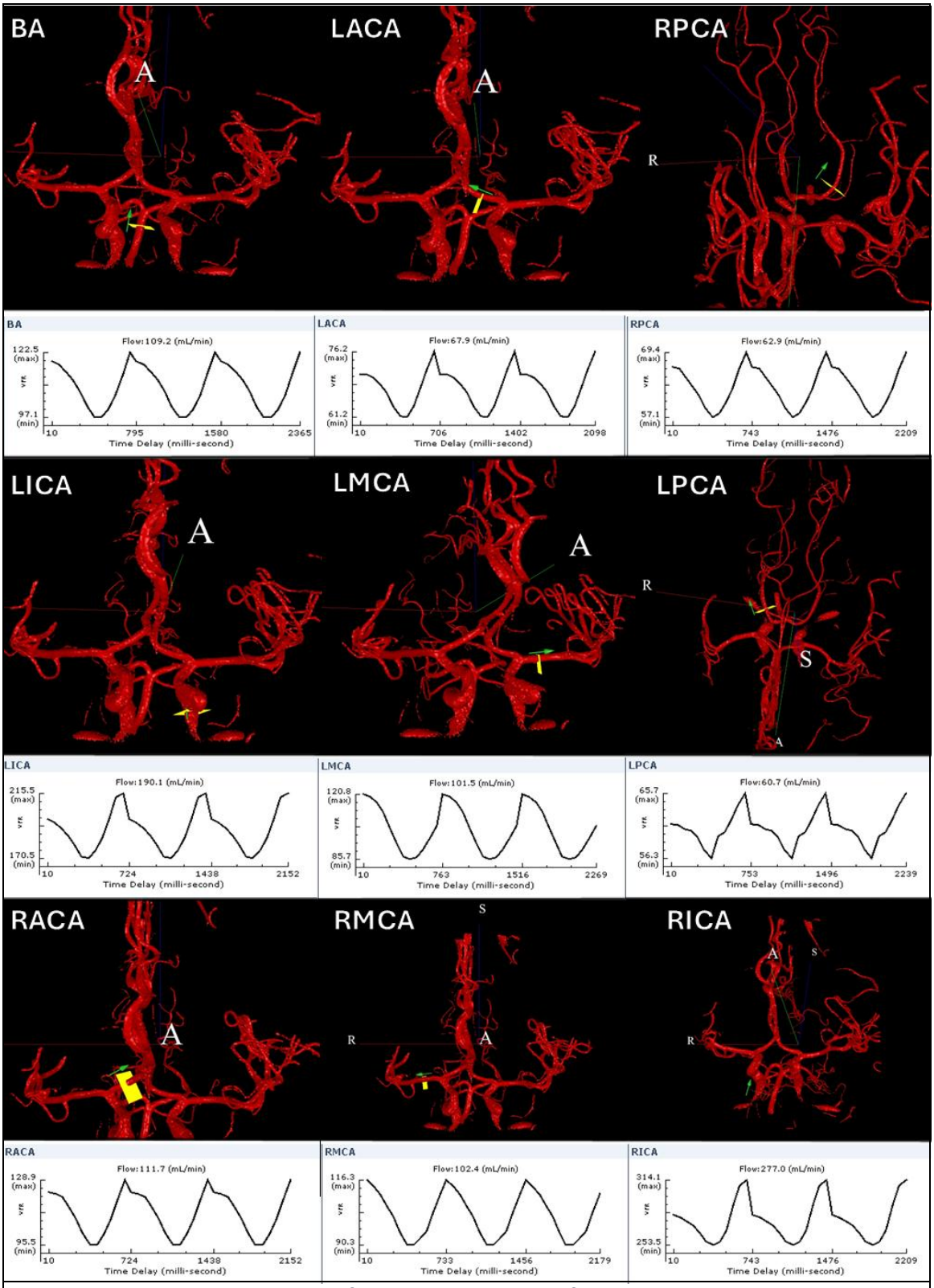

Figure 3 – Measurement planes for each main Artery for Subject 58.

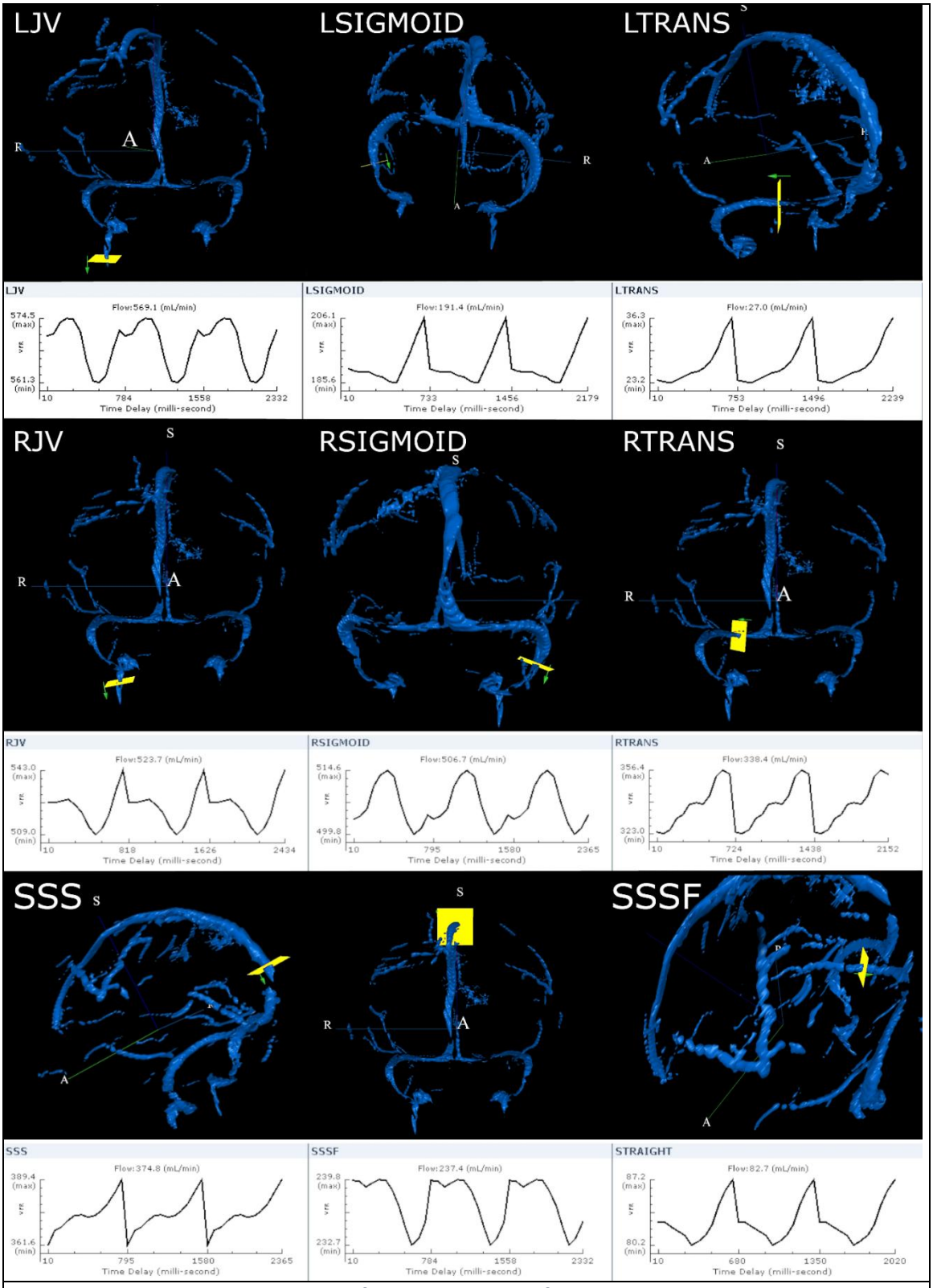

Figure 4 – Measurement planes of each main Vein for Subject 58.

1.8.1. Measurement analysis of Artery measurements for S58: As seen in Figure 5, all main arteries in the arterial tree backbone were measured. After inspecting all the main inlets and outlets, it is obvious that the average inflow from the ICAs and the BA results in 576 ml/min and the average outflow from the PCAs, MCAs and the ACAs results in 504 ml/min. The measurements contain an average flow discrepancy of 72 ml/min, which is 12.5 % of the total inflow. This discrepancy can vary throughout the systolic-diastolic cycle, the statement that this discrepancy has been caused by the measurement inaccuracy would be false. The accuracy of the technology used varies between 3 and 5 %[4]. This thesis proposes that those discrepancies are caused by vessels that draw blood from the main arteries, this effect cannot be measured by modern technology.

1.8.2. Measurement analysis of Venous measurements for S58: The procedure of the analysis of the Venous tree backbone are identical to the Arterial tree backbone. The total inflow from the Superior Sagittal Sinus (SSS) and the Straight Sagittal Sinus (STRAIGHT) result in a total average inflow of 458 ml/min, the total average outflow from the Jugular veins results in a total average outflow of 1093 ml/min, this discrepancy is caused by the Superior, Inferior Petrosal and other feeds.

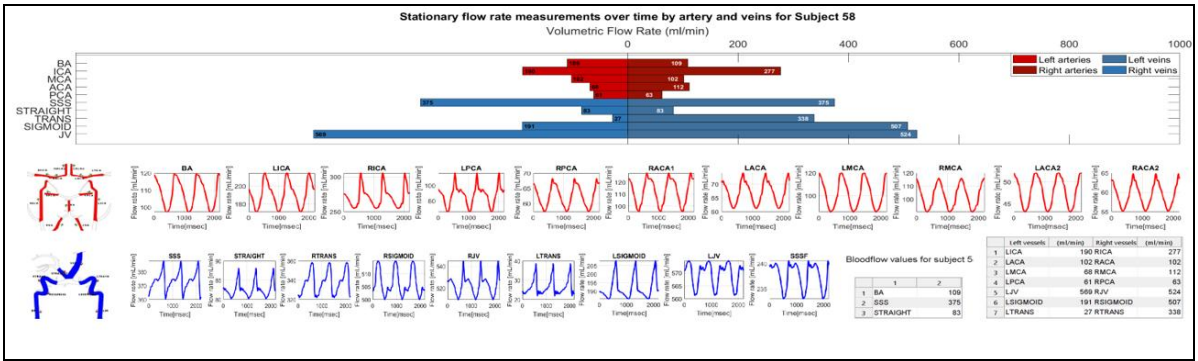

Figure 5 – Visual representation of the NOVA report for S58 as stationary values. For all measured arteries and veins the systolic-diastolic cycle was presented, all artery measurements are depicted as red, all vessels are depicted as blue. Further a bar graph is presented to compare the left and the right variation of vessels, if a vessel does not have a symmetric counter vessel (such as the Basilar artery), the flow value on both left and right side are equal in the graph.[5]

1.9. NOVA flow report of Subject S64: The NOVA report of subject 64 (S64) presents for all main Veins and Arteries of interest, in Figure 6 there is a depiction of all planes, where S58's measurements of Arteries were taken, Vein measurement planes are in Figure 7. The NOVA table of flows can be found in Appendix A. All used abbreviations are discussed in Figure 2.

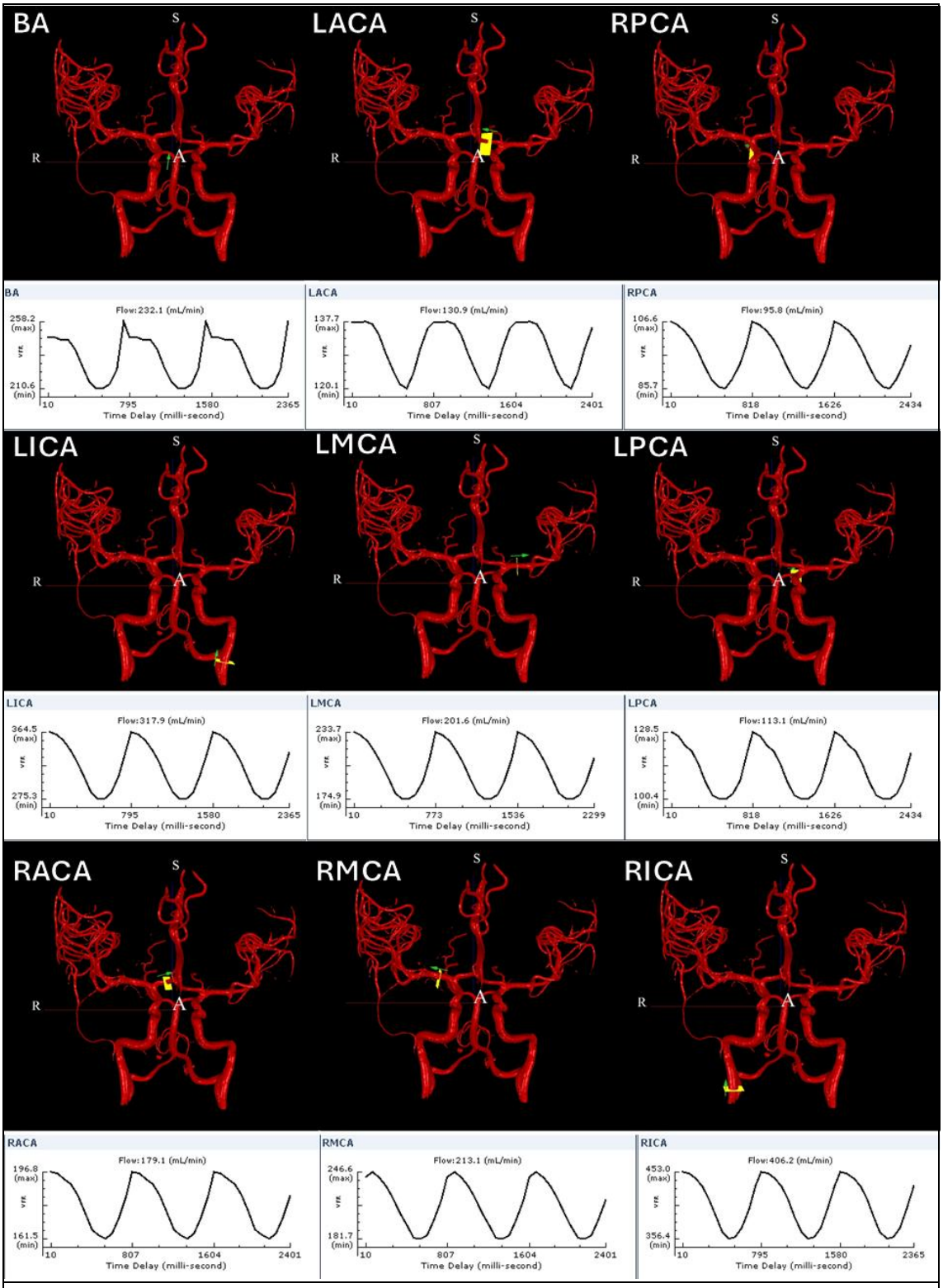

Figure 6 – Measurement planes for each main Artery for Subject 64.

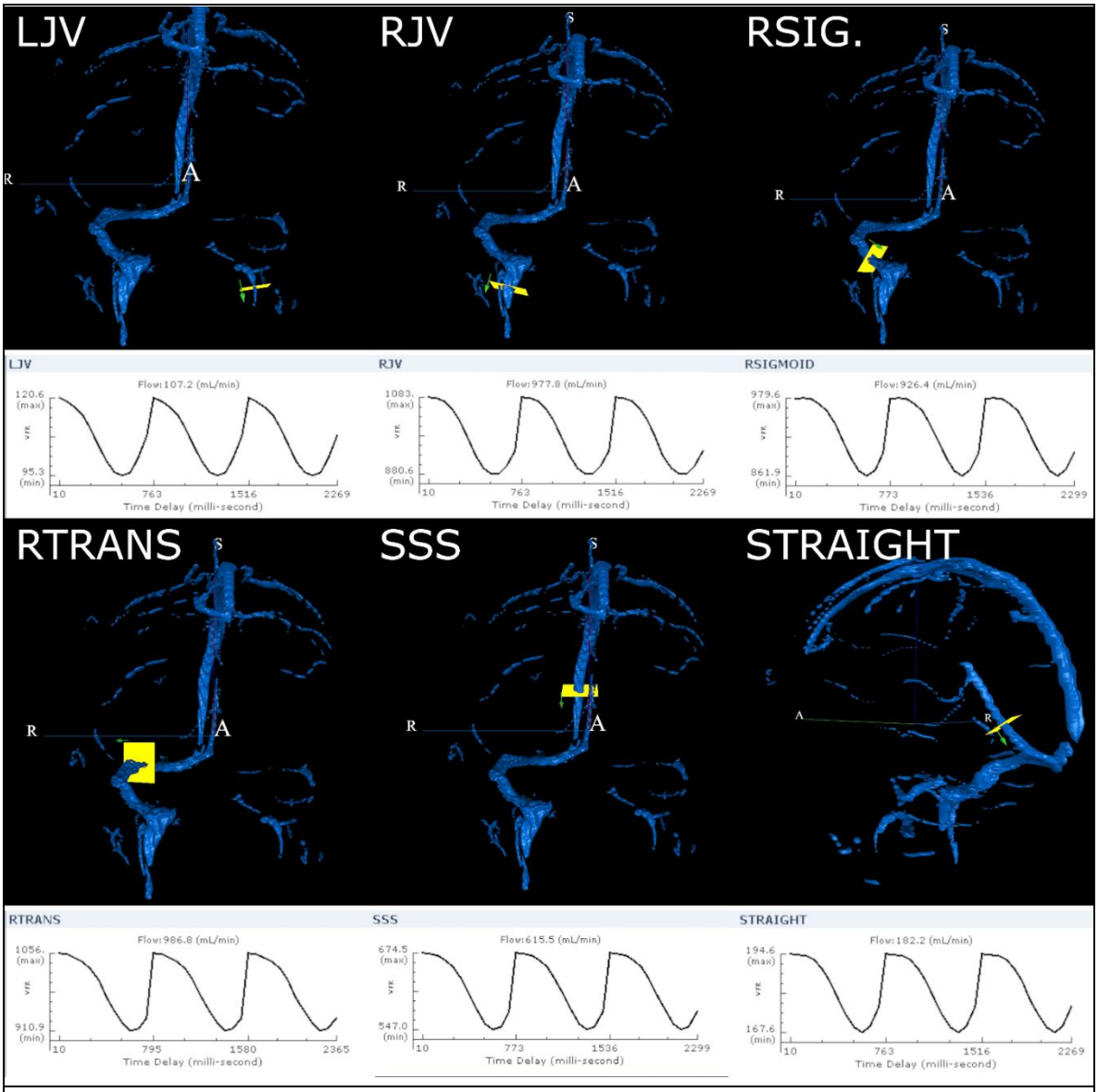

Figure 7 – Measurement planes of each main Vein for Subject 64.

1.9.1. Measurement analysis of Artery measurements for S64: As seen in Figure 8, all main arteries in the arterial tree backbone were measured. After inspecting all the main inlets and outlets, it is obvious that the average inflow from the ICAs and the BA results in 956 ml/min and the average outflow from the PCAs, MCAs and the ACAs results in 934 ml/min. The measurements contain an average flow discrepancy of 22 ml/min, which is 2.3 % of the total inflow. This discrepancy can vary throughout the systolic-diastolic cycle, the statement that this discrepancy has been caused by the measurement inaccuracy would be false, although the flow discrepancy percentage is within the tolerance of the measurement precision, it is not generally observed.

1.9.2. Measurement analysis of the Venous measurements for S64: The procedure of the analysis of the Venous tree backbone are identical to the Arterial tree backbone. The total inflow from the SSS and the STRAIGHT result in a total average inflow of 797 ml/min, the total average outflow from the Jugular veins results in a total average outflow of 1085 ml/min, this discrepancy is caused by the Superior, Inferior Petrosal and other minor feeds.

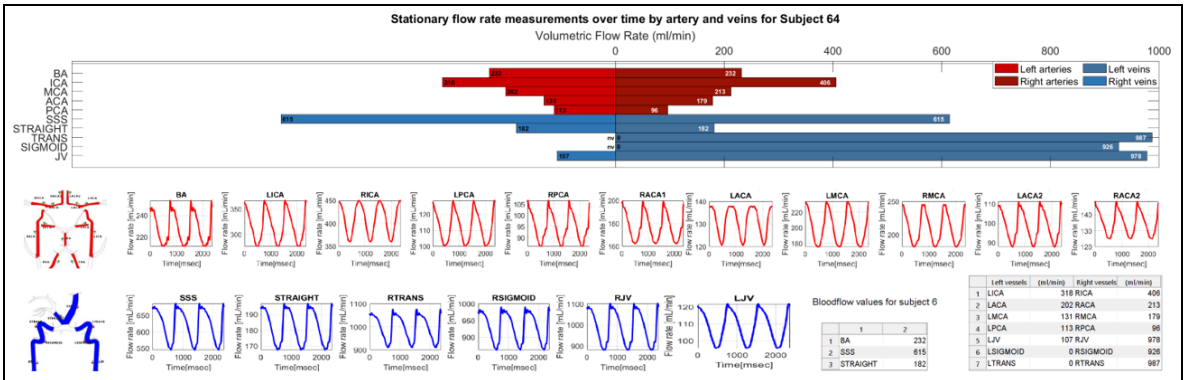

Figure 8 – Visual representation of the NOVA report for S64 as stationary values. For all measured arteries and veins the systolic-diastolic cycle was presented, all artery measurements are depicted as red, all vessels are depicted as blue. Further a bar graph is presented to compare the left and the right variation of vessels, if a vessel does not have a symmetric counter vessel (such as the Basilar artery), the flow value on both left and right side are equal in the graph.[5]

1.10. Reconstruction of the blood flow signal from NOVA measurements: As seen in Appendix A and E, the NOVA report contains 20 measurements for each vessel. To obtain the whole flow signal, the Fourier series and the Quateroni methods have been used.[5]

Chapter 2 – Simulation of blood flow in vascular networks

Summary

Flow simulations are widely used, ranging from industry to medicine. Flow simulations introduced in this section are aimed towards the implementation of the Hagen-Poiseuille and mass conservation equations. This section summarizes the mathematical background, and the implementation of matrix notation for essential input data. Multiple showcases of user input data used for flow simulation can be found in Chapter 4.

Introduction

The flow simulation is a method based on the Hagen-Poiseuille and mass conservation equations for the calculation of flows and pressure of the entire network. This method is used for network analysis where the geometry (length and diameter of vessel) of the network and the boundary conditions (pressure or flow rate) are known. This chapter explains the Matrix form approach of flow simulations. Further, this section explains the implementation into MATLAB and all necessary files this approach needs. The flow simulation is then showcased on multiple case studies, including the Circle of Willis backbone.

Methods

2.1. Mathematical background to simulating networks: All of the simulations are linear (all degrees of freedom satisfied), there is only one correct solution. To define all the needed equations, the **mass conservation** and **Hagen-Poiseuille laws** will be used. To have all the equations as compact as possible, all the necessary information will be stored in matrices (eq. 1– Hagen-Poiseulle law and eq. 2 – mass conservation equations). The **A** matrix is a matrix, where the flow resistances are stored on the main diagonal of the matrix (e.g. resistance 1 – A(1,1), resistance 2 – A(2,2)), The **f** and **p** are column vectors where the unknown flows and pressures are stored (Boundary condition variables have to be replaced for its values). The $\mathbf{C_1}$ Matrix is the connectivity matrix, which represents which flows are between what nodes.

$$A\,f = C_1\,p \tag{1}$$
$$C_1^T\,f = 0 \tag{2}$$

If we want to input all the data into MATLAB, a very effective way to transcribe it is the Master matrix form (eq. 3). It is based on the linear formula, The **I** is an identity matrix, the $\mathbf{D_1}$ matrix is a decision matrix, that enforces only the boundary conditions. The $\bar{\boldsymbol{p}}$ is a column vector, which notates the boundary conditions (e.g. BC for node 3 – $\bar{p}(3, 1)$).

$$Mx = b \rightarrow \begin{bmatrix} A & -C_1 \\ (I - D_1)C_1^T & D_1 \end{bmatrix} \begin{bmatrix} f \\ p \end{bmatrix} = \begin{bmatrix} 0 \\ D_1\bar{p} \end{bmatrix} \tag{3}$$

2.2. Definition of all necessary network files for simulations: Before it is possible to simulate any network, we need to get familiar with the needed files for any simulation. The main files for any simulation are the ".fMx", ".pMx", ".dia" and the ".BC" file. The fMx and pMx define how the network looks and what the expected direction of flows are. The dia file contains the diameters of the flows. The BC file contains the boundary conditions. It is the only file that can be changed without changing the network.

2.3. How to load and simulate a network in MATLAB: For running simulations using the script, you need to import all the files mentioned above for the network you want to simulate and the script itself into MATLAB. After doing so, all you need is to run the script, a dialogue window will pop up, where you need to select a fMx file of the network you want to simulate.

2.4. Definition of a BC file: A BC file is a simple file that can be created using for example notepad (Windows10 – .txt file extension). The structure logic behind inputting the desired is like a pseudo-matrix in a notepad separated with spaces and enters. It is composed of rows and columns. The first column is for noting for which node the boundary condition is meant. The second column is for marking which type of boundary condition it is. For network simulations, there are two types of BC – The Dirichlet BC (boundary pressure) or the Neumann BC (boundary flow), multiple showcases can be found in Chapter 4.

2.5. How to correctly input Dirichlet boundary condition values: The value of boundary conditions is the most important information in the file, so it is essential to know how to interpret the value. The Dirichlet boundary condition is very simple, it is the difference between the environment pressure and the pressure of the liquid (e. g. the air around us is approximately 100kPa – 1 bar, if we put pressure in our car tires, you know that you must put 2 bar inside = 2 bar difference relative to the atmosphere. The absolute pressure inside the tire will be 3 bar). It is possible to input absolute pressure also, but you have to take into consideration that the flows will be equal to the relative pressure example, but all calculated pressures will also be absolute pressures.

2.6. How to correctly input Neumann boundary condition values: The Neumann conditions have to be treated differently, because unlike pressure, flow has a direction. Generally, a network can only have an inlet, an outlet and an end of a pipe. If there is an inlet, mass is added, so the overall value is looked at as positive. If there is an outlet, the value is negative. It is crucial, that the mass conservation law is satisfied, that means that the sum of all in/out flows must equal zero. Because of the mass conservation having to be that way, For each simulation, at least one Dirichlet BC has to be stated, if only Neumann BCs were stated, the equations wouldn't be linearly independent. Multiple case studies can be found in Chapter 4.

2.7. What are source/sink terms and when are they used: To fully define a network system, as many BCs have to be stated, as there are degrees of freedom (All conditions have to be linearly independent). A network with a total inflow of 100 ml/min and a total outflow of 90 ml/min, there is a 10 ml/min flow discrepancy (this discrepancy can be caused by side draws of any kind). Without taking the side draw into consideration, it isn't possible to

simulate this network due to the simulations depending on inflow/outflow equality. The sink/source term introduces this side draw to the simulation and enables the simulation.

2.8. Mathematical background behind source/sink terms: When generating a mass balance, we always take the sum of all flows and set it equal to zero, but if we want to add a source/sink term we do not change the overall DOF of the system, because it is not dependent on any boundary conditions, it is just a constant, we can just add it to the mass balance equation (as seen in eq. 4)

$$f_1 - f_2 \pm C = 0 \tag{4}$$

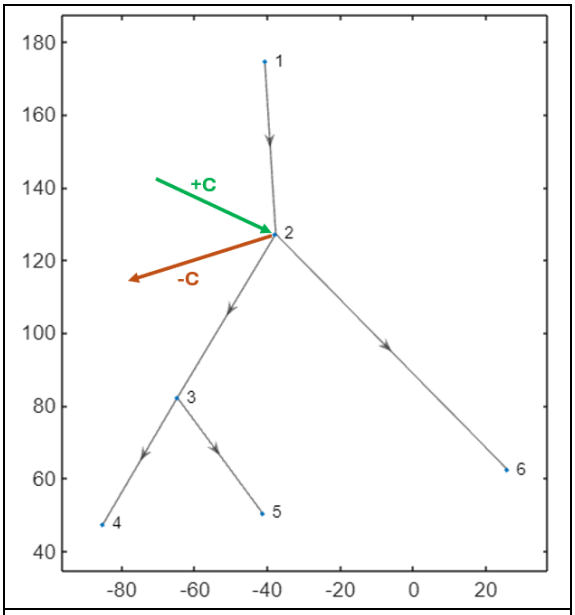

Figure 9 – Scheme of NW1Bioe532 with visualized source (green) and sink(red) terms with corresponding signs.

2.9. How to add source/sink term into the system: To add a source/sink term into the system, we will be writing it exactly the same like we were doing with the boundary conditions, also into the BC file. The **first column** says at what node the source/sink term is, the **second column** is going to be 3, which is the notation for a source/sink term, the **last column** is the value of the source/sink term. Case studies showcasing the source/sink terms can be found in Chapter 4.

2.10. How to use simulation Master matrix form with source/sink terms: If we want to add the source/sink terms we can use the master matrix form of the network analysis (eq. 3) and add the source sink values into the equation (eq. 5). $\bar{\boldsymbol{Q}}$ is a column vector of source/sink values.

$$\begin{bmatrix} \boldsymbol{A} & -\boldsymbol{C_1} \\ (\boldsymbol{I}-\boldsymbol{D_1})\boldsymbol{C_1^T} & \boldsymbol{D_1} \end{bmatrix} \begin{bmatrix} \boldsymbol{f} \\ \boldsymbol{p} \end{bmatrix} = \begin{bmatrix} \boldsymbol{0} \\ \boldsymbol{D_1}\bar{\boldsymbol{p}} \end{bmatrix} + \begin{bmatrix} \boldsymbol{0} \\ (\boldsymbol{I}-\boldsymbol{D_1})\bar{\boldsymbol{Q}} \end{bmatrix} \tag{5}$$

Results

2.11. Boundary conditions with only Dirichlet boundary conditions: This case study is a showcase of NW1Bioe532 with pure Dirichlet boundary conditions, the resistances are calculated as a function of vessel diameter and its length. In NW1Bioe532 there is one inlet node and three outlet nodes, so for the network to be solvable, pressures for each terminal node has to be specified (Assigned pressures are marked as bold in Table 1).

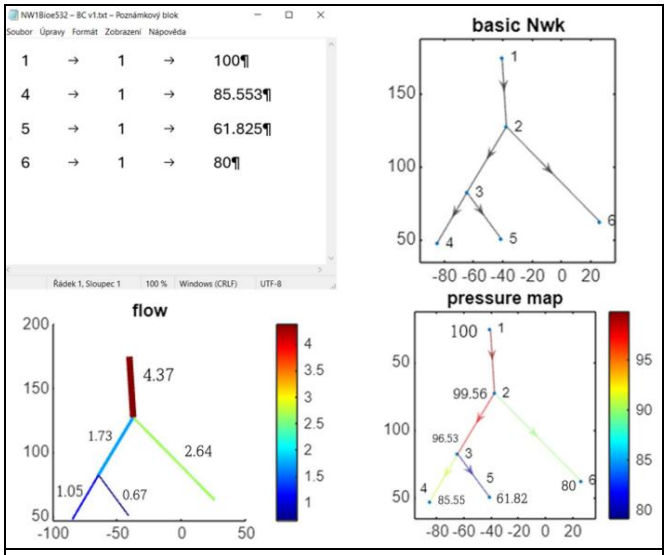

Figure 10 – BC file including purely Dirichlet Boundary conditions, calculated flow and pressure map visualized with superimposed values. Nwk name: NW1Bioe532.fMx; code: testBloodFlow_2024_withSources.m

Table 1 – Calculated pressures for NW1Bioe532. Assigned values are marked as bold.

Node	Pressure
[-]	[mmHg]
1	**100.00**
2	99.56
3	96.53
4	**85.55**
5	**61.83**
6	**80.00**

Table 2 – Calculated flows and resistances for NW1Bioe532.

Face	Flow	Resistance
[-]	[ml/min]	$\left[\frac{\text{mmHg} \cdot \text{min}}{\text{ml}}\right]$
1	4.3772	0.0990
2	1.7318	1.7511
3	1.0573	10.3856
4	0.6745	51.4603
5	2.6454	7.3965

2.12. Boundary conditions with combined forms of BC: This example is a presentation of mixed BC types. The face flowing through node 1 is an inlet node and therefore must have a positive value. Faces flowing through nodes 4 and 5 are outlet nodes and therefore must have a negative value. To have a fully defined system of linear equations, at least one Dirichlet BC has to be stated.

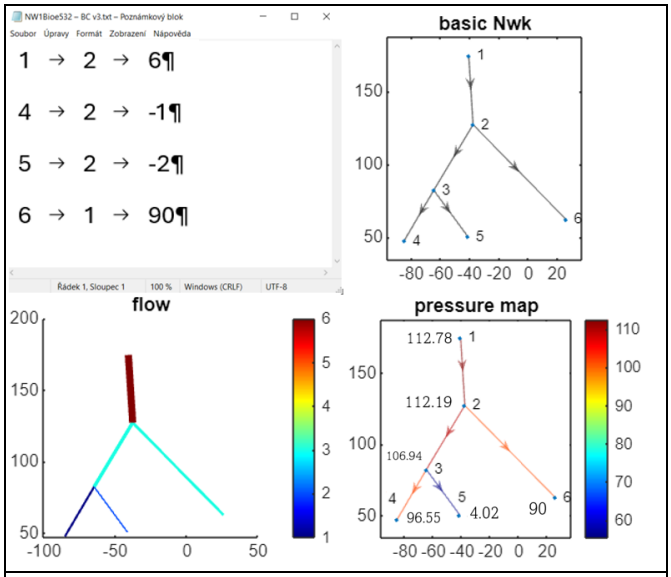

Figure 11 – Flows and Pressures for NW1Bioe532 – mixed boundary conditions, calculated flow and pressure map visualized with superimposed values. Nwk name: NW1Bioe532.fMx;
code: testBloodFlow_2024_withSources.m

Table 3 – Calculated pressures for NW1Bioe532. Assigned values are marked as bold.

Node	Pressure
[-]	[mmHg]
1	112.7838
2	112.1895
3	106.9363
4	96.5507
5	4.0157
6	**90**

Table 4 – Calculated flows and resistances. Assigned values are marked as bold.

Face	Flow	Resistance
[-]	[ml/min]	$\left[\frac{\text{mmHg} \cdot \text{min}}{\text{ml}}\right]$
1	**6**	0.0990
2	3	1.7511
3	**1**	10.3856
4	**2**	51.4603
5	3	7.3965

2.13. Showcase of real value simulation of the Circle of Willis: The next example, a simplified Circle of Willis network has been simulated (file name "CoW.cs31.fMx"). The boundary conditions were taken from Dr. Charbel's research paper.

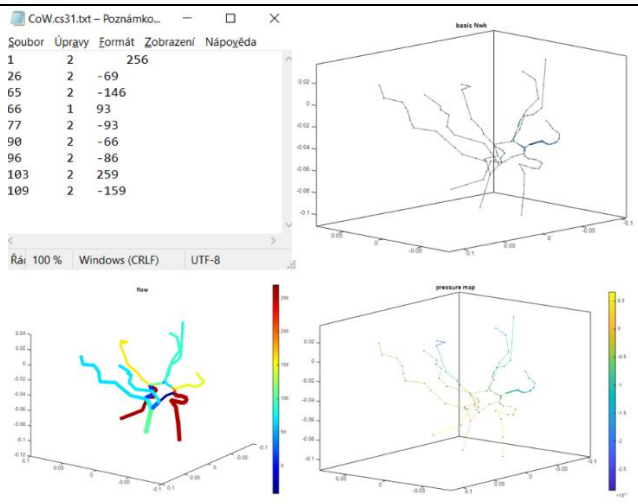

Figure 12 – Simulation of the Circle of Willis, measurements were taken from Dr. Charbel's paper.[3] Nwk name: CoW_simple1.fMx; code: testBloodFlow_2024_withSources.m

2.14. Simulation of NW1Bioe532 with a source/sink term: For showing how to use the source/sink terms, NW1Bioe532 was chosen to be simulated. The source term is going to be introduced at node 2. Due to choosing a source term, the value will have to be positive to be considered a source term (as seen in mass balance equation below). The calculations were done with eq. 5 in MATLAB using the backslash operator.

$$f_1 - f_2 - f_5 + 50 = 0 \qquad \bar{\boldsymbol{Q}} = \begin{bmatrix} \mathbf{0} \\ \mathbf{50} \\ \mathbf{0} \\ \mathbf{0} \\ \mathbf{0} \\ \mathbf{0} \end{bmatrix}$$

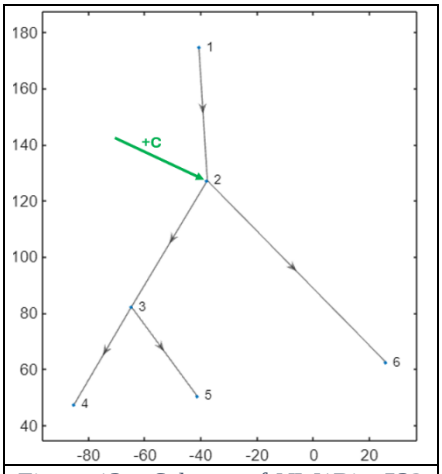

Figure 13 – Scheme of NW1Bioe532 indicating where stated source term was added.

Table 5 – Calculated pressures for NW1Bioe532. Assigned values are marked as bold.

Node	Pressure
[-]	[mmHg]
1	**100**
2	56.15
3	49.34
4	**50**
5	**40**
6	**20**

Table 6 – Calculated flows and resistances for NW1Bioe532.

Face	Flow	Resistance
[-]	[ml/min]	$\left[\frac{\text{mmHg} \cdot \text{min}}{\text{ml}}\right]$
1	146.16	0.3
2	75.66	0.09
3	-2.19	0.3
4	77.85	0.12
5	120.5	0.3

Chapter 3 – Flow estimation of vascular networks.

Summary

This section proposes a new methodology for estimating flows in a given vascular network. This new methodology is based on a multi-objective constrained optimization, which can receive explicit flow measurements, as well as flows expressed as a fraction of an arbitrary vessel. This implicit flow input enables to infer flows based on the cross-section ratio between parent/child vessels. This method returns an anatomically correct flow distribution of the whole neurovascular system. The method is also able to reconcile imperfections in flow measurements, which were caused by insufficient imaging quality of modern non-invasive technologies. We were further able to estimate flows in vessels that cannot be detected. By estimating anatomically accurate networks, the estimation method enables the acquisition of flow data in vessels that are otherwise unmeasurable, while preserving original flow measurements.

Introduction

When working with biological systems and desiring accurate values, it is quite challenging, so we have to come up with ideas on how to make our values more precise. When calculating flows with only the Hagen-Poiseuille and mass equations we can have a pretty good image of how the flow will behave, however in real cases the mass balances of the visible arteries are in most cases not satisfied because of vessels that are not visible at a MR scan. To find a good compromise between measured values and calculated ones, one way is to optimize it with the same approach as we calculate constrained function in mathematics.

Methods

This section is devoted to showing how to find the optimal flow field on a network that satisfies mass balance and differs minimally from real measured values. The optimization is set up as a least-squares problem with equality constraints for which the solution is computed by finding the stationary point of the Lagrangian function.

3.1. Mathematical background to flow optimization: To get a compromise between the measured flows and the expected ones, we can use the least-square optimization. The least-square optimization is based on the square of the difference between measured and optimized flow to be minimal.

3.2. What optimization method to use: The flow optimization that we are using is based on searching for flows that are as close to the measured flows as possible with a mass balance constraint. There are multiple ways of setting the equations up.

3.2.1. Method 1 – minimizing the difference between selected flow sets: This method minimizes the objective function by making network flows match as close as possible. If the flow vector $\bar{f}$ contains measurement errors, they are reconciled. Unfortunately, this approach can become singular when the network contains internal or terminal loops that are not decided by the flow vector$\bar{f}$. This is due to the absence of internal flows in the objective function, the optimality conditions are rank deficient, and the resulting system matrix can become singular.

3.2.2. Method 2 – minimizing the difference between all flows: This method has an objective function that contains all nodes. Measured flows are set to the measured value, while all the remaining (unmeasured) flows are set to a "desired" value of zero. Thus, all flows are included in the objective function with a desired value. This method was found to eliminate problems with singularity. These problems always converged; however, the estimated flows were often far away from the desired values. This undesired behavior can be explained as follows. By including all flows in the desired objective, we are treating all flows (measured and assumed to be zero) as equally important. Thus, the tradeoff often pushed measured flows down to zero as a compromise to measured levels and assumed zero flow levels. Because of the large deviations from the measure flows. This method is therefore not recommended.

3.2.3. Method 3 – Multi-objective optimization approach (recommended): Here we adopt a multi-objective optimization approach. We set the first goal of measured values with a high weight, for example, W = 10 000. Then set the second objective to avoid singularity with low weight, say w=1. Again, the objective function is designed to contain all nodes: Measured flows are set to the measured value of heavyweight (w=10 000), while all the remaining (unmeasured) flows are set to the desired value of zero with a low level of confidence (w=1). Again, all flows are included in the objective function but with different weights. These problems always converged without encountering singularity. Estimated flows were exactly equal to desired values in networks without singularity. Estimated flows were very close to the desired values in networks with singularities. **This method is recommended**.

3.3. Flow Estimation using Constrained Optimization: To set up the general multi-objective optimization solution, a least square model was chosen (eq. 6) as the objective function for which an equality constraint was set (eq. 7) enforcing the mass balance equations to be satisfied.

The objective function includes 2 least-square terms for accepting measurements as well as fraction terms of calculated flows as valid input. Lagrangian multipliers were introduced to merge the objective function and its constraint (eq. 8). This method produces a flow field which obeys to mass balance and will tend toward the flows prescribed in the $\bar{f}$ vector. Should the prescribed flows not allow for mass balance the mass discrepancy is reconciled by a compromise proportional to the weight of the prescribed flows. It is now possible to

express this function in matrix form and arrive at a general solution (eq. 9) for the design problem. The derivation of eq. 9 is stated in Appendix C.

Equation 9 is the Master objective function, it consists of 2 least-square terms – one is set up to seek the closest-to-prescribed flow values, the second allows to input partial flow inputs, the input doesn't have to be a number, but can be expressed as a fraction of a different flow. It is worth noting that fractional input is not required, if it is not used, the objective equation can be simplified to just one term as shown in eq. 9.

$$min.\ z(f) = \left[W_1\left(f - \bar{f}\right)\right]^T \cdot \left[W_1\left(f - \bar{f}\right)\right] + [W_2 \Delta M f]^T \cdot [W_2 \Delta M f] \tag{6}$$

To reconcile the flow discrepancies, the system is constrained with a nodal mass balance equality, this resolves to the total inflow/outflow balance to be equal.

$$s.t. \quad g(f) = C_1^T f = (I - D) \cdot C_1^T \cdot f + D \cdot \lambda_p = 0 \tag{7}$$

To access a general solution, the objective function and the constraint were combined into one Lagrangian function using the Lagrange multipliers.

$$\mathcal{L}(f, \lambda) = \left[W_1\left(f - \bar{f}\right)\right]^T \cdot \left[W_1\left(f - \bar{f}\right)\right] + [W_2 \Delta M f]^T \cdot [W_2 \Delta M f] + \lambda^T \left[(I - D) \cdot C_1^T \cdot f + D \cdot \lambda_p\right] \tag{8}$$

By deriving the equation and setting the derivation to zero, we access 2 equations, which were transcribed into matrix form (eq. 9). It is worth mentioning that the λ_p variable has been introduced by Professor Linninger as an elegant way of preserving the equation order by including *dummy equations* for preserving the otherwise removed boundary equations.

$$\begin{bmatrix} (\mathbf{2W_1^T W_1 + 2\Delta M^T W_2^T W_2 \Delta M}) & \boldsymbol{C_1(I - D)} \\ \boldsymbol{(I - D)C_1^T} & \boldsymbol{D} \end{bmatrix} \begin{bmatrix} \boldsymbol{f} \\ \boldsymbol{\lambda_p} \end{bmatrix} = \begin{bmatrix} \mathbf{2W_1^T W_1 \bar{f}} \\ \mathbf{0} \end{bmatrix} \tag{9}$$

3.4. Simplified equation for measurements only: The Master equation (eq. 9) contains all introduced methods, this implies that both flow measurements as well as outflow conditions (Visit section 3.6). For many cases, the use of the Master matrix form is disproportionate to the number of input types. When having only measurements, the equation can be simplified into eq. 10, which removes multiple variables.

$$\begin{bmatrix} \boldsymbol{2W^T W} & \boldsymbol{C_1(I - D)} \\ \boldsymbol{(I - D)C_1^T} & \boldsymbol{D} \end{bmatrix} \begin{bmatrix} \boldsymbol{f} \\ \boldsymbol{\lambda} \end{bmatrix} = \begin{bmatrix} \mathbf{2W^T W \bar{f}} \\ \mathbf{0} \end{bmatrix} \tag{10}$$

3.5. Flow optimization of non-constant flow: A standard flow optimization accepts an input of measured flows for single instant in time. This approach is suitable for stable systems, where one measurement is sufficient for the description of the flow. However, the volumetric flow in the neurovascular system is constantly changing because of the heart beating, this

system would require multiple measurements at different time instances to describe the flow. This method will be called *pseudo-dynamic* optimization.

3.6. Flow splitting: The flow splitting method is based on assigning outflow conditions dependent on morphological properties and Murray's law[6]. Dr. Park presented four different methods which can be interpreted as outflow splitting methods – Equal flow, outlet area ratio, outlet volume ratio, volume-to-end ratio[3]. Those methods were implemented as an additional objective function element in the form of a least-square error method.

3.7. Pseudo-dynamic flow optimization: Measured blood flows are waveforms representing the cardiac cycle, to estimate flows, it is inferred to have flow measurements for multiple time instances. To emulate a dynamic simulation, it is possible to estimate multiple consecutive time instances, this simplifies the solution to eq. 10, where the only input, that changes is the known flow vector with respect to time.

This method returns the flow values of every arbitrary time instance between the first and the last measurements. It is suitable to mention that this method is based solely on linear equations making this method a non-compute-intensive way of approximating dynamic methods.

$$\begin{bmatrix} (2\boldsymbol{W_1^T W_1} + 2\Delta\mathbf{M}^{\boldsymbol{T}}\boldsymbol{W_2^T W_2}\Delta\boldsymbol{M}) & \boldsymbol{C_1}(\boldsymbol{I}-\boldsymbol{D}) \\ (\boldsymbol{I}-\boldsymbol{D})\boldsymbol{C_1^T} & \boldsymbol{D} \end{bmatrix} \begin{bmatrix} \boldsymbol{f} \\ \boldsymbol{\lambda} \end{bmatrix}_{\boldsymbol{t}} = \begin{bmatrix} 2\boldsymbol{W_1^T W_1}\bar{\boldsymbol{f}} \\ \mathbf{0} \end{bmatrix}_{\boldsymbol{t}} \tag{11}$$

3.8. Estimating pressure with known flows and resistances: To calculate the pressure from flows, the Hagen-Poiseuille law can be used – The product of *flow resistance* and the *flow value* is equal to the *pressure drop* along that vessel. The resistance is calculated beforehand from the vessel diameter and length.

The flow optimization method is based on enforcing nodal mass balances, the flows are simultaneously ensured to be as close to the entered measurements thanks to the minimal least square error objective. By following those objectives, the system returns appropriate results, but when simulating networks, the calculations can be based on the Hagen-Poiseuille law (eq. 12) – The product of *flow resistance* and the *flow value* is equal to the *pressure drop* along that vessel.

By optimizing the flow measurements, we have already enforced the mass balance condition, the resistance can be calculated from the vessel's properties. This statement implies that if we know at least one pressure, we can derive a formula for calculating pressures, which satisfy the Hagen-Poiseuille law (eq. 13). Full deduction of eq. 13 can be found in Appendix D.

$$A \cdot f = C_1 \cdot p \tag{12}$$

$$\boldsymbol{p} = \left[(\boldsymbol{I} - \boldsymbol{D})\boldsymbol{C_1^T C_1} + \boldsymbol{D}\right]^{-1} \cdot \left[(\boldsymbol{I} - \boldsymbol{D})\boldsymbol{C_1^T A}\bar{\boldsymbol{f}} + \boldsymbol{D}\bar{\boldsymbol{p}}\right] \tag{13}$$

3.9. Adjusting Non-Physiological Inferred Flows in Added Source/Sink Terms: It is valuable to examine the flow present in the source and sink terms added to these networks, as in some cases the flows estimated in these regions provide insight into difficult to measure areas of the brain. For instance, a sink term added to the BA represents the flow in the pre-pontine arteries. The pre-pontine arteries supply blood to the pontine which is a critical region of the brain. However, in some cases the flows predicted in these added side draws do not exhibit the expected systolic-diastolic cycle that would be expected.

This is corrected by taking the original signal estimated in that region, removing the non-physiological portion of the signal, and then interpolating the absent portion of the signal with a more accurate representation of the systolic diastolic cycle. The newly generated flow is then prescribed to the side draw and the estimation is then reperformed and examined.

3.10. Summary on assigning confidence levels to input: This section is a summary of guidelines on what confidence levels to assign for various input information. A brief summary can be found in Table 7.

Table 7 –Summary of Confidence levels commonly used in the estimation methods.

Confidence level	Description
0.00	Used for unknown values, **not recommended**
0.10	Used for unknown values
1.00	Used for input with minor significance
100.00	Used for input for major significance

3.10.1. Confidence level "0": Confidence level "0" is the basic form of noting, that this flow, pressure or other input type is not known. When this confidence level is assigned, the potential change in value throughout the estimation will not have any effect on the least square error, this means that this value can be changed arbitrarily. This confidence level can be used either, when only a few measurements are known, or if the network is very small. This confidence level input **is not** recommended, because when being used on a bigger network, the Master matrix may turn **singular**.

3.10.2. Confidence level "0.01": Confidence level "0.01" is similar to confidence level "0". It is used in the same scenarios as confidence level "0", the main difference is that it bypasses the plausible singularity, thus bigger and more complex networks can be estimated. This confidence level has to be used with caution, even though an error would occur while inputting data, the system will most likely simulate and return invalid data. This confidence level is not the specific number, but rather the representation of a close-to-zero number.

3.10.3. Confidence level "1": Confidence level "1" is the base level for measurements, this level is assigned to known values, which have no major significance for the input data set and can be changed throughout the estimation procedure.

3.10.4. Confidence level "100": Confidence level "100" is a high confidence information, which cannot be changed throughout the estimation process. This weight is assigned on highly precise measurements. This confidence level is not exactly "100", but rather a great value number. This number can be greater or smaller, than "100", but in practice numbers above 100 guarantee the enforcement of the data input.

Results

3.11. Flow estimation of nw3_bifurcation with one flow assigned: This network has been created as a variation of NW1Bioe532 to understand the basic behavior of flow optimization. The case study has been given to me by Professor Linninger, his notes to the following case studies can be found in Appendix E. To observe the behavior of this case study, only the inlet flow value of 100 has been assigned. By changing the confidence level of the inflow, decreasing deviation from the assigned value can be observed. It is worth mentioning that due to only assigning one value, the calculation would be singular. This was bypassed by setting the non-assigned flow values confidence levels to a close-to-zero value instead of absolute zero.

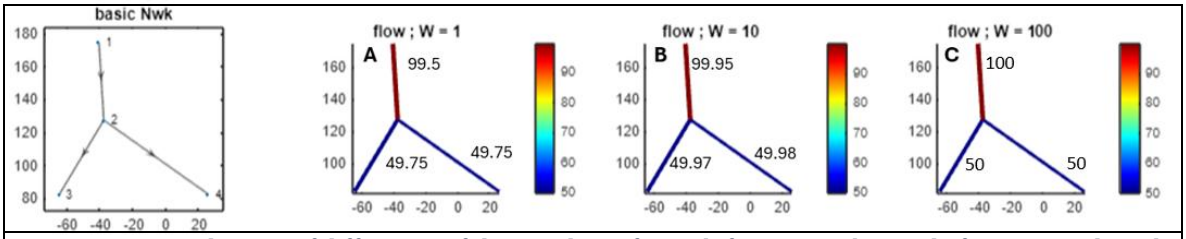

Figure 14 – Visualization of different confidence values of nw3_bifurcation, where only f1 is assigned. Nwk name: nwk_0.fMx; code: FlowEstimation_AutomaticBC_v4.m

Table 8 – Confidence levels, assigned and calculated values for nw3_bifurcation.

Flow	Desired [ml/min]	W^A	$Flow^A$ [ml/min]	W^B	$Flow^B$ [ml/min]	W^C	$Flow^C$ [ml/min]
1	100	1	99.50	10.0	99.95	100.0	100
2	0	0.1	49.75	0.1	49.97	0.1	100
3	0	0.1	49.75	0.1	49.97	0.1	100

3.12. Flow optimization of nw3_bifurcation with a flow discrepancy: This case study is an entrance model for real-life situations. In neurovascular imagery, the image resolution is fairly limited resulting into the illusion of disappearing mass (e.g. total inlet equal to 100 ml/min, total outlet equal to 90 ml/min). This case study has been assigned flow values, which do not satisfy the total inflow/outflow equality, this will showcase, how the estimation method results the discrepancy and returns values, which satisfy the mass balance.

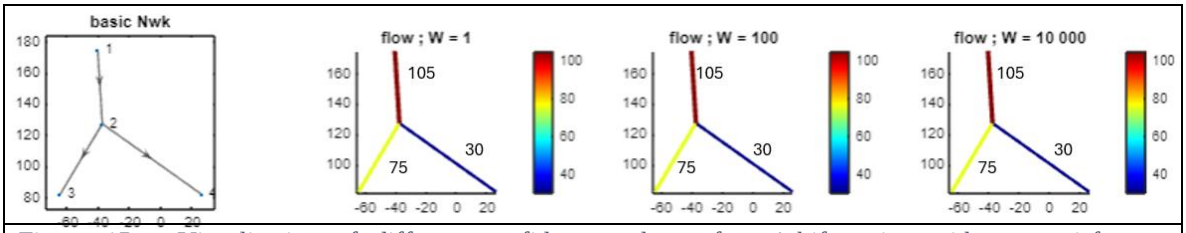

Figure 15 – Visualization of different confidence values of nw4_bifurcation with non-satisfactory inflow/outflow mismatch. Nwk name: nwk_0.fMx; code: FlowEstimation_AutomaticBC_v4.m

Table 9 – Confidence levels, assigned and estimated flows for nw3_bifurcation with a flow discrepancy.

Flow	Assigned [ml/min]	W^A	$Flow^A$ [ml/min]	W^B	$Flow^B$ [ml/min]	W^C	$Flow^C$ [ml/min]
1	100	1	105	100	105	10 000	105
2	80	1	75	100	75	10 000	75
3	35	1	30	1.0	30	1.000	30

3.13. Calculating missing flows of a network – NW1Bioe532: The flow optimization method is set up such a way that when enough flows are measured, the optimization can be used as a flow calculator, the flows will be calculated from the mass balance equations. For this example, network NW1Bioe532 was used.

3.13.1. Expected results: Three flows were assigned. Due to the system having enough degrees of freedom, the estimation will resolve the missing flows of the network.

3.13.2. Actual results: The system behaved as predicted, the non-assigned flows were calculated without changing the flows we assigned.

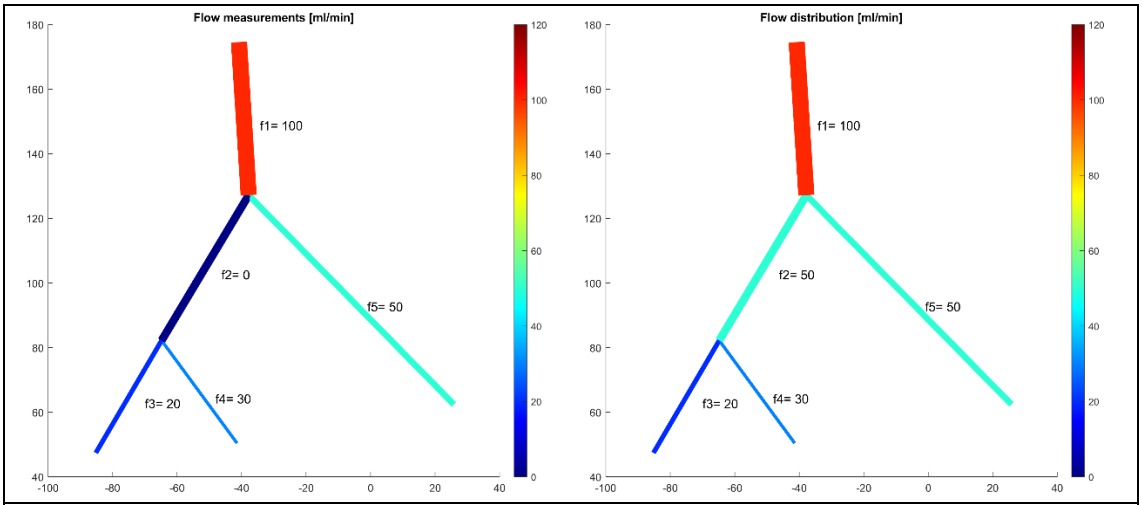

Figure 16 – Visual representation of the measured and estimated flows of the NW1Bioe532 with a satisfactory flow equality. Nwk name: NW1Bioe532.fMx; code: FlowEstimation_AutomaticBC_v4.m

Table 10 – Confidence levels, assigned and estimated flows of base NW1Bioe532.

Flow index	f1	f2	f3	f4	f5
Input value	100	0	20	30	50
Confidence value	1	0	0	1	1
Calculated flow	100	50	20	30	50

3.14. Flow optimization with mass balance error – NW1Bioe532: This flow optimization method accepts input values that do not satisfy the total inflow/outflow equality. This case study will be based on the previous NW1Bioe532 case study results. The results were altered to introduce the flow discrepancy.

3.14.1. Expected results: Every flow has been assigned a value, the total inflow is 100 ml/min, total outflow is 94 ml/min. Further, this system is fully defined – no degrees of freedom are available. This fact implies, that the flow estimation will have to change the assigned values to a certain point. The prediction is that the outflow values will be increased and the inflow values will be decreased. All confidence levels are equal – the total change of flows will be distributed throughout all flows equally.

3.14.2. Actual results: The system behaved as expected, the assigned outflow was lower than it had to be, so the total outflow was increased, and the total inflow was decreased. After the flow change, the total inflow/outflow equality is satisfied.

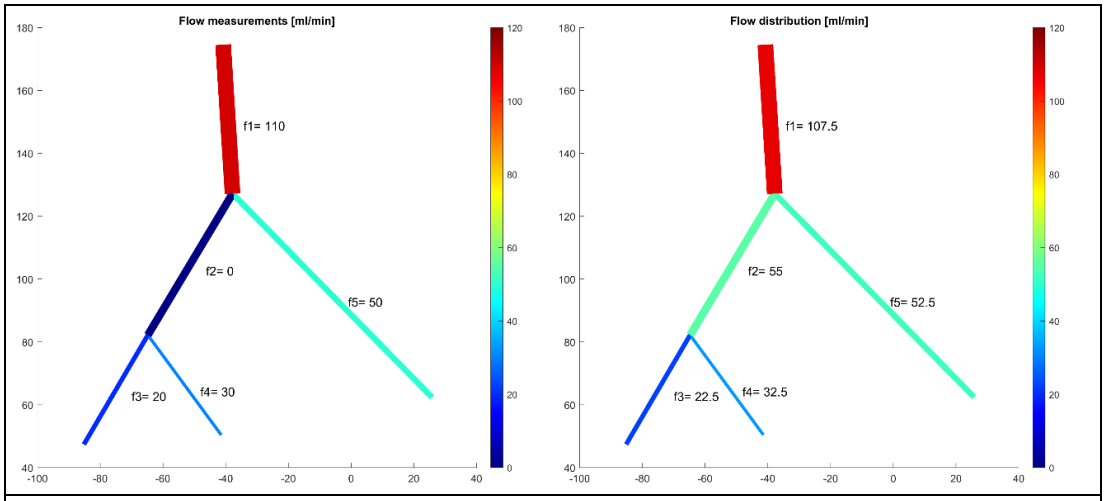

Figure 17 – Visual representation of the measured and estimated flows of the NW1Bioe532 with a flow discrepancy. Nwk name: NW1Bioe532.fMx; code: FlowEstimation_AutomaticBC_v4.m

Table 11 – Confidence levels, assigned and estimated flows of NW1Bioe532 with a flow discrepancy.

Flow index	f1	f2	f3	f4	f5
Input value	110	0	20	30	50
Confidence value	1	0	1	1	1
Calculated flow	107.5	55	22.5	32.5	52.5

3.15. NW1Bioe532 estimation with weighted measurements: The estimation method has the ability assign different confidence values to specific values. This allows the estimation to preserve values with a high confidence level and if necessary, change measurements with a high confidence. In Figure 18, it is apparent that by increasing the confidence level of flow 1, the deviation is marginal, when compared to the previous case study.

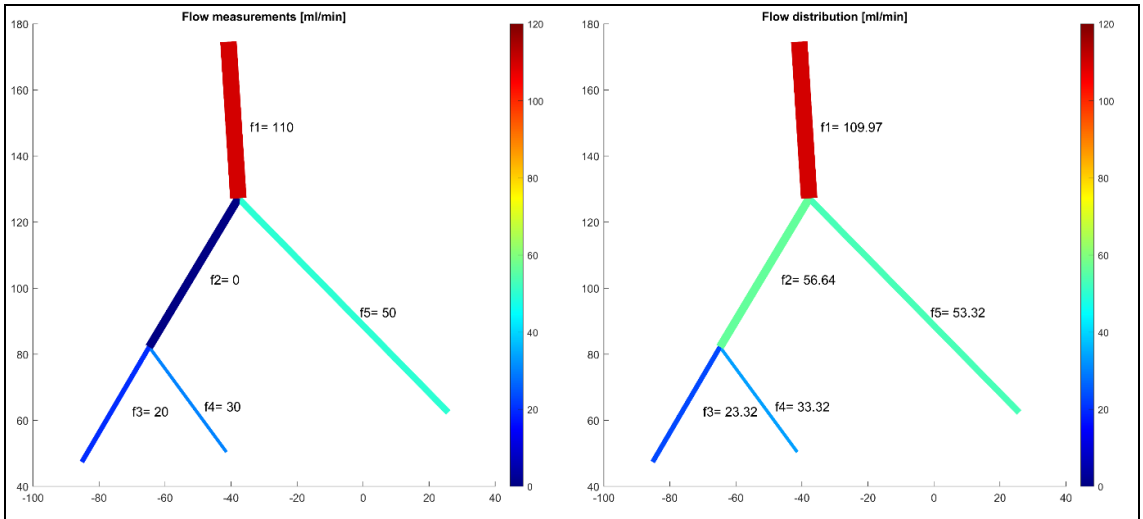

Figure 18 – Visual representation of the measured and estimated flows of the NW1Bioe532 with a flow discrepancy, the inflow and one of the outflow's confidence level has been increased. Nwk name: NW1Bioe532.fMx; code: FlowEstimation_AutomaticBC_v4.m

Table 12 – Confidence levels, assigned and estimated flows of NW1Bioe532 with a flow discrepancy and the inflow confidence level increased.

Flow index	f1	f2	f3	f4	f5
Input value	110.0	0.00	20.00	30.00	50.00
Confidence value	10.0	0.00	1.00	1.00	1.00
Calculated flow	109.9	56.64	23.32	33.32	53.32

3.16. NW1Bioe532 estimation with an inferred flow: The estimation method accepts multiple data types, up until now, only explicit flow measurements were demonstrated. The following case study is going to demonstrate the inferring of a flow. This type of input can be used to infer non-measurable vessels by multiplying the parent flow with the cross-section ratio of the parent and daughter vessels

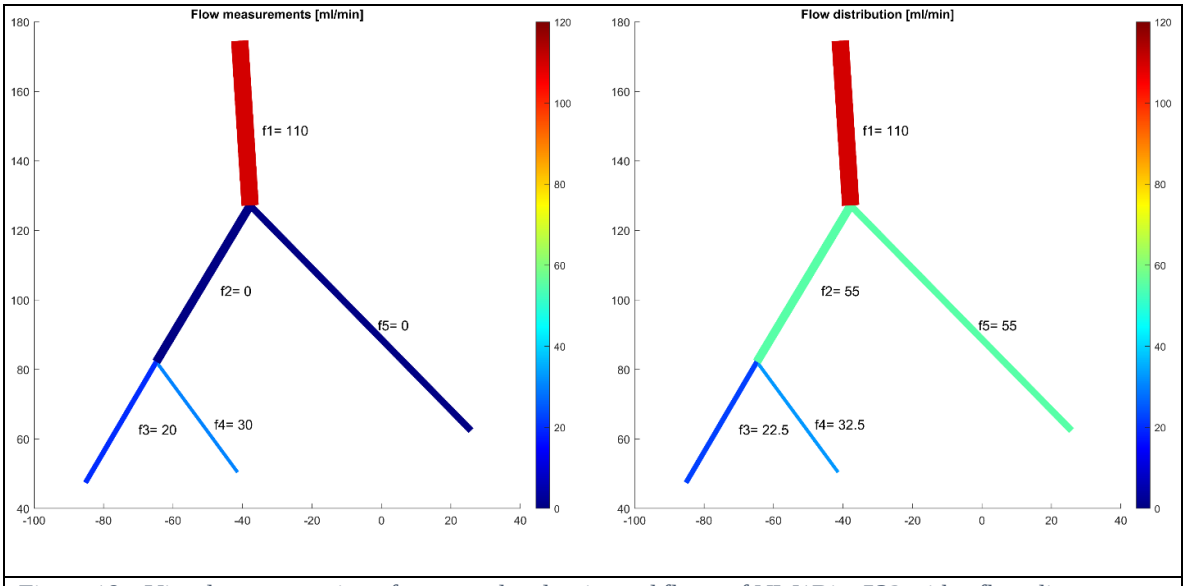

Figure 19 – Visual representation of measured and estimated flows of NW1Bioe532 with a flow discrepancy, multiple confidence levels increased and an inferred flow. Nwk name: NW1Bioe532.fMx; code: FlowEstimation_AutomaticBC_v4.m

Table 13 – Confidence levels, assigned and estimated flows of NW1Bioe532 with a flow discrepancy, several flow confidence levels increased and an inferred flow.

Flow index	f1	f2	f3	f4	f5
Input value	110	0	20.0	30.0	0.5f1
Confidence value	100	0	1.0	1.0	100
Calculated flow	110	55	22.5	32.5	55

3.17. NW1Bioe532 Oscillatory flow estimation: This case study expands on the NW1Bioe532 model, by introducing flow measurements that vary in time, it is possible to estimate a pseudo-dynamic case study. As seen in Figure 20, the measurements have a flow discrepancy. By estimating the network flows, it was possible to reconcile this discrepancy, but at the cost of devaluating the measurements, which is not desired.

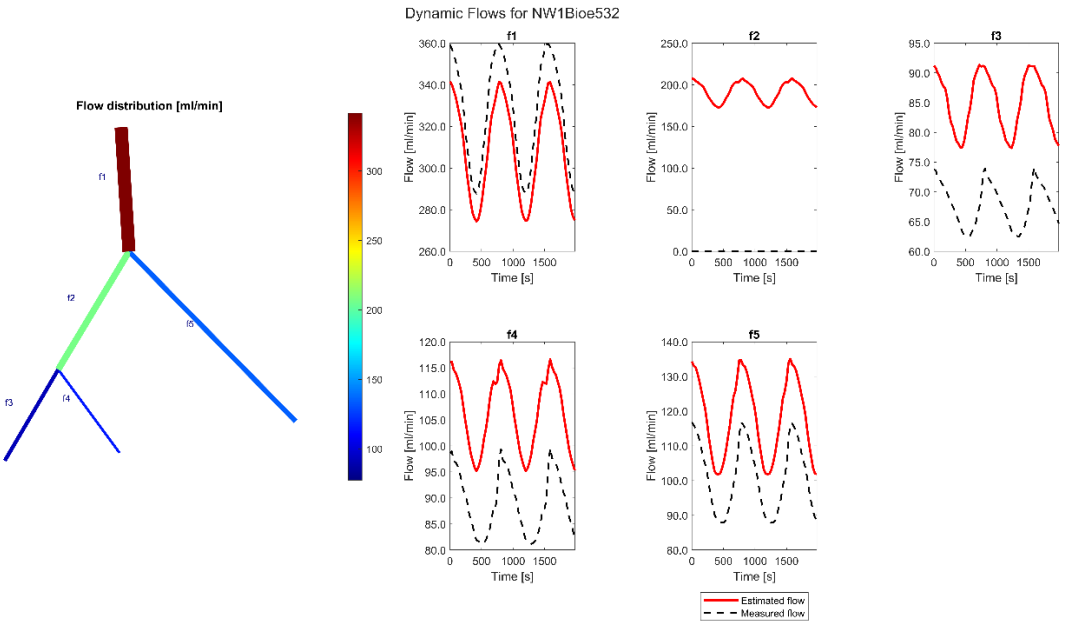

Figure 20 – Oscillatory flow estimation of NW1Bioe532. Nwk name: nwk_0.fMx; code: DynOptDemo.m

3.18. NW1Bioe532 Oscillatory flow estimation with side draws: This case study expands on the previous one. This case study will demonstrate that it is of great importance to have anatomically accurate networks. Due to this network being fictional, lets assume it to be a real neurovascular system, which is incomplete. In the previous case study, there was a flow discrepancy, the claim here is, that the discrepancy was caused by not including the full network, thus one or more outflows are not considered which causes the discrepancy. To test this hypothesis, another vessel will be added to the network, fulfilling the system and resolving the discrepancy.

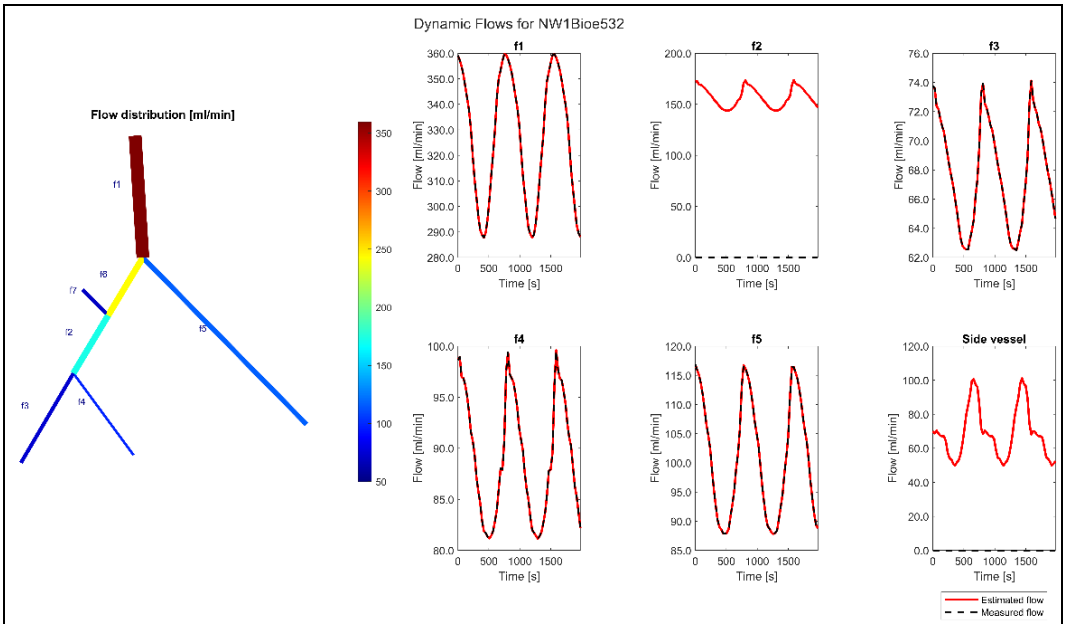

Figure 21 – Oscillatory flow estimation of NW1Bioe532 with a side vessel. Nwk name: NW1Bioe532.fMx; code: DynOptDemo.m

3.19. Circle of Willis flow estimation: To demonstrate, how the estimation method handles bigger networks, this case study will demonstrate the flow estimation of a Circle of Willis (CoW) network. The network is made up of 109 faces, the main in/outflows have been measured resulting into 9 measurements. This case study does not have a discrepancy, resulting into a simple quasi-simulation of the flow distribution. Dr. Park and Dr. Charbel's measurements[3] have been used as user input.

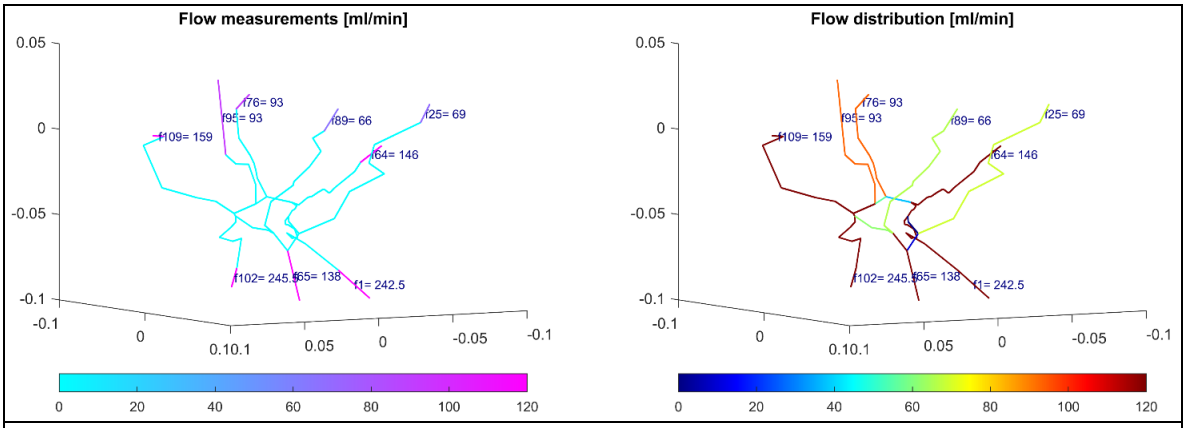

Figure 22 – Visual representation of measured and estimated flows of the Circle of Willis. Nwk name: CoW_simple1.fMx; code: FlowEstimation_AutomaticBC_v4.m

3.20. Circle of Willis estimation with a discrepancy: The following case study is going to demonstrate the flow estimation of the CoW, unlike the previous case study, this contains a

flow discrepancy. By estimating the network, how it currently is, the estimation method has altered the measurements, devaluating them.

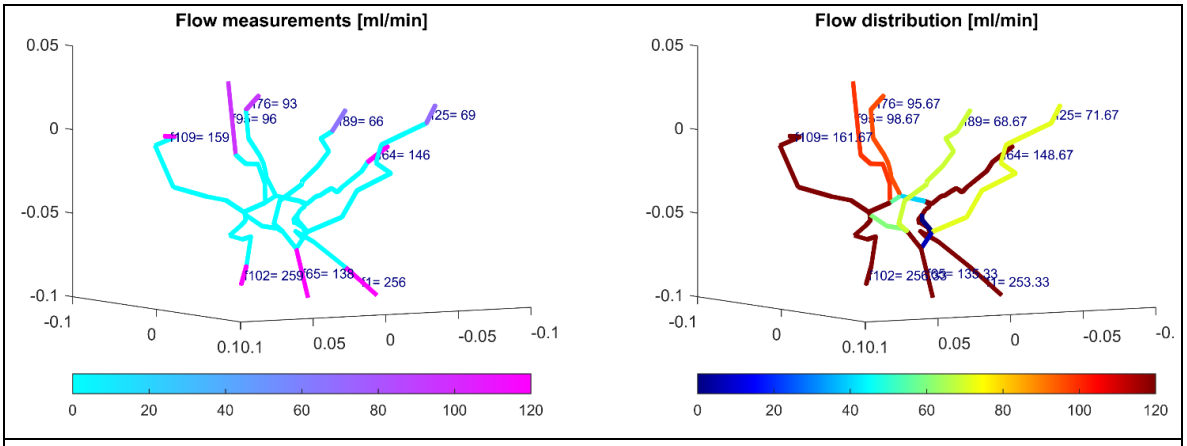

Figure 23 – Visual representation of measured and estimated flows of the Circle of Willis including a flow discrepancy. Nwk name: CoW_simple1.fMx; code: FlowEstimation_AutomaticBC_v4.m

3.21. Circle of Willis estimation with side draws: The flow discrepancy in the previous case study has been caused by the vessels not recognized by the measurement device (MRI, or different measurement method). The proposal of this research is that by adding those vessels to the network and inferring the flow as the ratio of cross-sections, the flow in the side vessels will be anatomically correct. In Figure 24, the same boundary conditions as in the previous case study were used. It is apparent that the measured flows have not been altered, also anatomically correct side vessel's flows have been acquired.

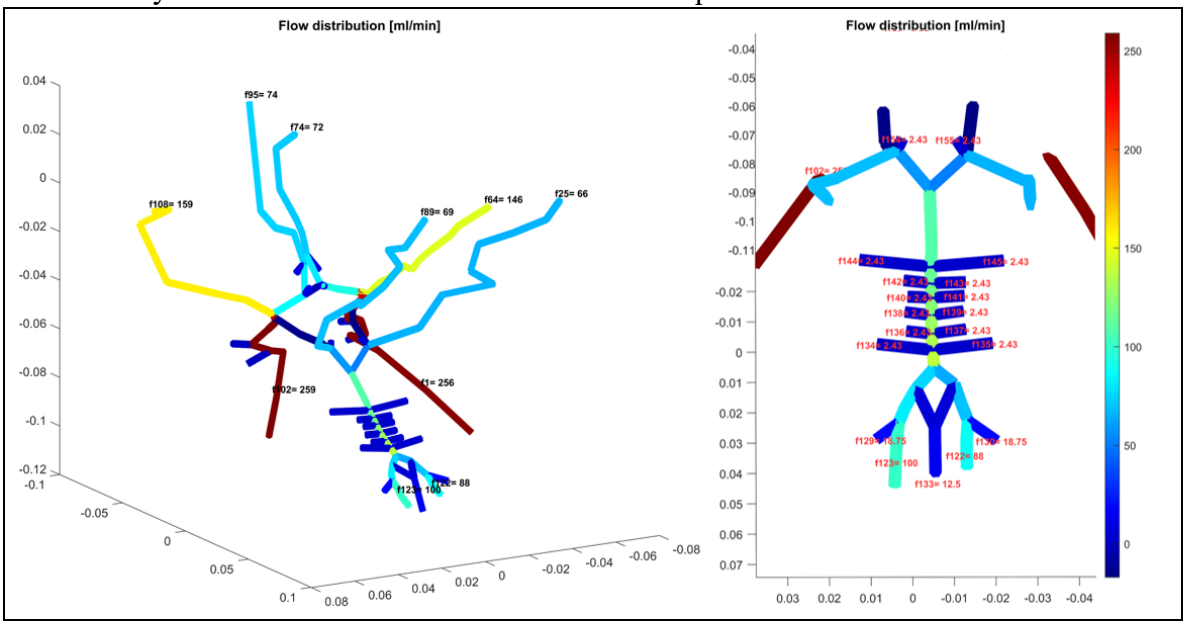

Figure 24 – Visual representation of estimated flows of the Circle of Willis with anatomically correct side vessels, including a detail on flows in the Pontine and Cerebellar arteries. Nwk name: CoW_Aug.fMx; code: FlowEstimation_AutomaticBC_v4.m

3.22. Circle of Willis Pressure estimation: The results of the pressure estimation show that the pressure at the inlet nodes is higher than the outlet nodes, which meets the anatomical behavior if the pressure distribution. The pressure distribution is almost symmetrical with light deviations due to slight differences in diameter. In the Right MCA there is a larger pressure drop, this is caused by the diameter being significantly smaller than the Left MCA.

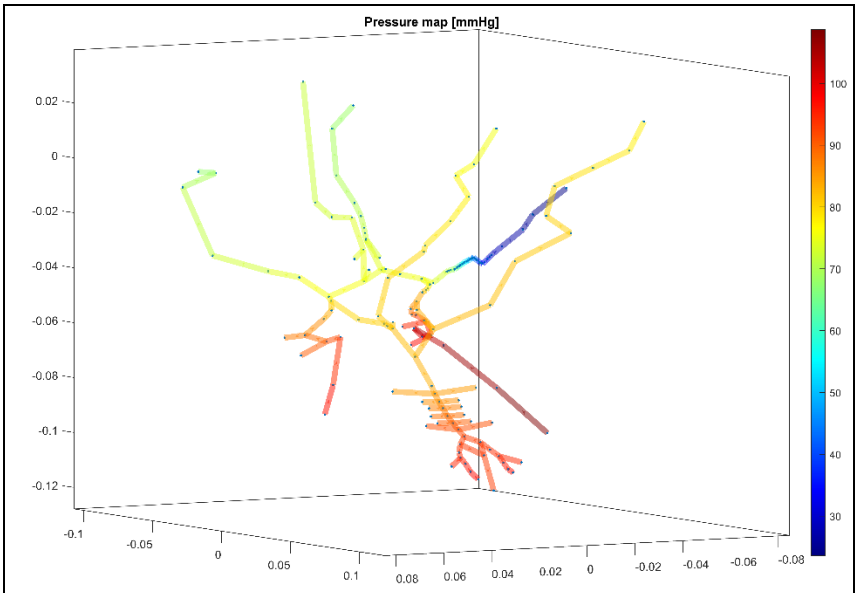

Figure 25 – Pressure map of the Circle of Willis with anatomically correct side vessels.Nwk name: CoW_Aug.fMx; code: FlowEstimation_AutomaticBC_v4.m

Chapter 4 – Implementation

Summary

This Chapter is a summary of the various boundary conditions for the Flow simulation, stationary and oscillatory estimation methods. Every type of boundary condition has been briefly defined, and all user inputs have been explained.

Methods

4.1. Summary of flow and pressure simulation user inputs: This section is a summary of input assignment for flow and pressure simulations using the Hagen-Poiseuille equation. The **Dirichlet** boundary condition is very easy to get a grasp, the pure Dirichlet BC should be used by novices due to its simplicity. The **Neumann** boundary condition is an intermediate boundary condition because of its counterintuitive behavior – the flow value is assigned to a specific node. The user has to think of it like flow flowing through a node, instead of a flux value. The fact that you must specify if the flow is flowing into or out of the node justifies the intermediate difficulty. The **Source and Sink** terms can be stated for any internal node, if the term is positive, mass is added to the system, and if negative, mass is removed from the system.

4.2. Summary of stationary flow and pressure estimation user inputs: This section is a summary of input assignment for flow and pressure estimations using the multi-objective constrained estimation method. The **flow measurement** input is the target value the flow estimation method aims towards. If the system has no flow discrepancy, the method estimates the flow distribution without altering the flow measurements. If the assigned flows have a flow discrepancy, the method either resolves the discrepancy at non-assigned terminal faces or deviates from the assigned measurements. The **Pressure measurement** input is at least one measurement, which will resolve all Hagen-Poiseuille equations and calculate all pressures of the network. The **Inferred flow** is a boundary condition, which enables to express a flow by referring to a target flow. The inferred flow option can refer to any flow in the network.

4.3. Summary of oscillatory flow and pressure estimation user inputs: The oscillatory **Flow measurements** data type is a file containing flow measurements for multiple time instances. The file contains two columns, the column on the left contains time [s] starting from zero. The column on the right contains corresponding flow values. The **Pressure measurements** data type is identical to the flow measurements data type, with the exception, that instead of flow values, it contains pressure values. The **inferred flow** is identical to the stationary data type.

Table 14 – Summary of BC and BCopt file input types; Stat. – Stationary; Osc. – Oscillatory

	Boundary type	Concept	Index	Input
Simulation	Dirichlet condition	Pressure at terminal nodes	1	Scalar
	Neumann condition	Flux through ext. node	2	Oriented scalar
	Source term	Additional inflow at int. node	3	Positive scalar
	Sink term	Additional outflow at int. node	3	Negative scalar
Estimation	Stat. flow measurement	Fux at face	102	Oriented scalar
	Stat. Pressure measurement	Pressure at terminal nodes	101	Scalar
	Stat. Inferred flow	Fraction of target flow	103	Multiple of target flow
	Osc. Flow measurements	Flux at face	1002	Measurement file name
	Osc. Pressure measurements	Pressure at ext. nodes	1001	Measurement file name
	Osc. Inferred flow	Fraction of target flow	103	Multiple of target flow

Results

4.4. BC file for Section 2.12– NW1Bioe532: This case study has been defined by one pressure at node 1 and 3 flows at face 1,3 and 4. It is crucial to assign the values as negative, if the target node is an outflow node.

4.5. BC file for Section 2.14 – NW1Bioe532: This case study has been defined by three pressures at nodes 1, 4, 5 and 6. The network was also assigned a **Source** term, resulting in additional 50 ml/min being supplied at node 2.

Table 15 – BC file for the standard flow and pressure simulation of NW1Bioe532 – Section 2.12.

NW1Bioe532 – Standard simulation		
Node	Type	Value
6	1	90
1	2	6
4	2	-1
5	2	-2

Table 16 – BC file for the standard flow and pressure simulation of NW1Bioe532 – Section 2.14.

NW1Bioe532 – Simulation with source term		
Node	Type	Value
1	1	90
4	1	50
5	1	40
6	1	20
2	3	50

4.6. BCopt file for Section 3.15 – NWIBioe532: This case study has 3 flow measurements of face 1, 3 and 4. Flow 5 has not been measured, but can be inferred from face 1, the cross-section ratio between face 5 and face 1 equals 0.5. Input values for face 1 and 5 have an increased confidence level.

4.7. BCopt file for Section 3.16 – Oscillatory NW1Bioe532: The BCopt file for the oscillatory NW1Bioe532 has three flow measurements for faces 1, 3 and 4. Flow 5 does not have any measurements but can be inferred from flow 1. The cross-section ratio between flow 5 and 1 is equal to 0.39. All data inputs have a high confidence value.

Table 17 – BCopt file of the stationary NW1Bioe532 flow estimation. Conf – Confidence level; Multi – Multiplier.

NW1Bioe532 – St. Inferred flow				
Face	Type	Conf.	Multi	Value
1	102	100	1.0	100
2	102	0	1.0	0
3	102	1	1.0	20
4	102	1	1.0	30
5	103	100	0.5	1

Table 18 – BCopt file of the Oscillatory NW1Bioe532 flow estimation. Conf – Confidence level; Multi – Multiplier.

NW1Bioe532 – Dyn. Inferred flow				
Face	Type	Conf.	Multi	Value
1	1002	100	1.00	f1
3	1002	100	1.00	f3
4	1002	100	1.00	f4
5	103	100	0.39	1

Chapter 5 – Applications of the Flow estimation method on Subjects 58 and 64

Summary

This section is dedicated to showcasing the oscillatory estimation method on two real patients – S58 and S64. For S58, the arterial tree was estimated both stationary and oscillatory. By estimating the network without side vessels, the measurements have been devaluated because of the anatomical inaccuracy. Side vessels have then been added after estimating, the discrepancy has been reconciled and anatomically correct flows in side-vessels have been acquired. To showcase the flexibility of the estimation method, a showcase of prescribing flow in the pre-Pontine arteries has been done next to estimating the pressure from one pressure measurement. Further, the venous backbone with and without side vessels has been estimated both stationary and oscillatory. The macro-tree – venous tree with much more vessels than the backbone, has also been estimated. For both For S64's arterial tree and the venous tree backbone, the flows and pressures for the arterial tree have been estimated with and without side vessels, stationary and oscillatory.

Methods

The following section is an extraction of measurement data of Subjects 58 and 64, a more detailed description of the measurement techniques can be found in Section 1.7-1.10.

5.1. NOVA flow report of Subject S58: The NOVA report of subject 58 (S58) presents for all main Veins and Arteries of interest, in Figure 26 there is a depiction of all planes, where S58's measurements were taken. The NOVA table of flows can be found in Appendix B.

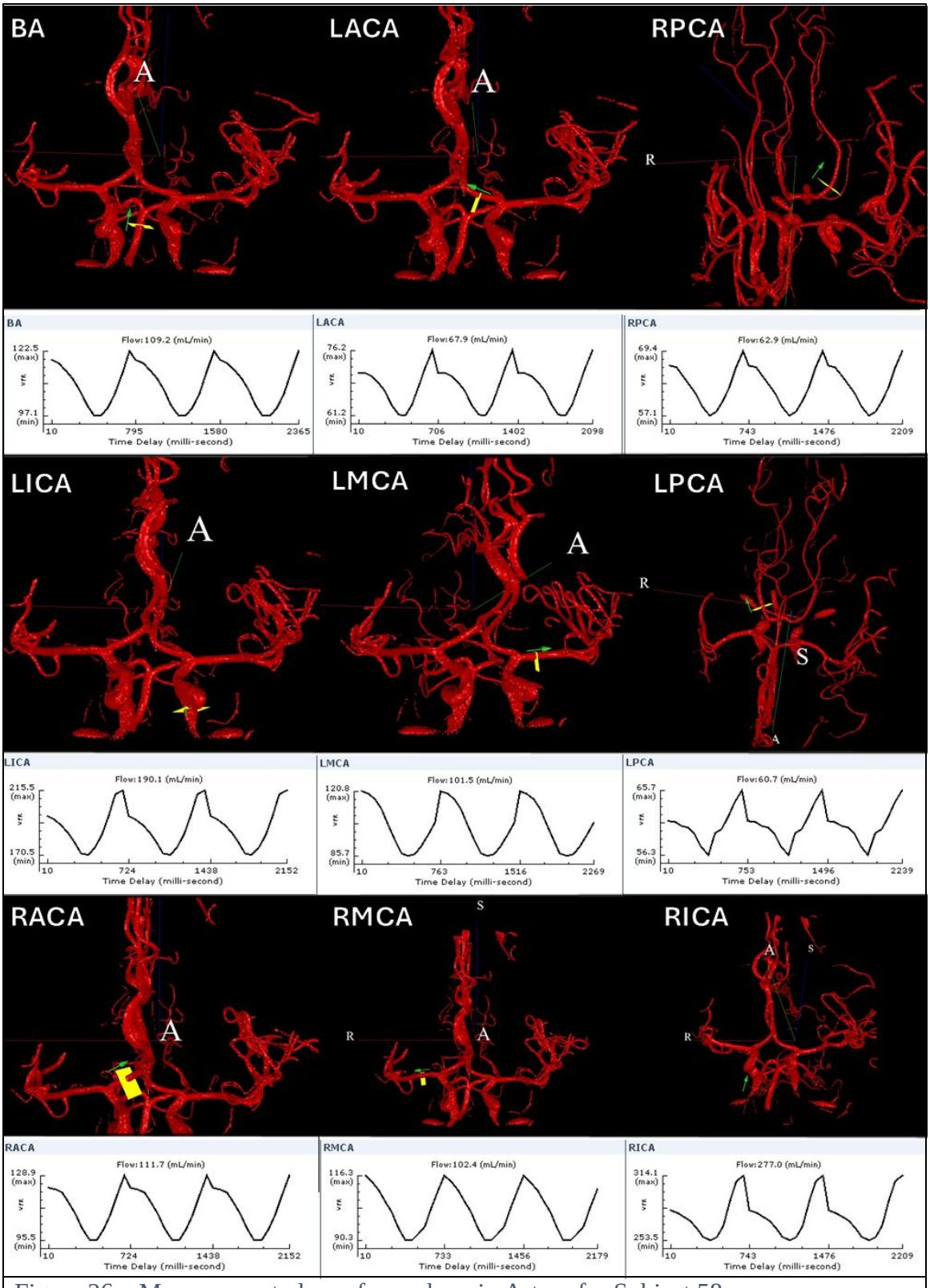

Figure 26 – Measurement planes for each main Artery for Subject 58.

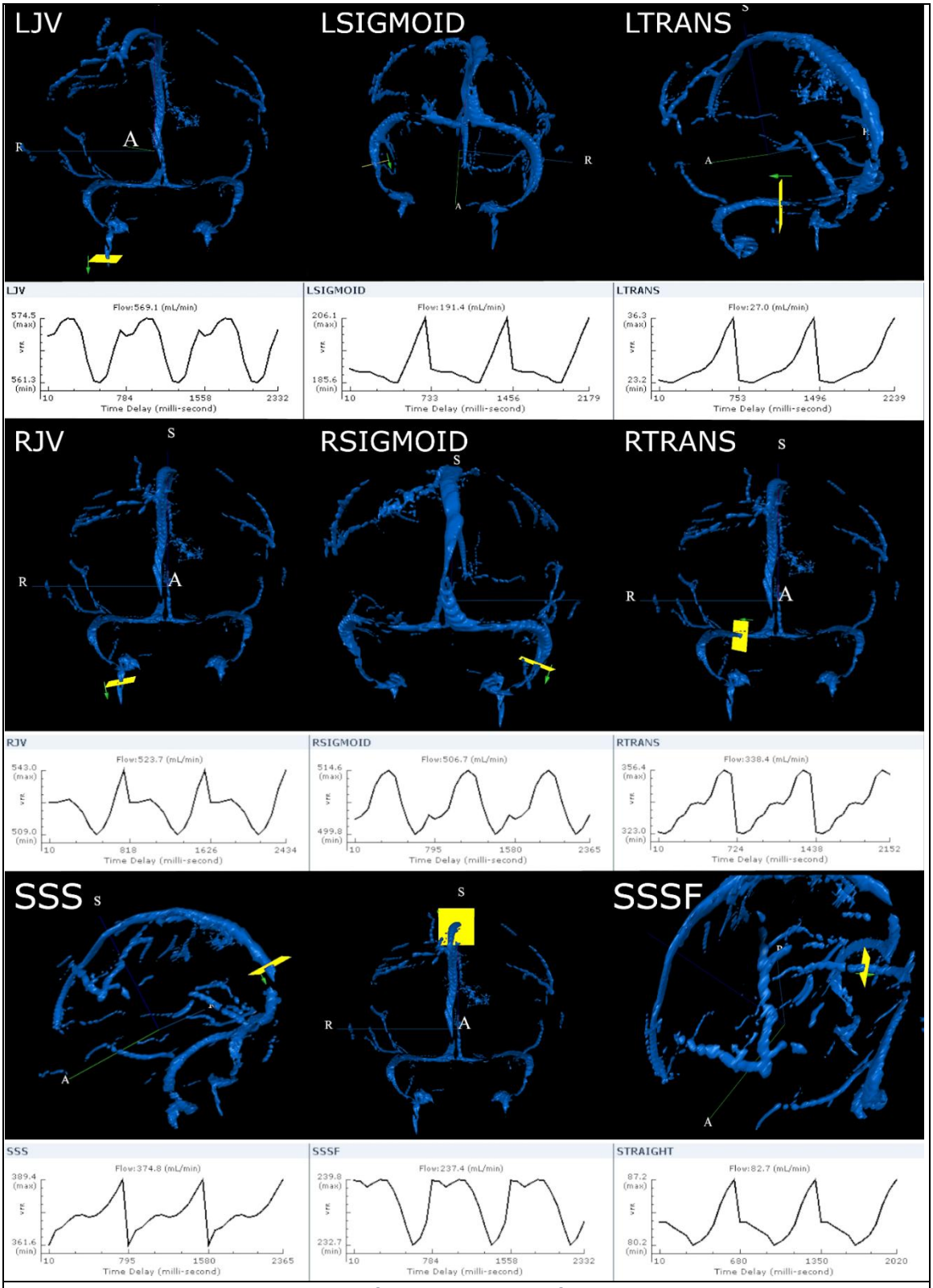

Figure 27 – Measurement planes of each main Vein for Subject 58.

5.1.1. Measurement analysis of Artery measurements for S58: As seen in Figure 28, all main arteries in the arterial tree backbone were measured. After inspecting all the main inlets and outlets, it is obvious that the average inflow from the ICAs and the BA results in 576 ml/min and the average outflow from the PCAs, MCAs and the ACAs results in 504 ml/min. The measurements contain an average flow discrepancy of 72 ml/min, which is 12.5 % of the total inflow. This discrepancy can vary throughout the systolic-diastolic cycle, the statement that this discrepancy has been caused by the measurement inaccuracy would be false. This thesis proposes that those discrepancies are caused by vessels that draw blood from the main arteries, this effect cannot be measured by modern technology.

5.1.2. Measurement analysis of Vein measurements for S58: The procedure of the analysis of the Venous tree backbone are identical to the Arterial tree backbone. The total inflow from the Superior Sagittal Sinus (SSS) and the Straight Sagittal Sinus (STRAIGHT) result in a total average inflow of 458 ml/min, the total average outflow from the Jugular veins results in a total average outflow of 1093 ml/min, this discrepancy is caused by the Superior, Inferior Petrosal and other feeds.

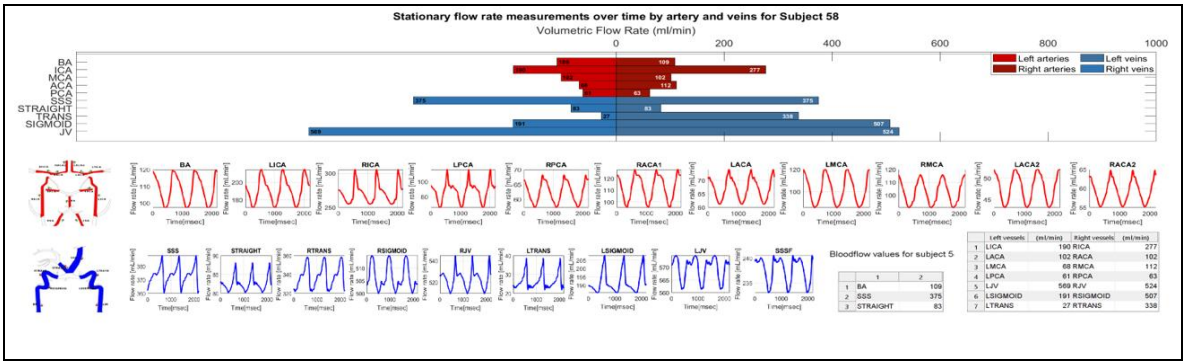

Figure 28 – Visual representation of the NOVA report for S58 as stationary values. For all measured arteries and veins the systolic-diastolic cycle was presented, all artery measurements are depicted as red, all vessels are depicted as blue. Further a bar graph is presented to compare the left and the right variation of vessels, if a vessel does not have a symmetric counter vessel (such as the Basilar artery), the flow value on both left and right side are equal in the graph.[5]

5.2. NOVA flow report of Subject S64: The NOVA report of subject 64 (S64) presents for all main Veins and Arteries of interest, in Figure 29 there is a depiction of all planes, where S58's measurements were taken. The NOVA table of flows can be found in Appendix A.

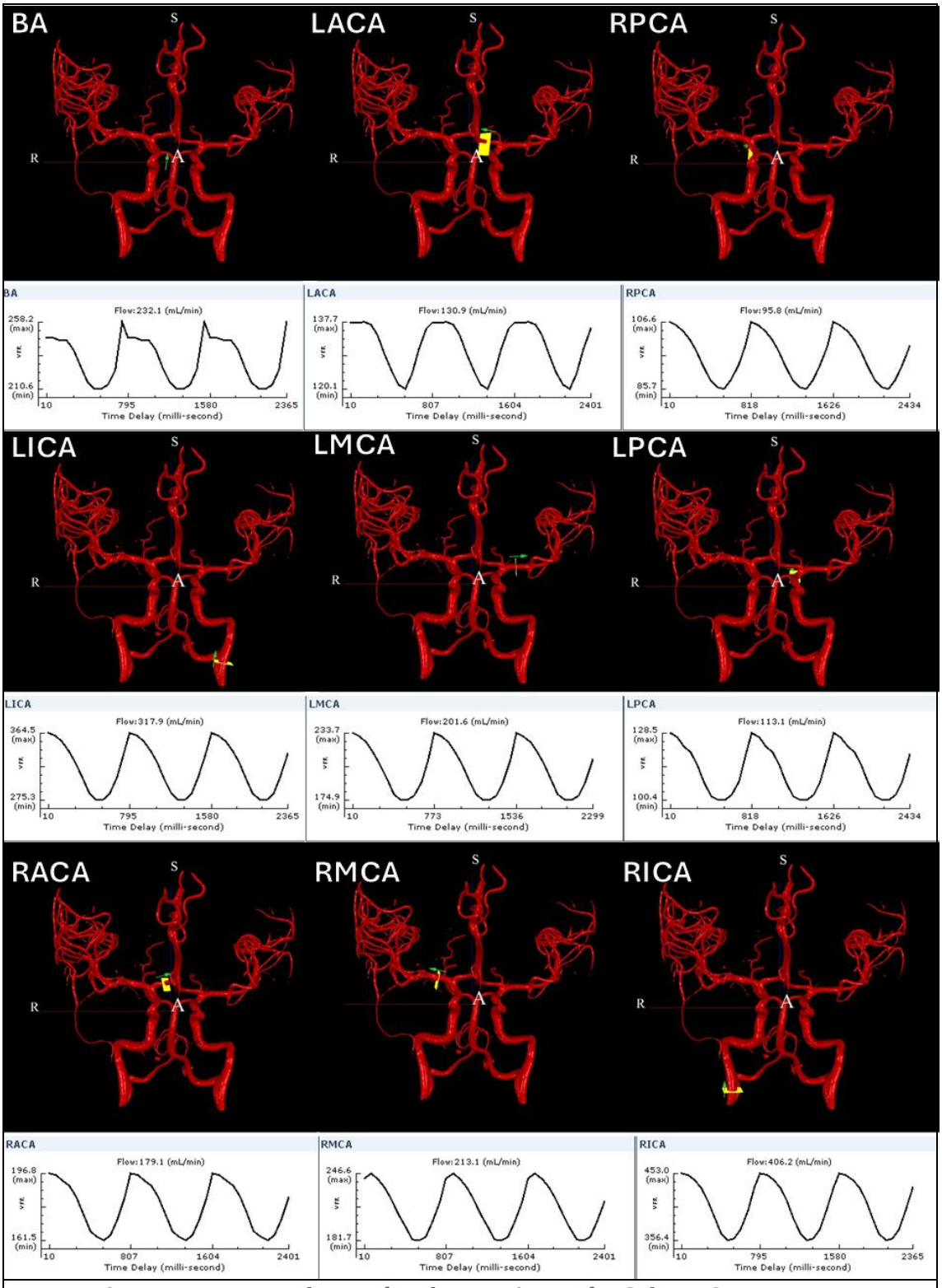

Figure 29 – Measurement planes of each main Artery for Subject 64.

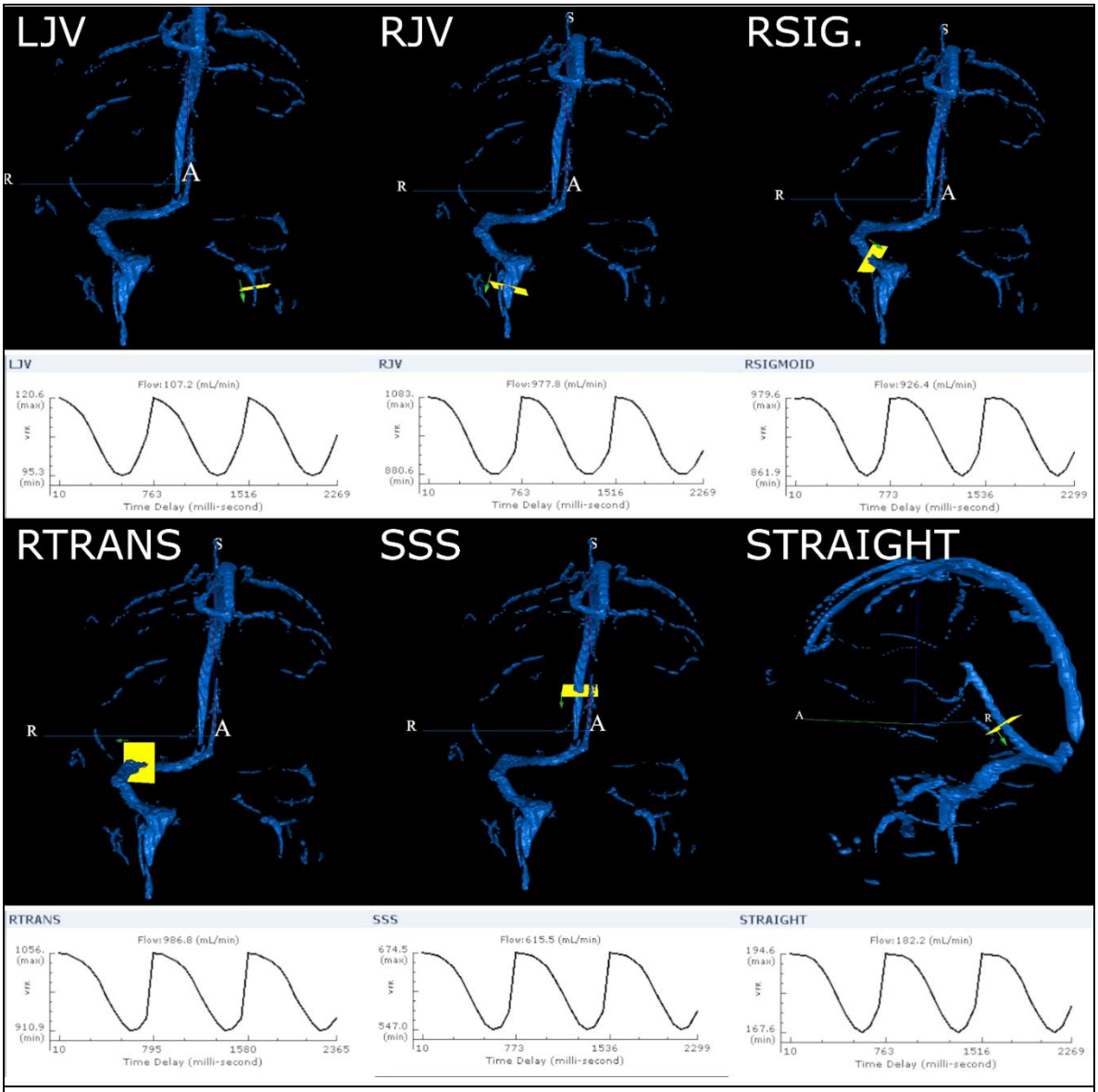

Figure 30 – Measurement planes of each main Vein for Subject 64.

5.2.1. Measurement analysis of Artery measurements for S64: As seen in Figure 31, all main arteries in the arterial tree backbone were measured. After inspecting all the main inlets and outlets, it is obvious that the average inflow from the ICAs and the BA results in 956 ml/min and the average outflow from the PCAs, MCAs and the ACAs results in 934 ml/min. The measurements contain an average flow discrepancy of 22 ml/min, which is 2.3 % of the total inflow. This discrepancy can vary throughout the systolic-diastolic cycle, the statement that this discrepancy has been caused by the measurement inaccuracy would be false, although the flow discrepancy percentage is within the tolerance of the measurement precision, it is not generally observed.

5.2.2. Measurement analysis of the Venous measurements for S64: The procedure of the analysis of the Venous tree backbone are identical to the Arterial tree backbone. The total inflow from the SSS and the STRAIGHT result in a total average inflow of 797 ml/min, the total average outflow from the Jugular veins results in a total average outflow of 1085 ml/min, this discrepancy is caused by the Superior, Inferior Petrosal and other minor feeds.

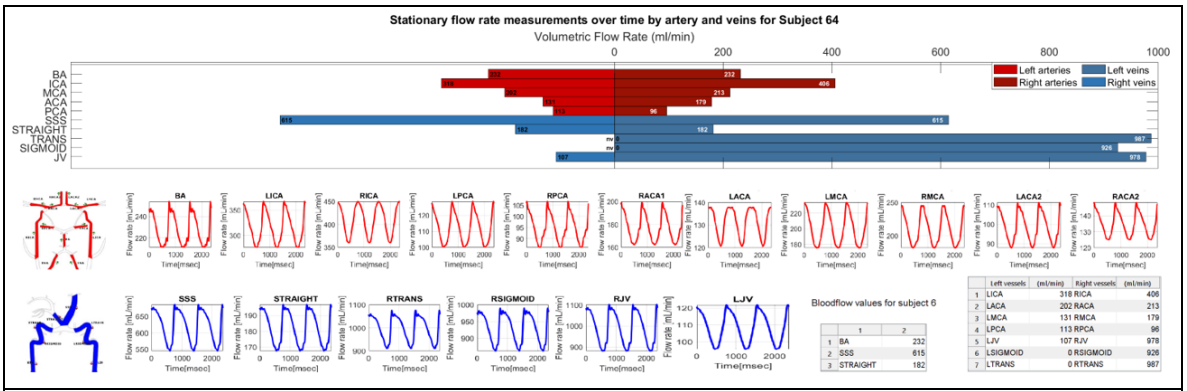

Figure 31 – Visual representation of the NOVA report for S64 as stationary values. For all measured arteries and veins the systolic-diastolic cycle was presented, all artery measurements are depicted as red, all vessels are depicted as blue. Further a bar graph is presented to compare the left and the right variation of vessels, if a vessel does not have a symmetric counter vessel (such as the Basilar artery), the flow value on both left and right side are equal in the graph.

Results

Flow and pressure estimation of Subject 58

5.3. Stationary (St.) S58's Arterial Backbone tree flow estimation: Since it is known that NOVA flow inputs into the Circle of Willis have been proven to not satisfy mass balance in this network[3], as there is more inflow than outflow, the arterial tree will be modified to enforce mass balance and to recover prescribed flows.

As shown in Figure 32, the prescribed mean flows in the CoW must be heavily attenuated by the estimation procedure to enforce mass balance. This is what was expected, as previous work has shown the inability to rectify in vivo measurements with networks that do not contain small side draw vessels.

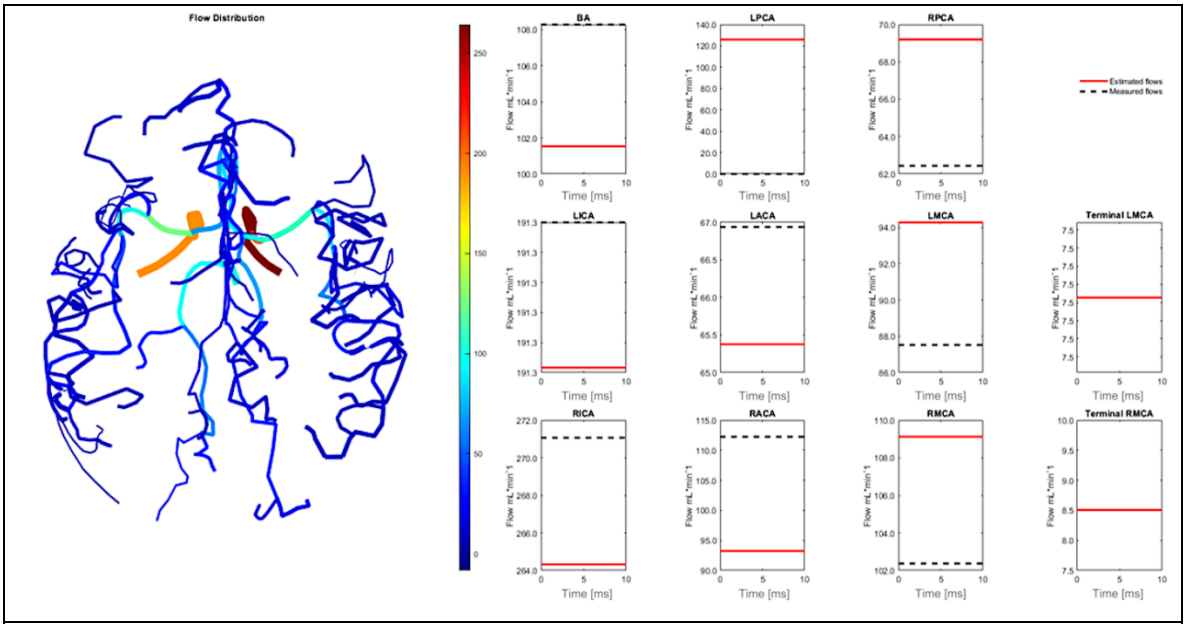

Figure 32 – Left: a heat map showing the flow in each vessel. Right: a series of plots showing the comparison for measured and estimated flows in key arterial vessels. As seen, the measured vessels do not match the estimated flows. This is due to the lack of side draws present in the Circle of Willis, the lack of side draws in the network implies a mass imbalance that the optimization procedure must rectify. Nwk name: S58_bb7_plus.fMx; code: DynOptDemo.m

5.4. Oscillatory (Osc.) S58's Arterial Backbone tree flow estimation: This section presents the results for the original segmentation of Subject 58, the prescribed input flows are NOVA measurements. The fractional flow assignment was prescribed according to cross-sectional area. We expect this case study to demonstrate the optimization procedure generating a compromise between the inlet and outlet flows in the Circle of Willis. We expect this because, as mentioned before, it is known that mass balance is not preserved in this network when using NOVA flows as inputs.

The true results, as displayed in Figure 33, demonstrate that the flow distribution is not able to perfectly mimic the measured flow values. This is due to the procedures hard constraint to maintain mass balance. The measured values do not preserve mass balance, so the optimization procedure must make a compromise, matching our expected results.

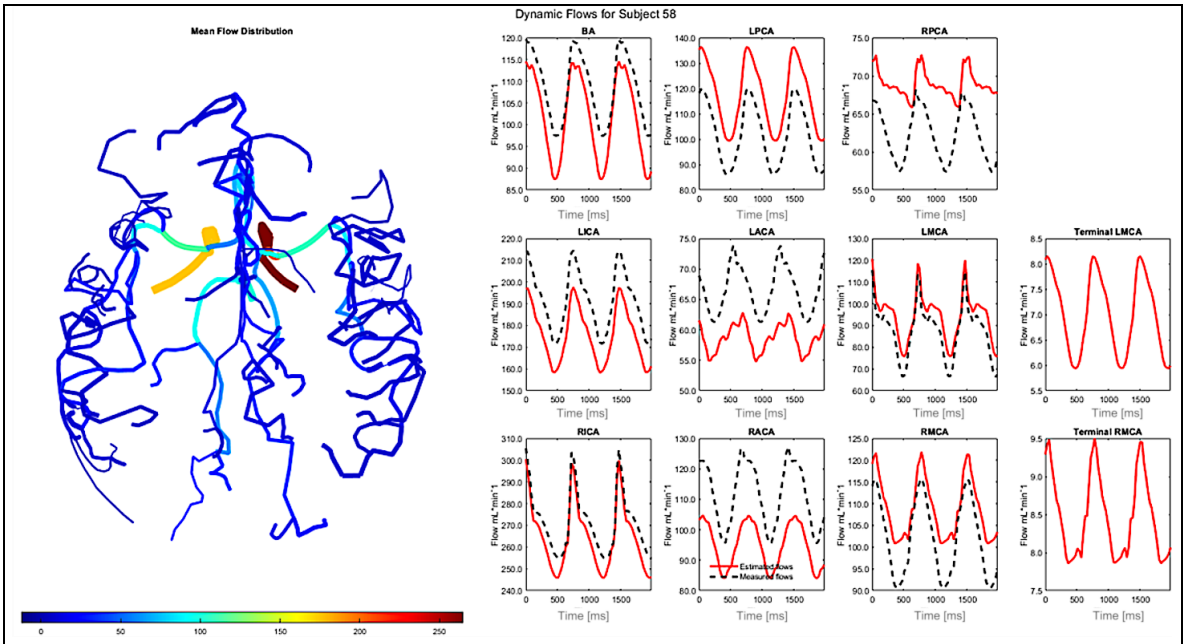

Figure 33 – Left: a heat map showing the mean flow in each vessel. Right: a series of plots showing the comparison for measured and estimated dynamic flow signals in key arterial vessels. As seen, the measured vessels do not match the estimated flows. This is due to the lack of side draws present in the Circle of Willis, the lack of side draws in the network implies a mass imbalance that the optimization procedure must rectify. Nwk name: S58_bb7_plus.fMx; code: DynOptDemo.m

5.5. Osc. S58's Arterial Backbone tree flow estimation with side draws: This case study utilizes an augmented version of the S58 network. This network is similar to the previous, but with added side draws. The first side draw is located in the BA and mimics the flow in the Pontine or Pre-pontine arteries. Two other side draws are located on the ACAs prior to the anterior communicating artery, these mimic the effect as the anteromedial central arteries. The last two side draws included in this diagram are located on MCAs and replicate the effect of the Anterior choroidal arteries.

The results of this case study should show that the optimization no longer has to compromise the flows to ensure mass balance. Instead the side draws should be assigned flows that allow for the mass balance in the CoW. As displayed in Figure 34 the flow estimation was able to perfectly recreate the input flows and no longer has to compromise in the CoW. We are also able to infer flows in the side draws based on the estimation procedures assignment.

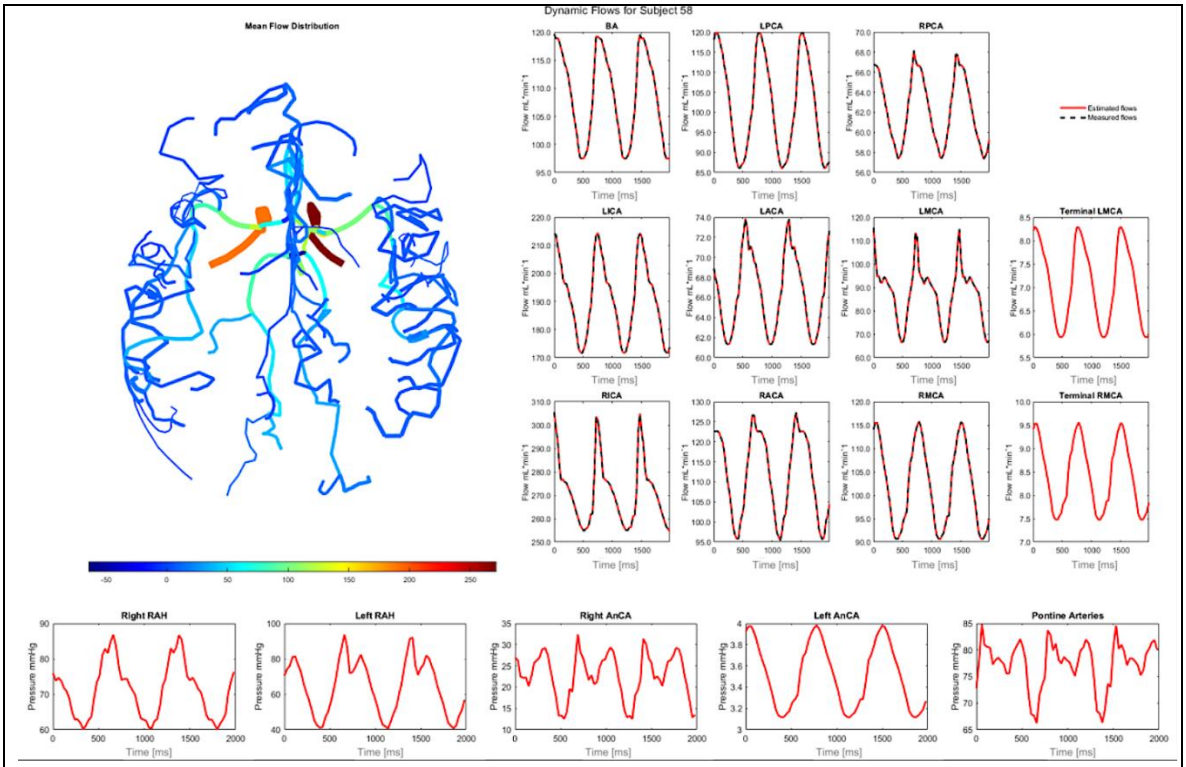

Figure 34 – Left: Heat map indicating the flow in the major arterial tree, Right: flows within the Circle of Willis and downstream terminal nodes indicating the terminating nodes of the MCA, Bottom: Flows in the Anterior Choroidal Anterior, Recurrent Artery of Huebner and Pontine Arteries acting as side draws. Nwk name: S58_bb7_plus.fMx; code: DynOptDemo.m

5.5.1. Results for Prescribing the flow in the Pre-Pontine Artery: As mentioned in section 3.9, the flow in the added side draws can exhibit non-physiological dynamics. This is the case with the prepontine artery flow that was inferred in Figure 35. Therefore, the procedure described in section 3.9 was applied and resulted in anatomically accurate flow values in the pre-pontine Arteries after the estimation.

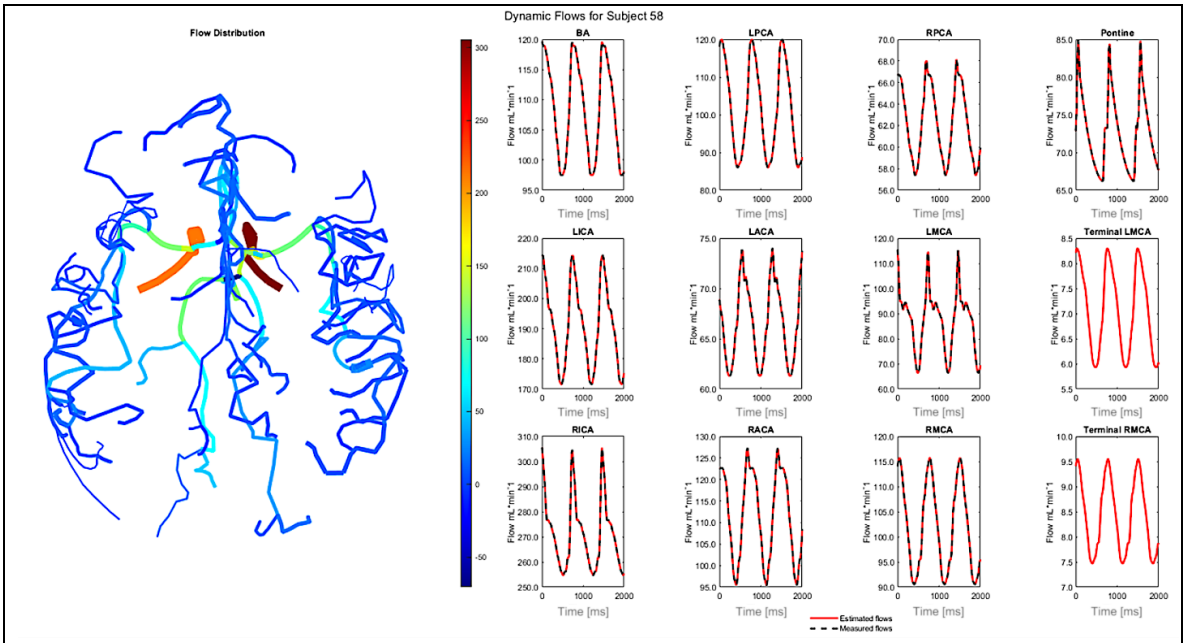

Figure 35 – Left: Heat map indicating the average pressure in the major arterial tree, Right: pressures within the Circle of Willis and downstream terminal nodes indicating terminating pressure of the MCA, Bottom: Estimated pressures in the Anterior Choroidal Artery, Recurrent Artery of Huebner and Pontine Arteries acting as side draws. Nwk name: S58_bb7_plus.fMx; code: DynOptDemo.m

The prescription of a systolic-diastolic cycle in the prepontine artery shows the amount of control that the estimation procedure allows over a network.

5.6. Osc. S58's Arterial Backbone tree pressure estimation with side draws: Pressures were recovered from the augmented version of S58 using the same procedure as the previous case study. The results expected should still display no physiological pressure drops in the distal branches because the side draws will only adjust the flow assignment in the CoW as none were added to these more distant branches.

As seen in Figure 36 the pressure drops are still too extreme in the distal branches. More side draws would need to be added in the further branches of the arterial tree to allow for more physiological pressure drops.

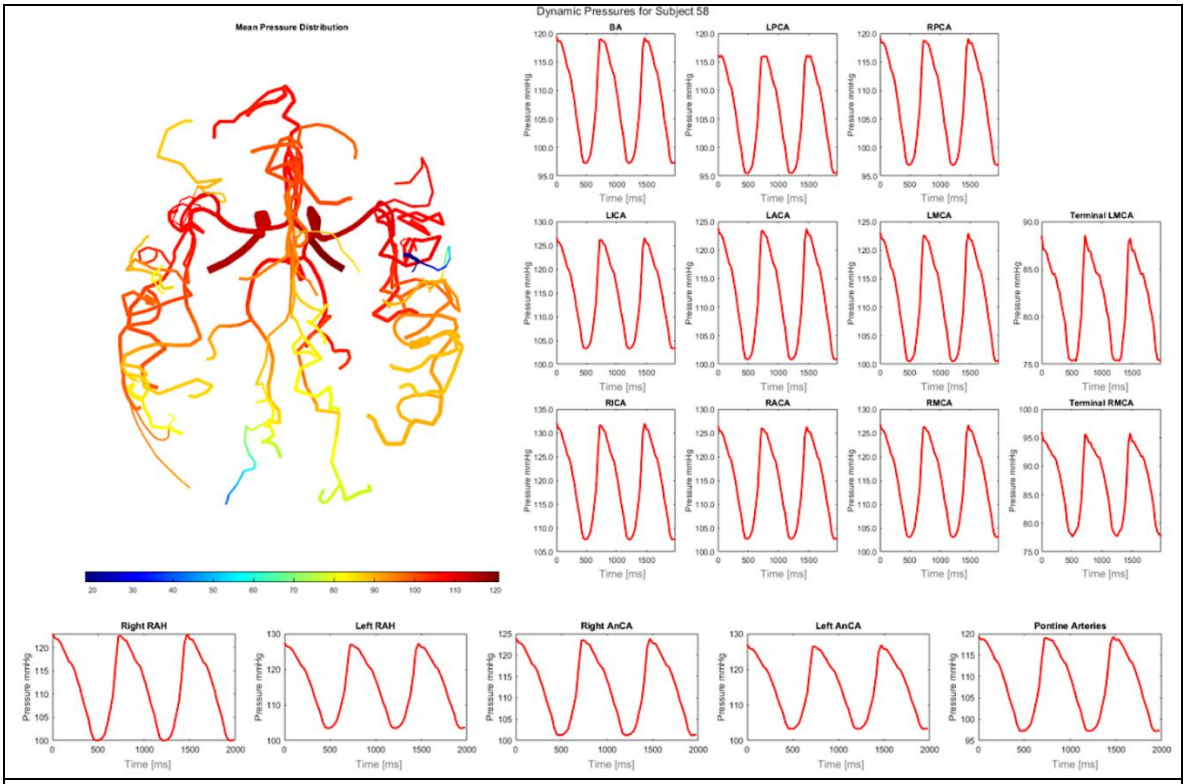

Figure 36 – Left: Heat map indicating the average pressure in the major arterial tree, Right: pressures within the Circle of Willis and downstream terminal nodes indicating terminating pressure of the MCA, Bottom: Estimated pressures in the Anterior Choroidal Artery, Recurrent Artery of Huebner and Pontine Arteries acting as side draws. Nwk name: S58_bb7_plus.fMx; code: DynOptDemo.m

5.7. Osc. S58's Arterial Macro tree flow estimation: The flow estimation of the Arterial Macro tree is based on the same measurements as the previous Arterial tree estimation. This network has more anatomical details than the Arterial tree backbone. Due to the increased anatomical detail, the flow estimation results do not have any flow discrepancies anymore.

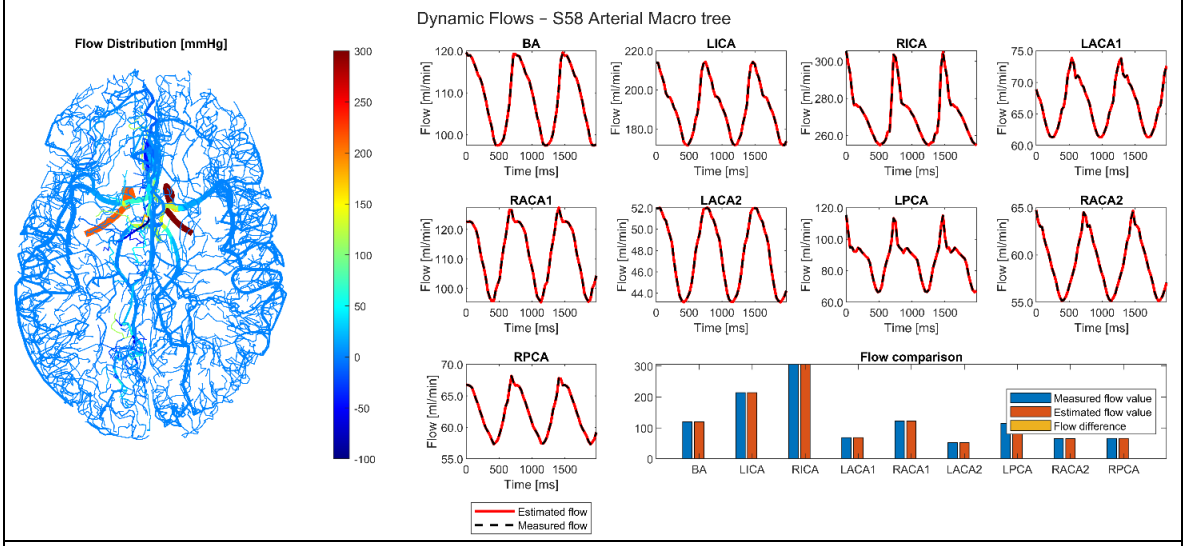

Figure 37 – Visualization of the dynamic S58 Arterial macro tree flow estimation. For each main artery a visualization of measured and estimated flow values has been displayed. A bar graph comparing the measurements and results to display the preservation of measured values. Nwk name: S58_macroTree.territoryLabeled.fMx; code: DynOptDemo.m

5.8. Osc. S58's Arterial Macro tree pressure estimation: The pressure estimation results in Figure 38 display a mostly satisfying pressure map, where the pressure drop goes along the flow direction. It can be seen, that some smaller branches undergo a rapid pressure drop, this effect is created by an occurred error during the network generation procedure, the diameter is smaller, that in reality.

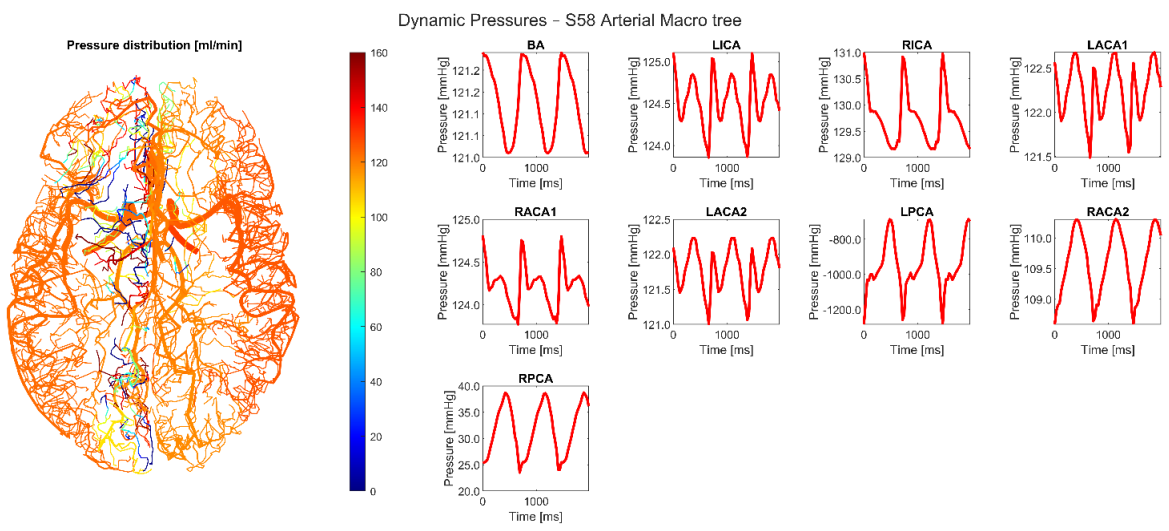

Figure 38 – Visualization of the dynamic S58 Arterial macro tree pressure map. For each main artery a visualization of estimated pressure values have been displayed. Nwk name: S58_macroTree.territoryLabeled.fMx; code: DynOptDemo.m

5.9. Osc. S58's Arterial Whole tree flow estimation: The whole Arterial tree builds upon the previous macro tree massively extending the anatomical detail. The extension of the network will also no longer deviate from the input flow measurements but mainly showcases the power of the estimation method on a network with just under half a million equations. The results may be used in further calculations thanks to the quantity of information this estimation returns.

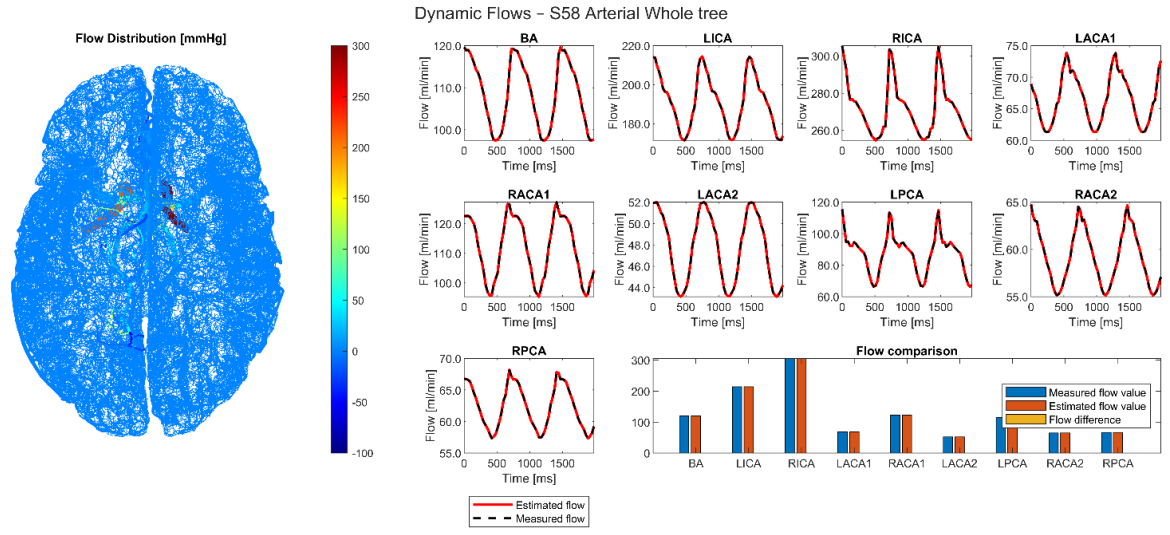

Figure 39 – Visualization of the dynamic S58 Arterial whole tree flow estimation. For each main artery a visualization of measured and estimated flow values has been displayed. A bar graph comparing the measurements and results to display the preservation of measured values. Nwk name: S58_wholeTree.territoryLabeled.fMx; code: DynOptDemo.m

5.10. Osc. S58's Arterial Whole tree pressure estimation: The pressure estimation of the whole tree show that the areas branching from the PCAs behave accordingly to the anatomical behavior. The remaining areas have an increased pressure to around 600 mmHg. This error couldn't be removed by removing extremely small diameters.

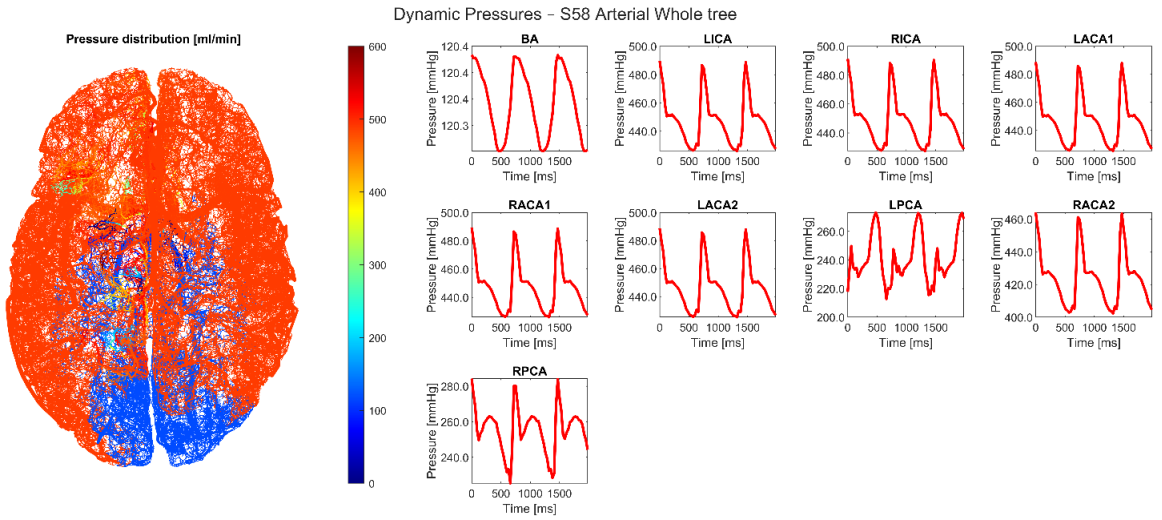

Figure 40 – Visualization of the dynamic S58 Arterial whole tree pressure map. For each main artery a visualization of estimated pressure values have been displayed. Nwk name: S58_wholeTree.territoryLabeled.fMx; code: DynOptDemo.m

5.11. St. S58's Venous Backbone tree flow estimation: The display of S58's flow estimation is displayed in Figure 41 where it is seen that the flows at the inlets are significantly lower and feed into the outlets at the left and right jugular veins. There is a significant jump in the estimated flow in the Straight Sinus but a significant decrease in the estimated flow in the SSS.

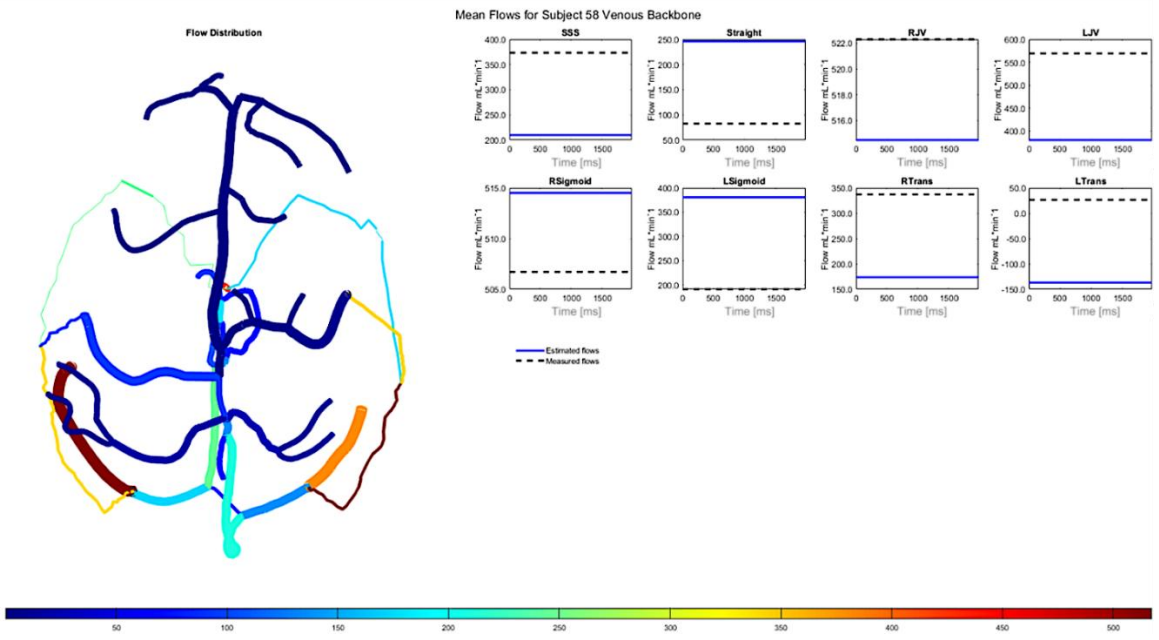

Figure 41 – S58_bb7 mean venous flows before and after estimation. There is a significant jump in some of the flow values which is a result of mass balance not being met within the system. This could be a result of several issues. Nwk name: S58_bbv.fMx; code: DynOptDemo.m

In Figure 42 we see that this trend is true in not just the static simulation but also the dynamic case as well. We also see the waveforms taking on different shapes in some of the vessels such as the LRJ vein and the LTrans sinus.

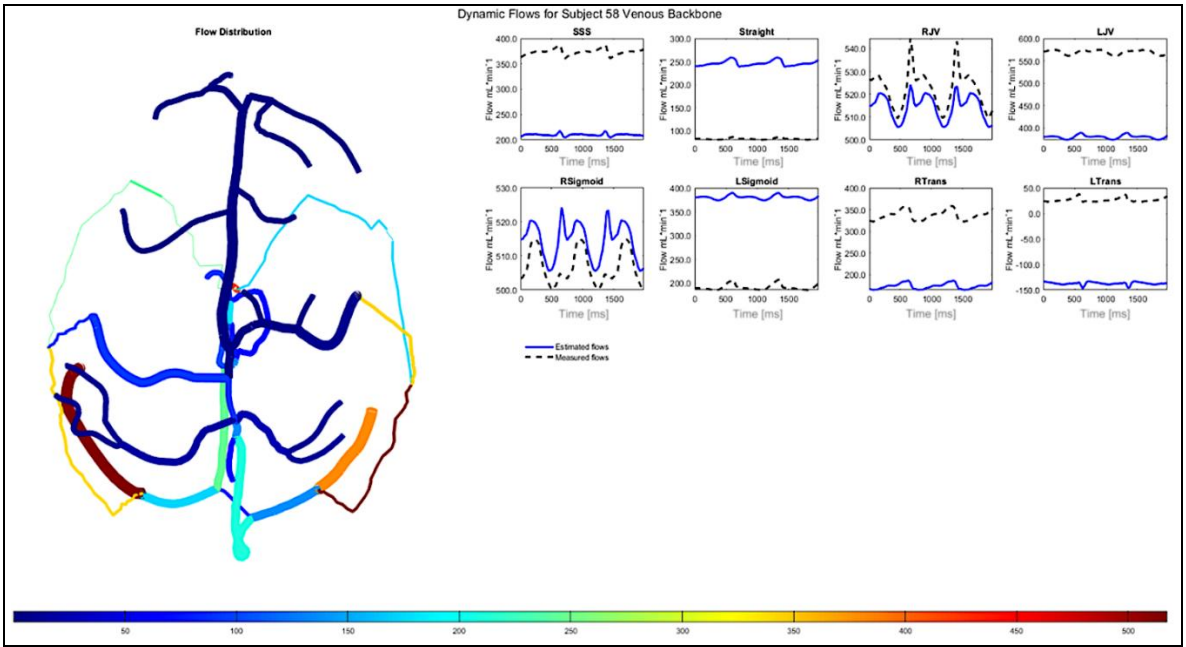

Figure 42 – Dynamic estimation of S58's venous tree. The waveforms shown before and after estimation highlight a discrepancy in the mass balance of the system, as well as being a possible result of measurement error meaning the flow signals need to be synchronized. Nwk name: S58_bbv.fMx; code: DynOptDemo.m

5.12. St. S58's Venous Backbone tree flow estimation with side draws: The next vessels added were between the SSS and the Left Transverse sinus, and between the Straight sinus and the Right Transverse Sinus.

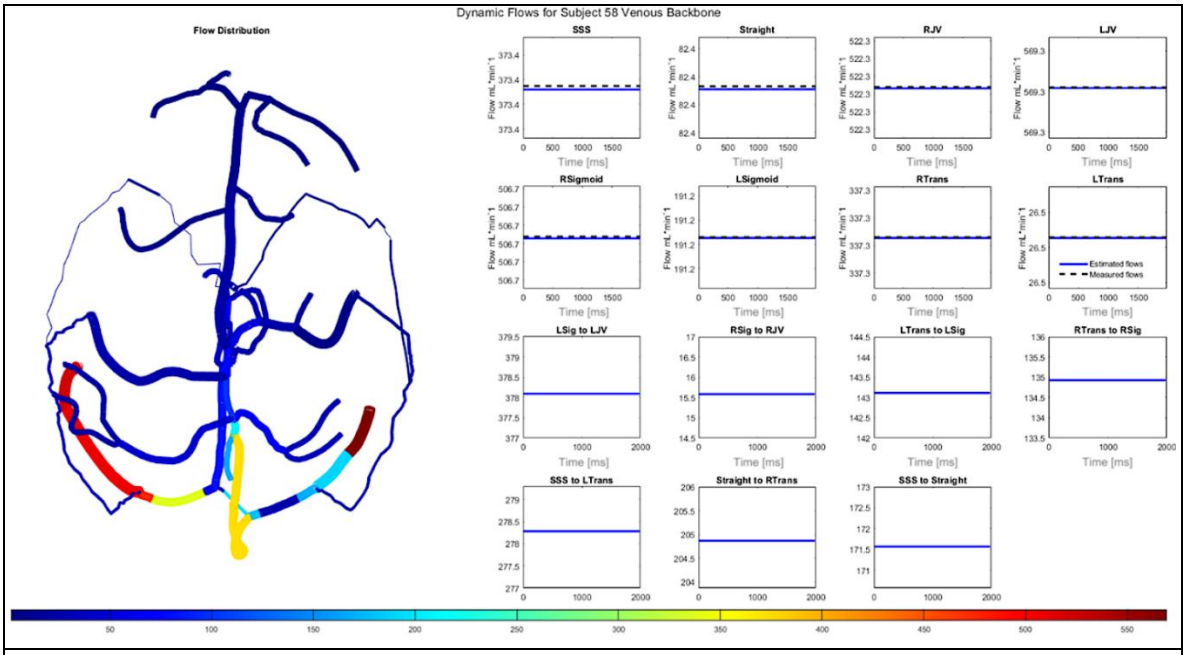

Figure 43 – The flow distribution for S58_bbv with side draws added between the transverse sinus, the sigmoid sinus, the jugular veins and between the SSS and the LSigmoid vessel and the Straight Sinus and the RSigmoid vessel. It can be seen that the flow reconciliation in the SSS and the Straight Sinus are much closer but are still not perfectly recovered Nwk name: S58_bbv.fMx; code: DynOptDemo.m

The effect of adding the side draws in this case study allowed for the SSS and the Straight Sinus flows to be almost perfectly recovered, as displayed in Figure 43. The flows in the side draw vessels are still quite high though.

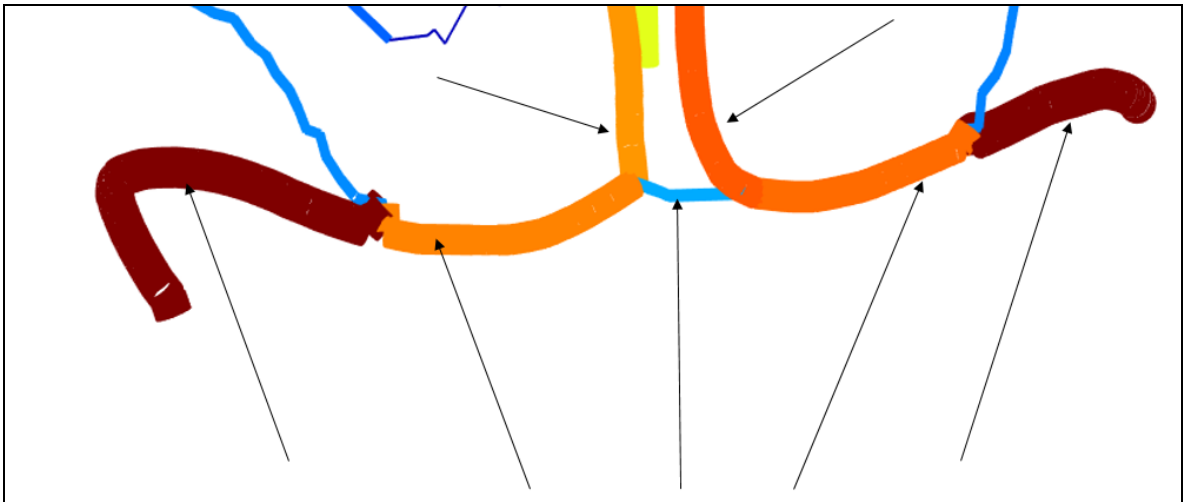

Figure 44 – A diagram showing the general location of added side draw vessels. These vessels are necessary for the measurements to maintain mass balance and thus be perfectly recovered in the simulation.

The final diagram for the side draw vessel locations can be seen in Figure 44, where they are indicated with a black arrow.

5.13. Osc. S58's Venous Backbone tree flow estimation with side draws: Having now determined the side draws necessary to preserve mass balance in the network, we perform the flow estimation with the dynamic signals as done in the first case study. The results of the dynamic flow estimation are displayed in Figure 45, where the flows signals are perfectly matched.

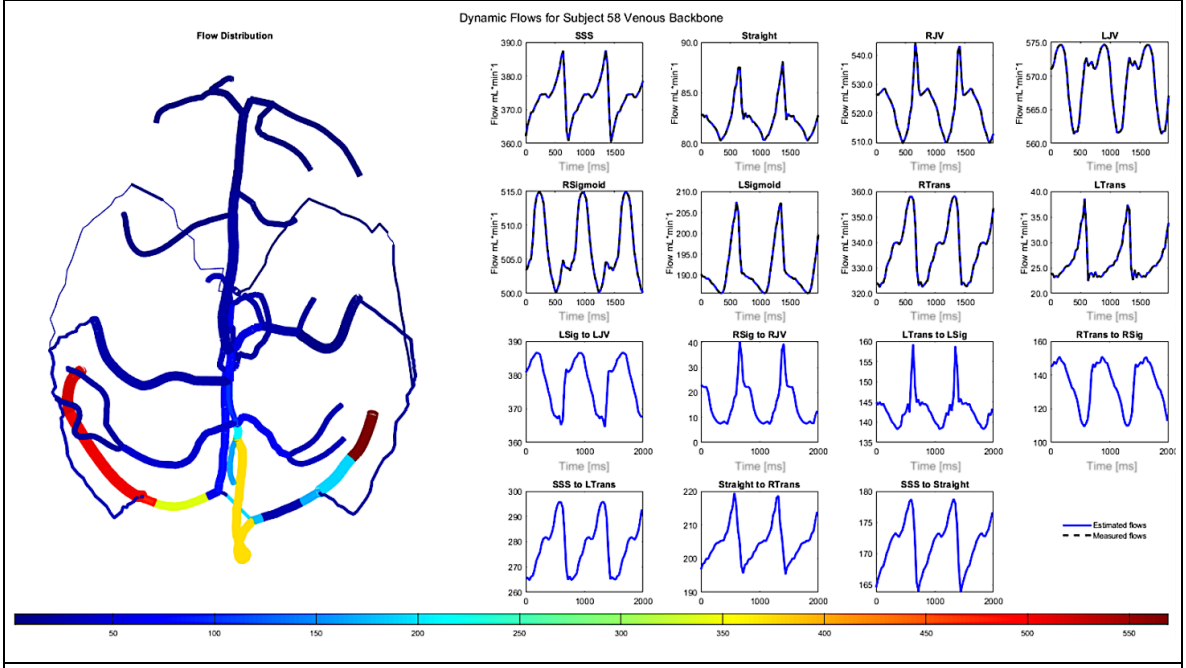

Figure 45 – A display of the mean flow distribution across S58_bbv, with the plots of the dynamic flow signals versus time on the right hand side. It can be seen that the flows recovered from the estimation procedure are equal to the measured flows at each time instant. Nwk name: S58_bbv.fMx; code: DynOptDemo.m

5.14. Osc. S58's Venous Macro tree flow estimation: The macro tree is a version of the venous tree that contains far more vessels than the backbone. This is why it was initially assumed that the macro tree would not need side draws added as the amount of vessels present could allow for the mass balance to already be met within the system. The results of prescribing NOVA flows on the macro tree are shown in Figure 46.

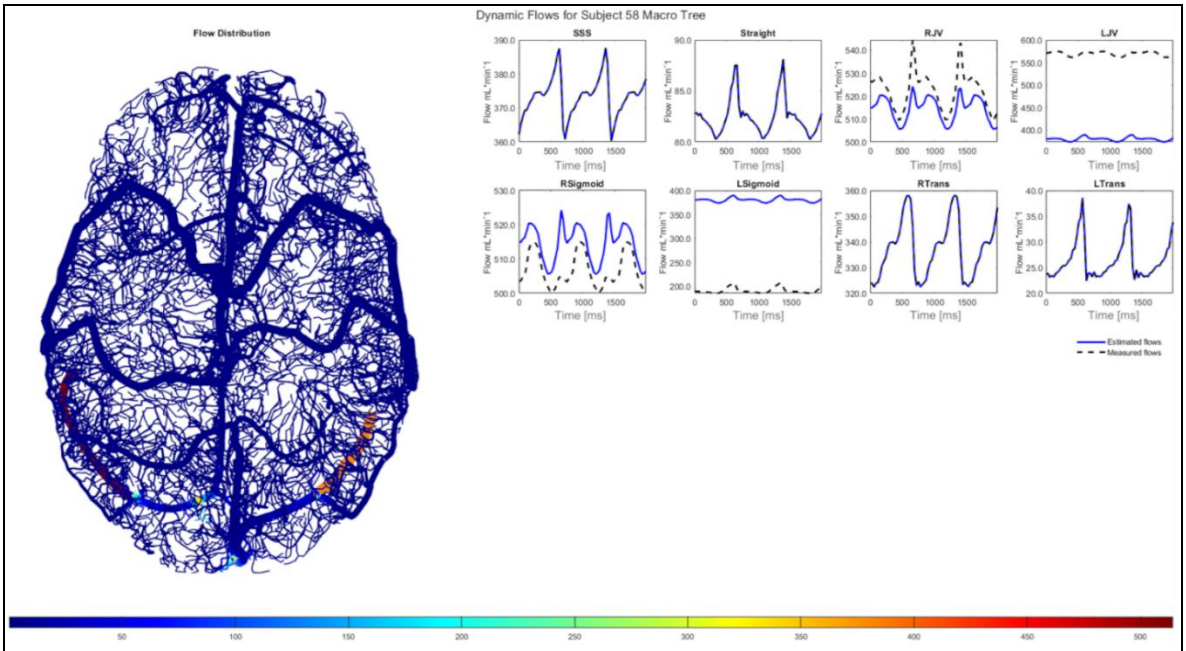

Figure 46 – A display of the mean flow distribution across S58_bbv, with the plots of the dynamic flow signals versus time on the right-hand side. It can be seen that the flows recovered from the estimation procedure are equal to the measured flows at each time instant. Nwk name: S58_macroTree.fMx; code: DynOptDemo.m

The expectation of perfectly matching measurements was not met, this is likely due to the choice to keep the jugular veins from having additional side branches during the segmentation process. As such, side draw branches are now reintroduced between the sigmoid sinus and the jugular veins.

5.15. Osc. S58's Venous Macro tree flow estimation with side draws: With side draws being added in the locations that mass balance was not being met, the estimation procedure was performed with the NOVA flows being the prescribed flows. The results of this simulation are shown in Figure 47.

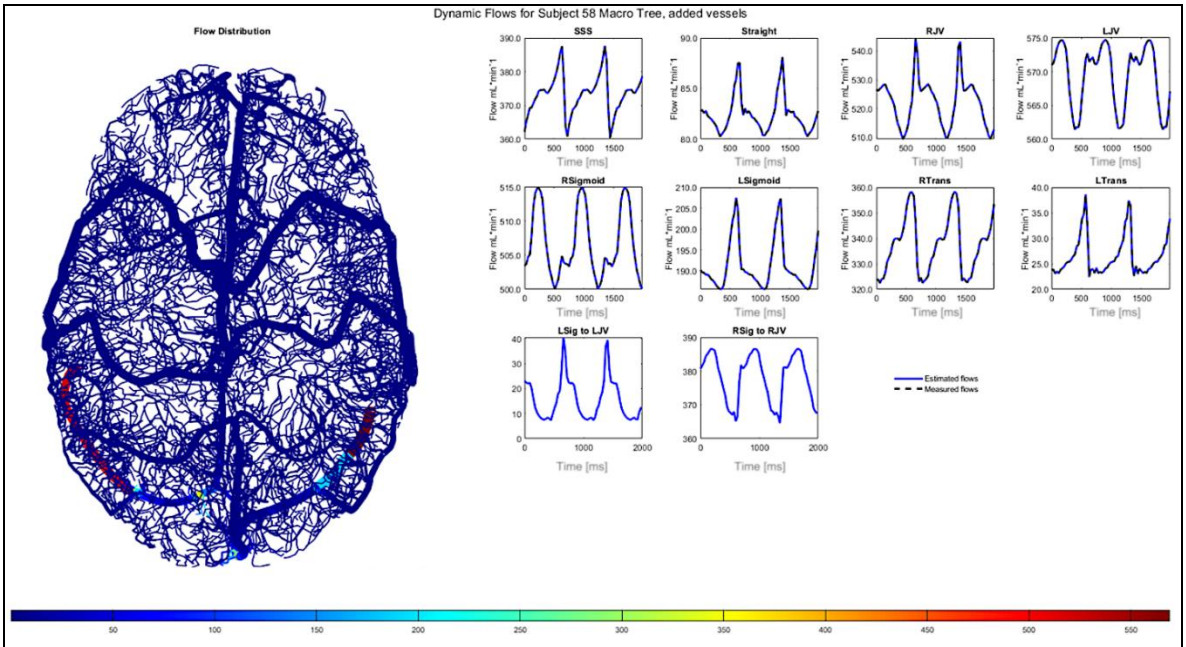

Figure 47 – A display of the mean flow distribution across S58_bbv, with the plots of the dynamic flow signals versus time on the right-hand side. It can be seen that the flows recovered from the estimation procedure are equal to the measured flows at each time instant. Nwk name: S58_macroTree.fMx; code: DynOptDemo.m

Flow and pressure estimation of Subject 64

5.16. St. S64's Arterial Backbone tree flow estimation: The stationary flow estimation is based on existing measurements, where only the first time instance has been used. In Figure 48, it is apparent, that a flow discrepancy is present. The estimation method has reconciled the discrepancies, but the measurements have also been devaluated.

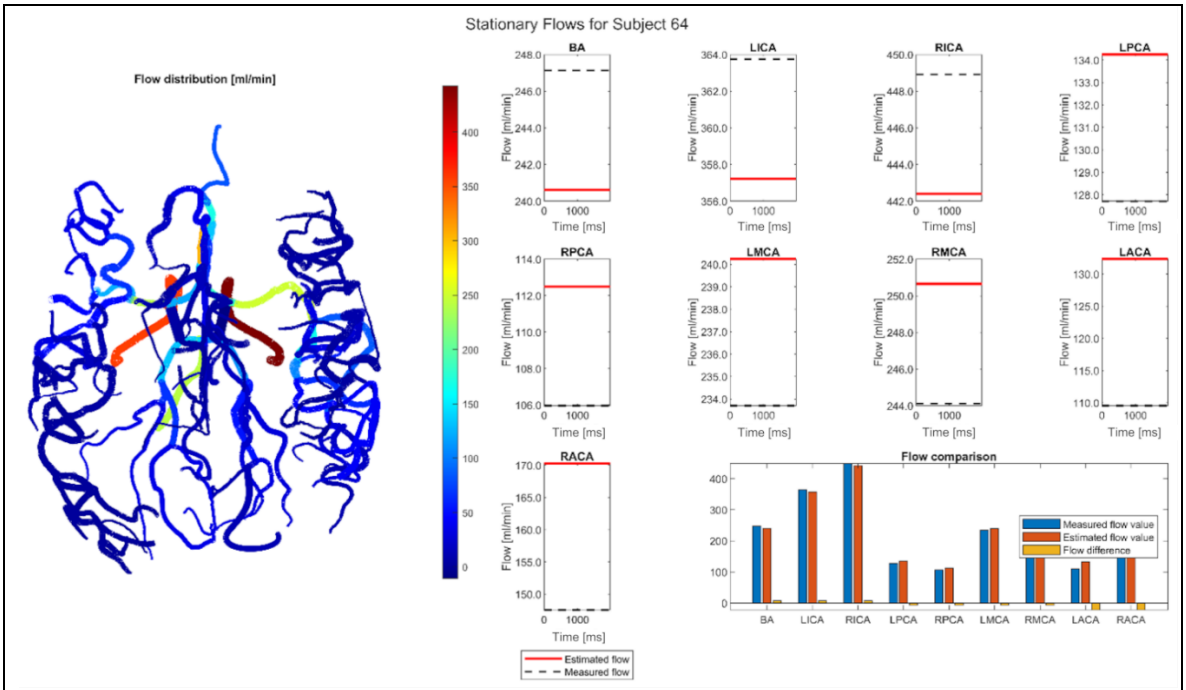

Figure 48 – Visualization of the stationary S64 flow distribution. For each main artery a visualization of measured and estimated flow values has been displayed. A bar graph comparing the measurements and results to display the preservation of measured values. Nwk name: S64_bba_plus.fMx; code: DynOptDemo.m

5.17. St. S64's Arterial Backbone tree pressure estimation: After estimating the flows, it is possible to calculate the pressures from the Hagen-Poiseuille equation.

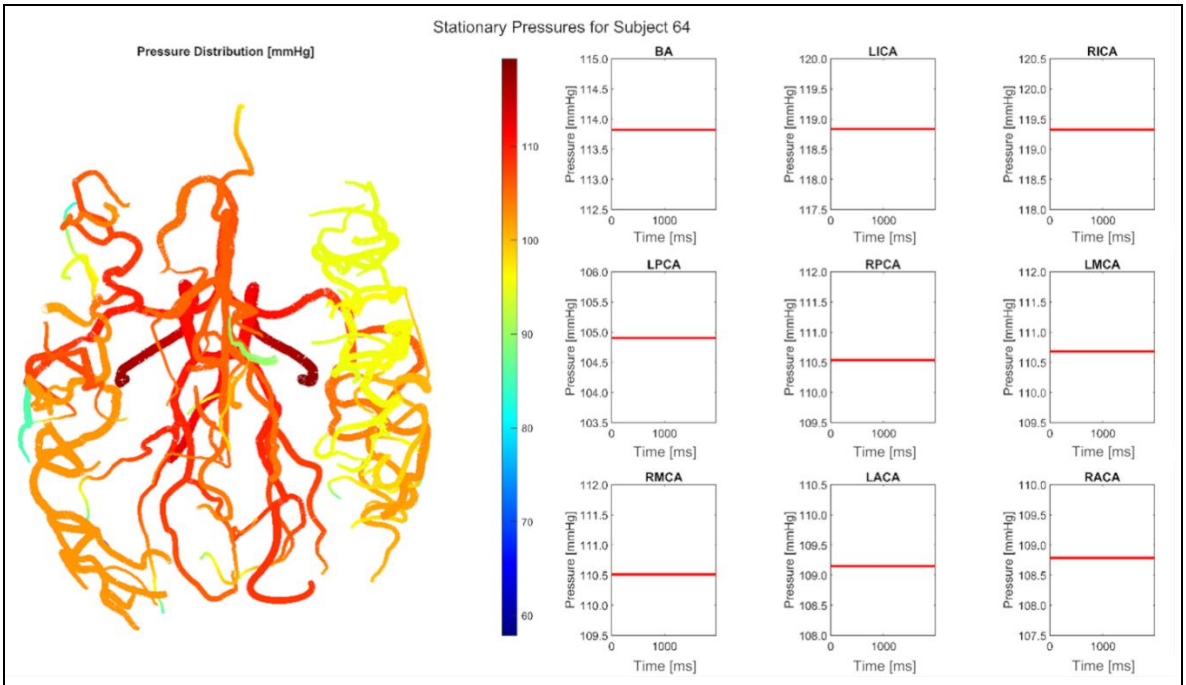

Figure 49 – Visualization of the stationary S64 pressure map. For each main artery a visualization of estimated pressure values have been displayed. Nwk name: S64_bba_plus.fMx; code: DynOptDemo.m

5.18. Osc. S64's Arterial Backbone tree flow estimation: This subject is based on in vivo measurements, after measuring the flows, it has been noticed that the inflow/outflow balance is not satisfied and will have to be reconciled using the estimation method. To present the format of NOVA flow measurements, The NOVA measurement for the RACA is in Appendix A.

The S64 Arterial tree has an inflow/outflow discrepancy due to not being able to measure small vessels. By estimating the model, the inflow/outflow equilibrium will be achieved, this method will alter the original measurements to achieve this goal, this will be addressed in the next case study. The estimation method has removed the discrepancy for each time instance. The estimated flow values have been deviated from the measurements.

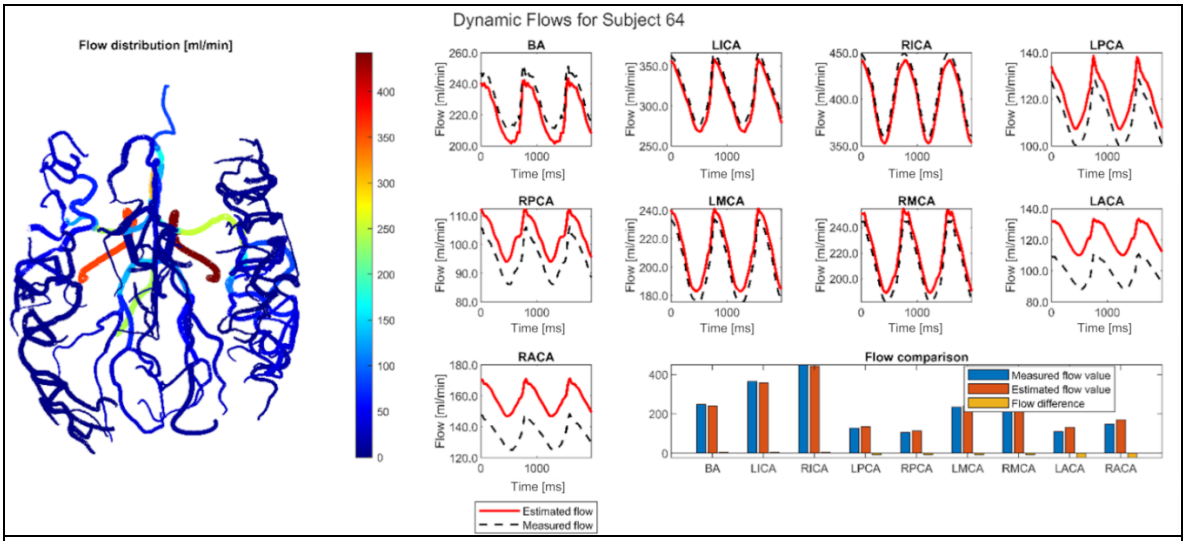

Figure 50 – Visualization of the oscillatory S64 flow distribution. For each main artery a visualization of measured and estimated flow values has been displayed. A bar graph comparing the measurements and results to display the preservation of measured values. Nwk name: S64_bba_plus.fMx; code: DynOptDemo.m

5.19. Osc. S64's Arterial Backbone tree pressure estimation: To estimate the pressure, it is necessary to have at least 1 measured pressure for each time instance. S64 doesn't have any pressure measurements, so to show the functionality of the method, the measurements of the right ICA have been multiplied by a scalar to oscillate between the values 130 and 100 mmHg throughout time instances, those values have been assigned to the BA and will mimic the desired pressure measurements.

The pressure estimation will calculate the pressure map for every time instance. The S64 arterial tree is made of thousands of faces, this leads to a certain problem – due to the network not being fully anatomically correct, the pressure drop is going to be distorted and it is not going to be physiologically accurate.

The expected results were met as the pressure drop in the arterial tree is beyond the physical range, this is due to the lack of physiological detail present in the network.

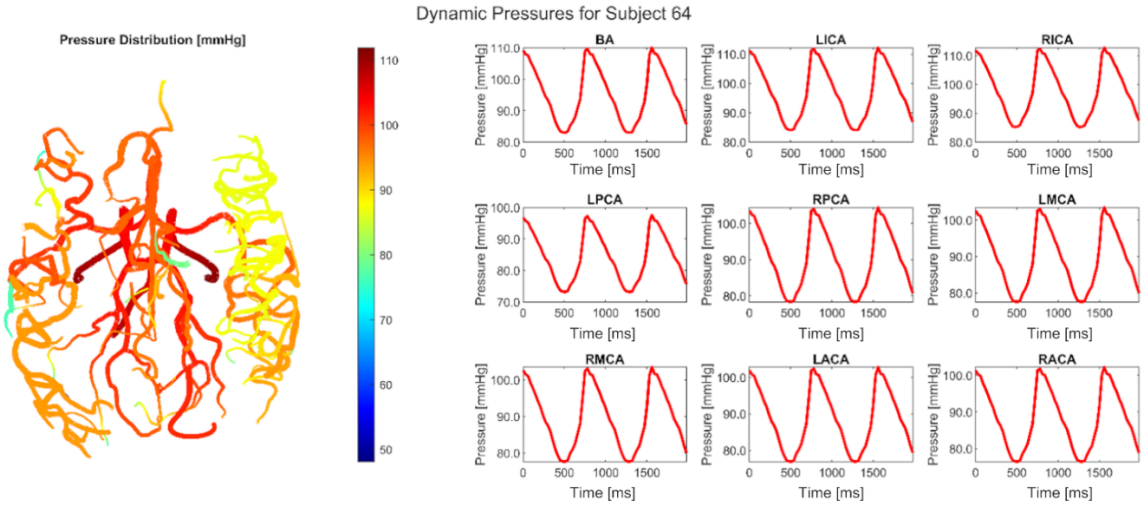

Figure 51 – Visualization of the oscillatory S64 pressure map. For each main artery a visualization of estimated pressure values have been displayed. Nwk name: S64_bba_plus.fMx; code: DynOptDemo.m

5.20. Osc. S64's Arterial Backbone tree flow estimation with side draws: The previous case study has shown that the flow estimation method is able to eliminate flow discrepancies, however, results have deviated from the original measurements devaluating them. The flow discrepancy in measured values is caused due to insufficient imaging quality – MR technology isn't able to register smaller vessels, thus not being able to see blood entering them. This implies that all the flow distributed into the mentioned "invisible" vessels is lost and won't be registered as outflow creating the discrepancy.

The S64_Aug model is based on the original S64 Arterial tree. To preserve measured values, anatomically correct "invisible" vessels to each main artery of the Circle of Willis – the Basilar artery, Posterior Cerebral artery, Middle, Anterior and Internal Carotid arteries have to be added.

By adding the invisible vessels, it is expected, that the arterial flows, which have been measured will be preserved throughout the process of estimation. The addition of invisible vessels will enhance the anatomical correctness, resulting in all potential flow differences equalizing by sinking (or adding) flow via the newly added vessels.

The estimation method has removed the discrepancy for every time instance. The measured values were preserved creating a system obeying mass conservation as well as obeying measured data.

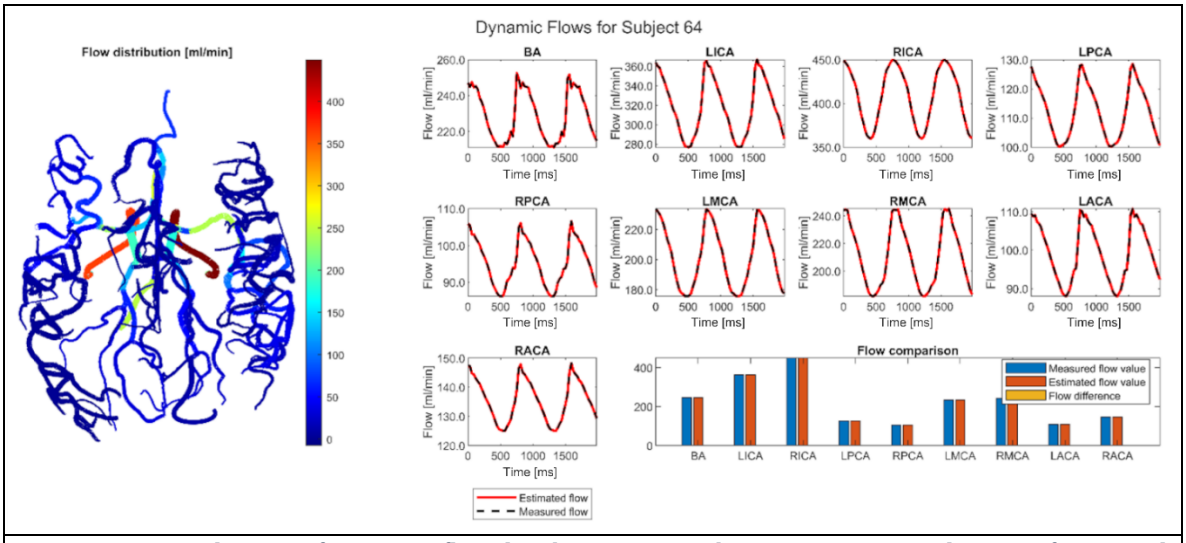

Figure 52 – Visualization of S64_Aug flow distribution. For each main artery a visualization of measured and estimated flow values has been displayed. A bar graph comparing the measurements and results to display the preservation of measured values. Nwk name: S64_bba_Aug_plus.fMx; code: DynOptDemo.m

5.21. Osc. S64's Arterial Backbone tree pressure estimation with side draws: The pressure estimation procedure is equivalent to the previous case study, by assigning the altered ICA measurements to the BA, it is expected to estimate the pressure for the augmented S64.

The expected results were met, the pressure drop in the arterial tree is within the physical range, the addition of side draws did not affect the pressure estimation.

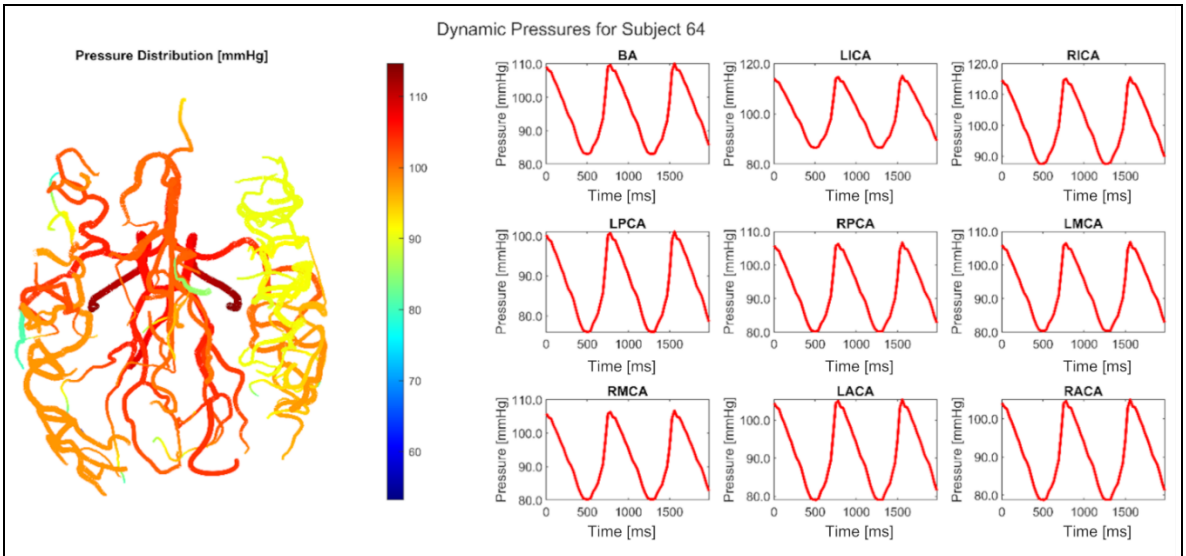

Figure 53 – Visualization of S64_Aug pressure map. For each main artery a visualization of estimated pressure values have been displayed. Nwk name: S64_bba_Aug_plus.fMx; code: DynOptDemo.m

5.22. Osc. S64's Venous Backbone tree flow estimation: This subject is based on in vivo measurements of the S64 Venous tree. After measuring the flows, it has been noticed, that the inflow/outflow balance is not satisfied and will have to be reconciled using the estimation method.

As stated, the S64 has an inflow/outflow discrepancy that must be reconciled. The estimation method should reconcile the discrepancy while having the least square error. This network has no side vessels added, this means that after estimation, it is expected that the estimated flows will have to deviate from the measurements to satisfy the inflow/outflow equilibrium.

The estimation method has removed the discrepancy for every time instance. The estimated flow values have been deviated from the measurements due to not including anatomically correct side vessels.

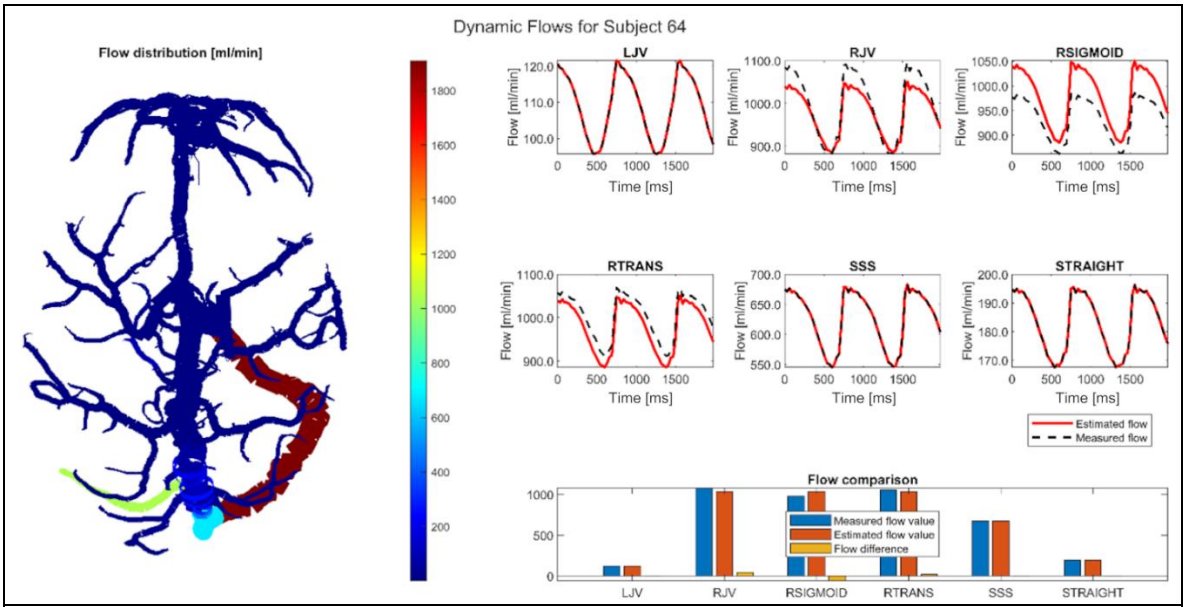

Figure 54 – Visualization of S64_Veins flow distribution. For each main Vein a visualization of measured and estimated flow values has been displayed. A bar graph comparing the measurements, results and the difference has also been shown. Nwk name: S64_bbVT.fMx; code: DynOptDemo.m

5.23. Osc. S64's Venous Backbone tree pressure estimation: To estimate the pressure for the S64 Venous backbone, LJV outflow has been set to a close-to zero pressure. It has been observed that the network shows immense pressures at some small terminal vessels. At the mentioned vessels, multiple faces have close-to-zero diameters, this causes the resistance of those vessels to be extremely big.

The pressure estimation is expected to be mathematically correct, due to the network having faces with close-to-zero diameters, the pressure drop is not expected to be locally physiologically accurate. The expectations have been met, the pressure estimation is mathematically correct, the pressure drop expectations have been met.

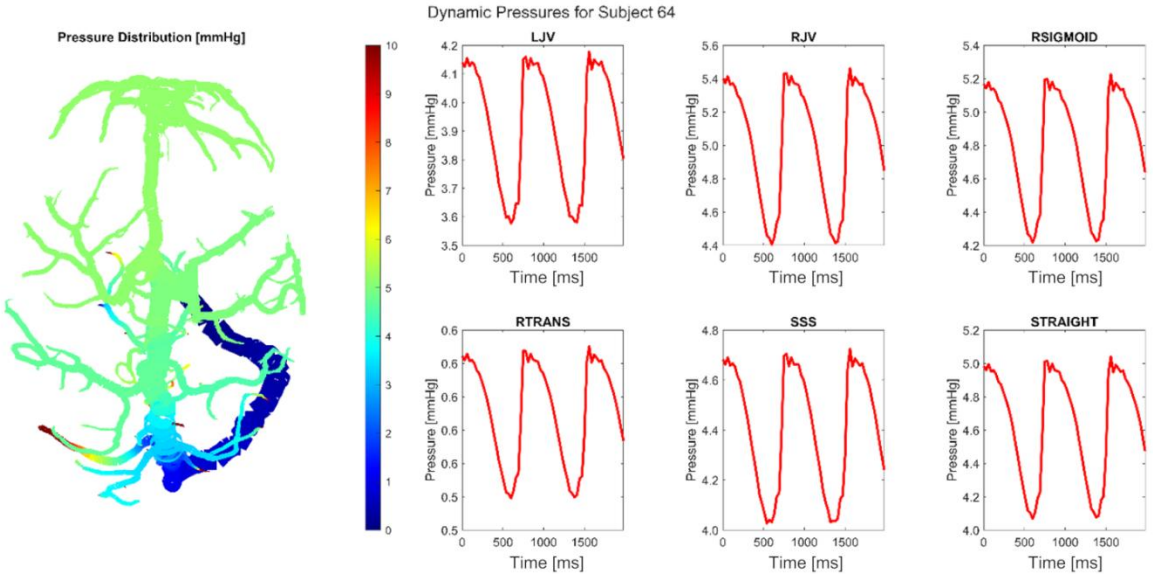

Figure 55– Visualization of S64_Veins pressure map. For each main Vein a visualization of estimated pressure values has been displayed. Nwk name: S64_bbVT.fMx; code: DynOptDemo.m

5.24. Osc. S64's Venous Backbone tree flow estimation with side draws: The first case study has shown that the flow estimation method is able to eliminate flow discrepancies, however, results have deviated from the original measurements devaluating them. The flow discrepancy in measured values is caused due to insufficient imaging quality – MR technology can't register smaller vessels, thus not being able to see blood entering them. This implies that all the flow distributed into the mentioned "invisible" vessels is lost and won't be registered as outflow creating the discrepancy.

The S64_Aug_Veins model is based on the original S64_Veins model. By adding side vessels to the network, the anatomical correctness of the network is increased – all potential inflow/outflow inequalities will be equalized through the added vessels, preserving the measurements.

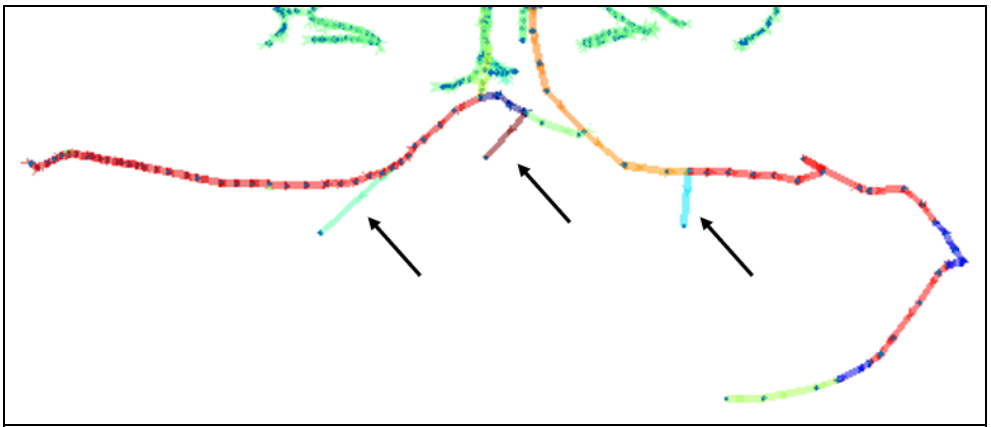

Figure 56 – Visualization of where the side vessels on S64_Aug_Veins have been added

By adding invisible vessels, it is expected for the results to match the original measured values. The addition of invisible vessels will add a degree of freedom to the system, which will result in all potential flow differences to be equalized by sinking (or adding) flow via the newly added vessels.

The estimation method has removed the discrepancy for every time instance. Measured values were preserved, creating a system obeying mass conservation as well as obeying measured data.

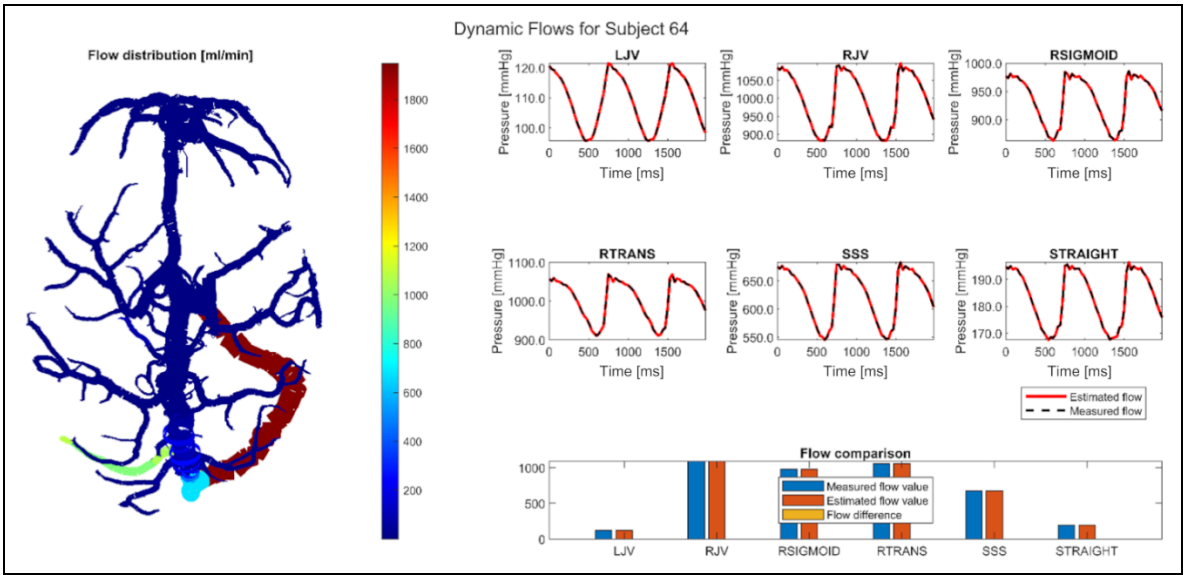

Figure 57 – Visualization of S64_Aug_Veins flow distribution. For each main vein, a visualization of measured and estimated flow values has been displayed. A bar graph comparing the measurements and results to display the preservation of measured values. Nwk name: S64_bbVT_Aug.fMx; code: DynOptDemo.m

5.25. Osc. S64's Venous backbone tree pressure estimation with side draws: The pressure estimation of the S64 Venous tree will be executed the same as in the previous case study, an LJV face has been set to a close-to zero pressure.

By adding the side vessels, no observable difference will be found in the pressure estimation, it is expected for the pressure estimation to be mathematically correct, the pressure drop is not going to be completely physiologically correct due to the networks size and the terminal vessels mentioned in Section 5.15.

The expectations have been met, the estimation is mathematically correct, and the pressure drop has been expected.

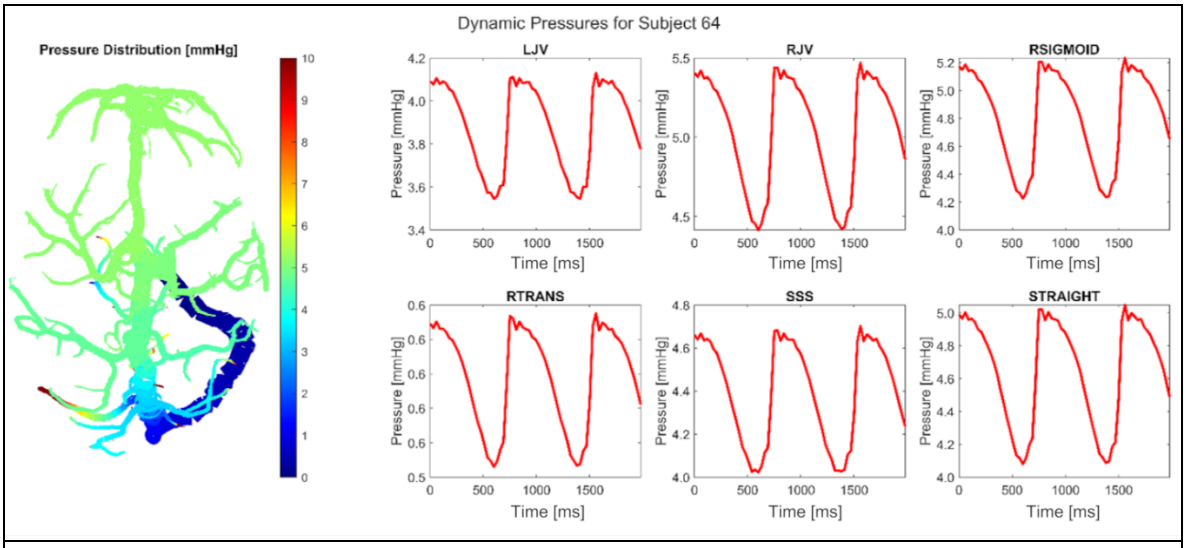

Figure 58 – Visualization of S64_Aug_Veins pressure map. For each main Vein a visualization of estimated pressure values have been displayed. Nwk name: S64_bbVT_Aug.fMx; code: DynOptDemo.m

Discussion of results

The oscillatory flow and pressure estimation of subjects S58 and S64 has shown the potential of real-life use of the estimation method. By estimating the networks without any side vessels, the method has successfully resolved the flow discrepancy enabling to simulate the results. However, when estimating both networks without side vessels, the results deviate majorly from the original measurements, devaluating them. To avoid devaluating the measurements, anatomically accurate side vessels have been added to the networks increasing their accuracy and resolving the flow discrepancy. The results support the hypothesis that by increasing the anatomical accuracy of the network, the flow discrepancies will be reconciled and flows, which cannot be measured can then be acquired with this indirect method.

Chapter 6 – Discussion, Conclusion, Outlook

This thesis explained, that even modern measuring techniques have not yet the required resolution to be able to record the full neurovascular system resolving into flow measurements with imperfections – flow discrepancies, caused by not capturing flow entering non-detectable vessels.

Because of this fact, the estimation method has been designed. By creating an anatomically more accurate neurovascular model and entering flows, which can be measured, the estimation method enables to calculate the flow distribution in all faces. Thanks to the ability to infer flows via the cross-section ratio, it was possible to acquire precise flow values, which cannot be measured with any technology. Also, by estimating the flows, it enabled to use the presented pressure estimation method to acquire a pressure map of the whole network with a single pressure measurement.

This thesis also introduced an oscillatory approach to the estimation method, which was presented on multiple case studies, including 2 real patients. For both patients, a full analysis was done – the flow and pressure estimation of the Arterial and Venous tree backbones. Further, for subject 58, the Venous and Arterial Macro trees were estimated. The S58 Arterial Whole tree has also been estimated to solidify the presented notion.

Estimating the measurements in multiple anatomical detail variations and assigning inferred flows according to the cross-section ratios has proven that by including more anatomical detail, the flow discrepancy will reconcile and return valid and anatomically correct flow values, which, to the best of our knowledge, has never been achieved before.

This tool has great potential. It can analyze the neurovascular blood flow patterns and how it would behave after a surgical procedure, before even coming into contact with the patient. This model is a potential pre-requisite for future heat models, supplying reliable flow measurements of the whole neurovascular system.

Bibliography

[1] RHCASTILHOS. *Schematic representation of the circle of Willis, arteries of the brain and brain stem.* [online]. 24. leden 2007 [vid. 2025-05-22]. Dostupné z: https://commons.wikimedia.org/wiki/File:Circle_of_Willis_en.svg

[2] *1b: Complete Arterial Anatomy with Neck Arteries - 3D model by The Neurosurgical Atlas - Sketchfab* [online]. [vid. 2024-08-13]. Dostupné z: https://sketchfab.com/models/1a6a0fece597461b81a9f55e02317741/embed?annotations_visible=1&api_version=1.5.2&autostart=1&graph_optimizer=0&merge_materials=0&ui_fullscreen=0&ui_help=0&ui_infos=0&ui_watermark=0

[3] PARK, Chang S., Grant HARTUNG, Ali ALARAJ, Xinjian DU, Fady T. CHARBEL a Andreas A. LINNINGER. Quantification of blood flow patterns in the cerebral arterial circulation of individual (human) subjects. *International Journal for Numerical Methods in Biomedical Engineering* [online]. 2020, **36**(1), e3288. ISSN 2040-7947. Dostupné z: doi:10.1002/cnm.3288

[4] HELTHUIS, Jasper H. G., Tristan P. C. VAN DOORMAAL, Sepideh AMIN-HANJANI, XinJian DU, Fady T. CHARBEL, Berend HILLEN a Albert VAN DER ZWAN. A patient-specific cerebral blood flow model. *Journal of Biomechanics* [online]. 2020, **98**, 109445. ISSN 0021-9290. Dostupné z: doi:10.1016/j.jbiomech.2019.109445

[5] GHARIB, Ines a Clara THEODOLY. *Analyze of the static and dynamic blood flow*. Lab Report. B.m.: Laboratory of Product and Process Design. 2022.

[6] MURRAY, Cecil D. The Physiological Principle of Minimum Work. *Proceedings of the National Academy of Sciences* [online]. 1926, **12**(3), 207–214. Dostupné z: doi:10.1073/pnas.12.3.207

List of Figures

List of Tables

Appendix A *S64 Nova flow report*

BA	LICA	RICA	LPCA	RPCA	RACA1	LACA	LMCA	RMCA	LACA2	RACA2
247.14	363.75	448.92	127.71	105.96	197.29	137.76	233.70	244.12	109.54	147.52
246.13	360.07	445.71	124.97	104.40	196.38	137.59	231.29	245.17	109.15	146.26
245.62	354.43	441.09	122.15	103.04	193.66	137.65	228.50	239.92	108.04	144.49
245.12	347.10	433.98	120.65	102.00	192.49	137.71	223.68	231.51	106.93	143.15
242.26	339.21	426.52	118.54	100.96	189.52	136.69	217.00	226.47	105.62	141.89
237.37	331.61	417.64	116.33	99.21	184.74	135.91	210.88	220.38	103.33	140.29
233.84	322.59	401.31	113.61	97.46	181.64	132.89	205.69	213.66	101.50	138.19
228.28	314.43	386.41	110.09	95.84	178.02	130.53	196.24	205.25	99.46	136.10
222.56	308.80	375.05	106.75	93.90	172.72	128.24	188.08	197.48	97.11	134.50
218.86	298.67	364.39	103.93	91.05	169.88	125.64	181.22	190.34	95.01	132.32
215.66	287.98	360.83	101.11	88.98	165.49	123.11	177.89	184.03	92.85	130.14
212.96	280.38	360.11	100.22	87.55	163.55	121.60	176.58	182.14	91.21	127.53
211.45	276.97	366.83	100.56	86.38	162.90	120.70	175.65	182.14	89.12	125.77
211.62	276.66	379.22	101.24	86.11	162.38	121.55	176.01	184.24	88.14	125.26
212.29	280.00	394.80	102.11	86.63	163.15	123.90	178.78	187.82	88.27	125.00
213.47	287.29	408.26	104.39	89.59	165.08	129.41	184.70	191.18	89.65	125.92
215.66	293.17	428.10	107.71	90.95	167.91	133.58	190.62	195.38	92.67	127.66
219.19	305.23	439.09	112.88	92.56	173.59	135.63	199.87	209.24	94.83	130.00
222.73	324.31	444.40	119.54	93.92	176.03	137.21	207.28	225.21	98.51	133.93
251.52	362.20	449.36	127.68	96.69	180.68	137.69	225.05	243.28	110.12	138.53

SSS	STRAIGHT	RTRANS	RSIGMOID	RJV	LTRANS	LSIGMOID	LJV	SSSF
675.056	194.73	1057.32	976.852	1084.9	0	0	120.666	0
674.407	194.47	1055.42	977.319	1083.43	0	0	119.525	0
672.515	194.078	1055.2	977.743	1080.67	0	0	118.568	0
671.25	194.078	1050.39	976.164	1077.91	0	0	117.298	0
666.268	193.165	1045.96	974.563	1066.77	0	0	116.029	0
660.67	191.47	1042.25	968.912	1055.56	0	0	113.848	0
654.447	189.252	1036.78	964.669	1038.32	0	0	111.184	0
646.373	186.383	1028.71	956.993	1019.87	0	0	108.387	0
637.064	183.252	1014.37	947.25	997.828	0	0	105.12	0
625.276	179.73	1000.13	932.092	973.304	0	0	101.7	0
608.533	176.861	982.317	919.642	947.567	0	0	99.1982	0
593.027	173.209	965.411	905.188	925.471	0	0	96.5346	0
576.901	170.6	954.694	891.373	900.864	0	0	95.7143	0
562.013	168.904	938.628	879.583	889.691	0	0	96.1048	0
551.453	167.73	920.699	867.772	882.02	0	0	96.9867	0
547.085	168.513	912.506	864.017	882.816	0	0	100.311	0
550.145	169.426	915.709	868.512	899.473	0	0	104.555	0
562.487	172.557	926.885	880.468	920.901	0	0	108.953	0
590.922	176.991	967.966	903.274	949.611	0	0	114.608	0
675.688	194.336	1066.23	981.82	1083.74	0	0	121.324	0

Appendix B *S58 Nova flow report:*

BA	LICA	RICA	LPCA	RPCA	RACA1	LACA	LMCA	RMCA	LACA2	RACA2
118.97	196.37	276.21	94.60	66.61	122.703	71.22	120.00	115.59	52.00	63.38
118.08	193.90	275.41	93.00	66.21	122.165	71.03	118.19	113.60	51.44	63.11
116.69	190.39	273.41	91.03	65.02	120.655	70.52	115.99	110.54	50.94	62.33
114.84	187.75	271.29	89.44	64.05	118.711	69.54	112.92	107.21	50.36	61.13
113.73	183.36	268.63	88.06	62.81	113.74	68.75	109.48	104.68	49.46	60.38
112.18	178.10	265.57	83.93	61.71	109.526	67.63	106.28	101.53	48.67	59.33
109.75	172.84	262.11	75.90	60.43	106.285	66.65	101.37	98.38	46.69	58.29
107.09	171.78	259.32	70.22	59.64	101.314	64.78	95.96	94.32	45.29	57.57
104.13	172.11	256.53	66.50	58.98	97.2081	63.20	91.53	91.35	43.92	56.34
101.99	175.07	255.20	67.05	58.09	95.9128	61.94	88.10	90.63	43.33	55.49
98.66	179.08	255.20	72.11	57.34	96.1314	61.33	86.14	90.81	43.15	55.13
97.49	185.89	256.13	81.47	57.73	100.566	61.33	86.42	91.80	43.44	55.42
97.49	191.13	258.79	86.89	58.48	102.08	61.93	87.29	93.51	43.86	55.98
98.09	206.16	261.71	91.96	59.88	107.921	62.91	88.55	95.50	44.76	56.92
99.13	213.31	270.62	101.49	61.51	113.976	64.68	91.77	96.76	46.31	57.77
102.10	214.35	301.60	115.49	63.57	118.302	66.03	95.50	104.50	48.24	58.68
105.58	209.97	301.47	101.60	64.84	124.467	67.52	99.34	107.57	49.11	60.15
111.73	206.46	294.03	94.56	67.92	127.279	71.19	104.54	110.45	50.45	61.58
118.99	201.21	281.66	93.36	67.30	123.605	72.64	115.43	113.42	51.80	62.69
119.08	196.64	276.47	91.78	66.68	122.526	73.98	119.52	115.14	51.96	64.74

SSS	STRAIGHT	RTRANS	RSIGMOID	RJV	LTRANS	LSIGMOID	LJV	SSSF
362.153	82.7482	323.89	503.436	526.624	23.7647	190.182	571.002	239.783
365.611	82.7383	323.259	503.963	526.308	23.5766	189.633	571.385	239.728
368.377	82.7274	323.027	504.857	527.09	23.3069	189.34	572.727	239.498
369.345	82.5036	324.162	506.576	527.878	23.202	189.109	574.074	239.226
370.452	82.1441	326.071	511.873	528.448	23.6913	188.816	574.538	239.389
371.973	81.9629	330.89	514.227	526.486	24.096	188.01	574.675	239.684
373.218	81.6925	332.603	514.938	525.17	24.6701	187.583	574.006	240.102
374.601	81.3776	335.669	514.641	523.431	25.2411	186.773	572.207	239.96
374.463	80.8883	339.326	513.698	521.704	25.3902	186.106	567.838	239.556
374.739	80.2683	339.86	510.273	517.844	25.7933	185.674	564.841	238.935
373.771	80.5595	339.807	506.479	514.413	26.4489	185.772	562.327	237.923
373.909	80.8111	339.358	504.07	512.474	27.4433	187.255	561.499	236.866
375.016	81.3211	342.046	502.302	509.666	28.6918	190.973	561.799	235.549
376.399	82.0055	346.295	500.997	510.454	30.5331	194.574	562.743	234.143
378.335	82.6918	352.889	500.059	512.499	33.8031	199.05	566.657	233.001
380.687	84.2447	356.551	500.951	516.249	35.8969	202.528	569.933	233.248
383.868	85.6659	358.259	502.305	520.833	37.1469	205.754	572.725	233.63
387.74	86.9554	357.232	504.762	529.207	23.9325	206.735	571.735	234.752
378.75	87.6397	347.404	504.003	544.287	23.7538	195.366	571.792	236.658
362.153	83.0533	326.448	503.806	537.036	23.5672	190.308	572.023	240.351

Appendix C *Hand-written derivation of General flow estimation formula:*

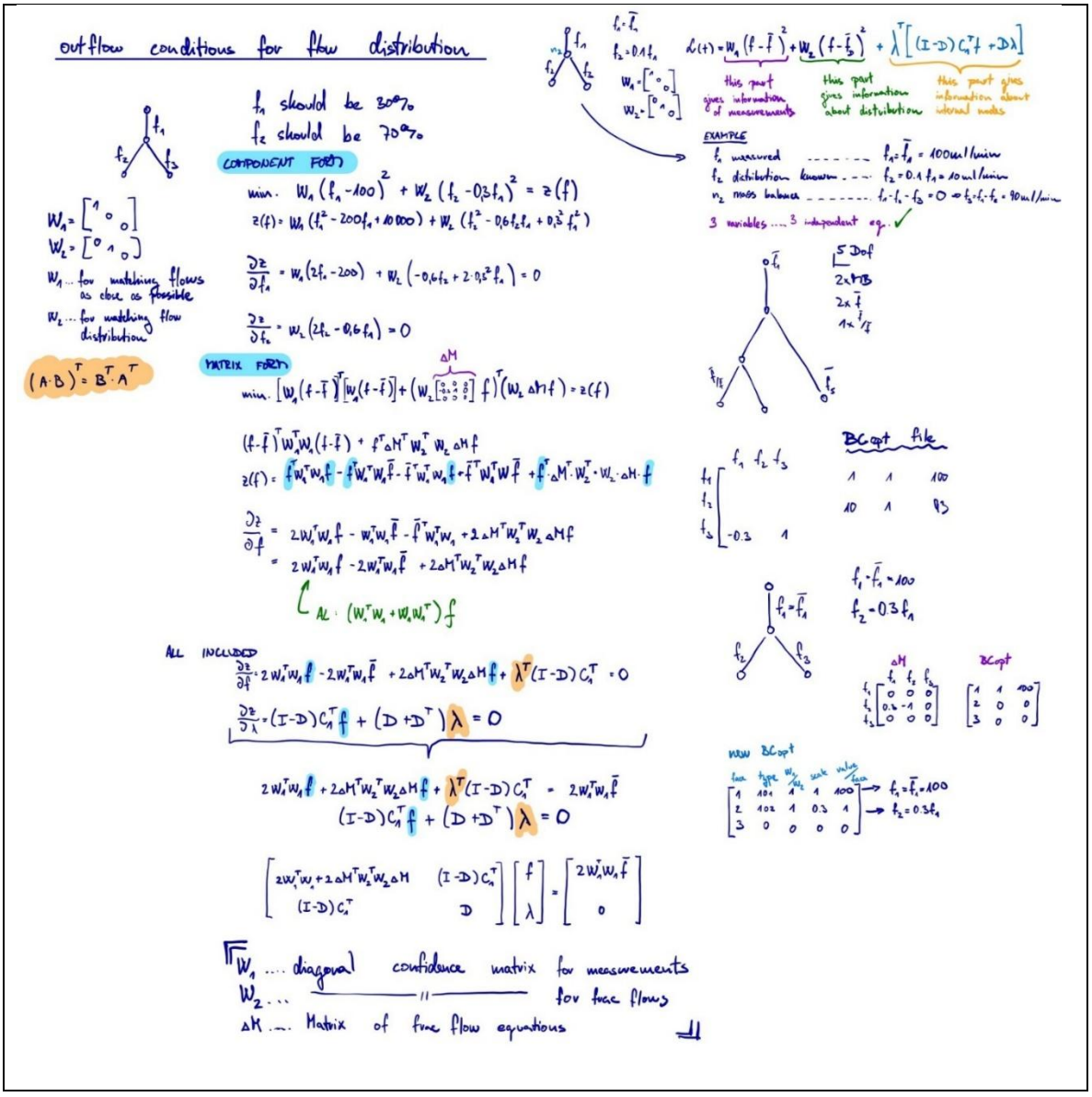

Appendix D *Hand-written derivation of General pressure estimation formula*

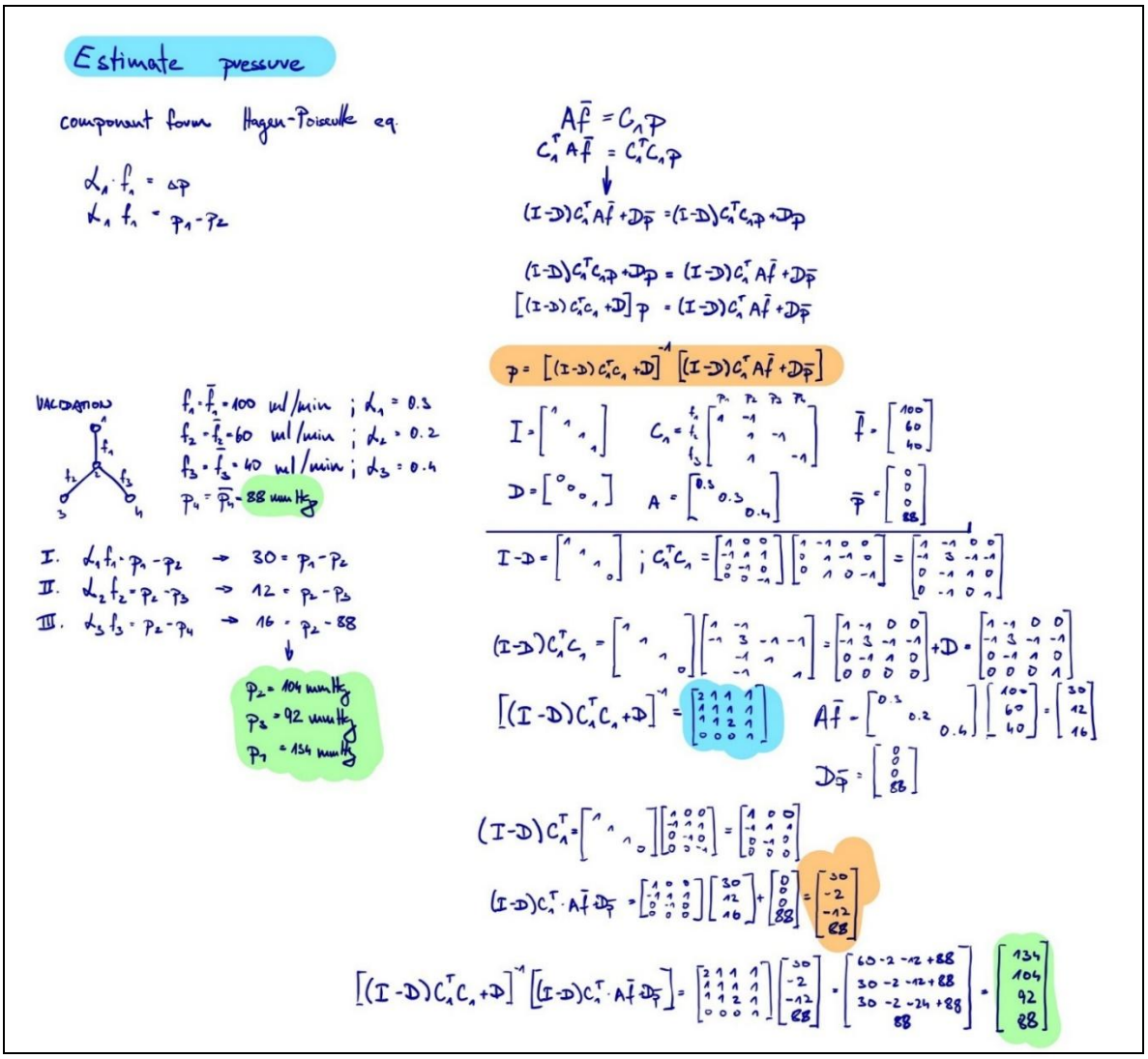

Appendix E *Professor Linningers hand-written notes on Flow estimation:*

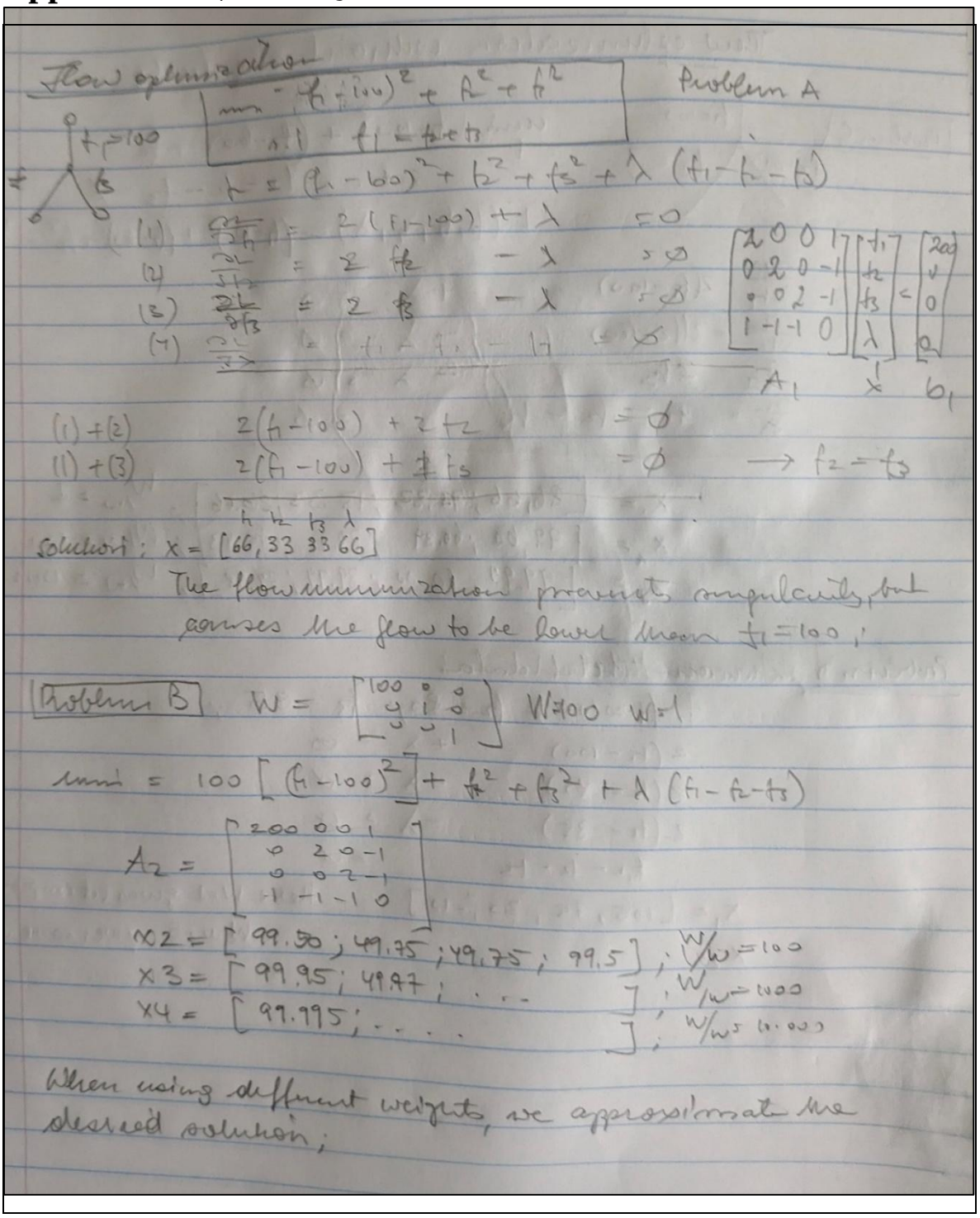

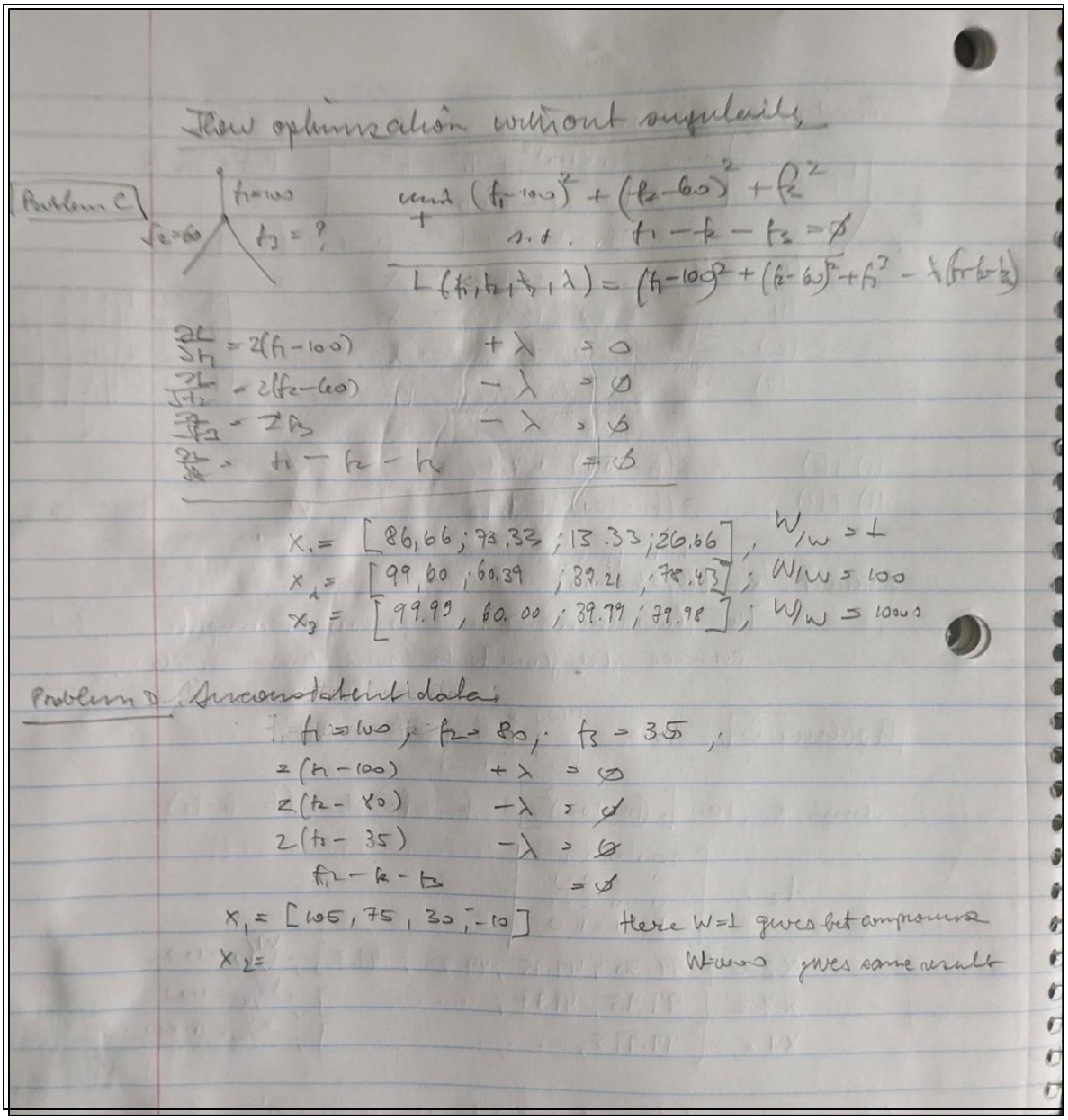

Flow optimization without singularity

Problem C

$f_1 = 100$

$f_2 = 60$

$f_3 = ?$

$\min (f_1 - 100)^2 + (f_2 - 60)^2 + f_3^2$

s.t. $f_1 - f_2 - f_3 = 0$

$L(f_1, f_2, f_3, \lambda) = (f_1 - 100)^2 + (f_2 - 60)^2 + f_3^2 - \lambda(f_1 - f_2 - f_3)$

$\frac{\partial L}{\partial f_1} = 2(f_1 - 100) + \lambda = 0$

$\frac{\partial L}{\partial f_2} = 2(f_2 - 60) - \lambda = 0$

$\frac{\partial L}{\partial f_3} = 2f_3 - \lambda = 0$

$\frac{\partial L}{\partial \lambda} = f_1 - f_2 - f_3 = 0$

$X_1 = [86,66; 73.33; 13.33; 26.66]$, $W/w = 1$

$X_2 = [99,60; 60.39; 39.21; 78.43]$, $W/w = 100$

$X_3 = [99.99, 60.00; 39.99; 79.98]$, $W/w = 1000$

Problem D. Unconstrained data

$f_1 = 100$; $f_2 = 80$; $f_3 = 35$;

$2(f_1 - 100) + \lambda = 0$

$2(f_2 - 80) - \lambda = 0$

$2(f_3 - 35) - \lambda = 0$

$f_1 - f_2 - f_3 = 0$

$X_1 = [105, 75, 30; -10]$ Here $W=1$ gives bet ampouva

$X_2 =$ $W=100$ gives same result